EFFECT OF IDENTIFICATION ON SEISMIC PERFORMANCE ASSESSMENT OF A TALL BUILDING

by

Korkut Kaynardağ

B.S., Civil Engineering, Bogazici University, 2013

Submitted to the Institute for Graduate Studies in
Science and Engineering in partial fulfillment of
the requirements for the degree of
Master of Science

Graduate Program in Civil Engineering

Boğaziçi University

2016

EFFECT OF IDENTIFICATION ON SEISMIC PERFORMANCE ASSESSMENT OF A TALL BUILDING

APPROVED BY:

Assoc. Prof. Serdar Soyöz (Thesis Supervisor)	.....
Assoc. Prof. Kutay Orakçal	.....
Prof. Necati Çatbaş	.....

DATE OF APPROVAL: 16.06.2016

ACKNOWLEDGEMENTS

My sincere thanks are to Associate Professor Serdar Soyöz who always trusted in me and accepted me to his research team. His valuable guidance and support in every field are absolutely precious. His knowledge and experience brought me to a higher level of thinking and helped me to gain important research skills. In addition, he always challenged me to do my best, which helped me to improve myself considerably. Actually, there is actually no words to thank to him.

Besides my advisor, I would like to thank to Kutay Orakçal for his help and insightful comments about my project. I also thank Necati Çatbaş for his interest in my thesis.

I thank my fellow research assistants in our group: Hüseyin Çolak and Oğuz Şenkardeşler for the stimulating discussions with me about my project, for their help through many laboratory and field works, and for all the fun and friendship that we have had in the last three years.

I acknowledge my gratitude to my friends: Diyap Esen Kaba and Yiğit Çetinel, who squeeze time from their busy schedule to help me for the stages of my thesis that are related to advanced programming. Their skills and experience enhanced my capabilities in programming.

Finally, I take this opportunity to express the profoundest gratitude from my deep heart to my beloved parents, grandparents, and my brother for their sacrifices, love, and continuous support – both spiritually and materially. Without their extreme sacrifices, supports and the carefree environment that they provided, it would not be possible for me to follow a graduate degree.

ABSTRACT

EFFECT OF IDENTIFICATION ON SEISMIC PERFORMANCE ASSESSMENT OF A TALL BUILDING

In this study, a twenty-six story, core-wall tall building was instrumented with data acquisition system. Modal parameters were obtained by using Enhanced Frequency Domain Decomposition (EFFD) method and a detailed FEM of the structure was updated based on the identified modal characteristics in order to represent the actual dynamic characteristics of the building. Updating of a fine FEM allows to minimize the uncertainties in structural parameters such as the effects of soil springs and seismic gaps with frictional plates which are usually omitted in updating procedures. Along this line, nonlinear time history (NLTH) analyses were performed with the updated and the non-updated FEM with 5% damping ratio. Additionally, NLTH analyses were carried out with updated FEM considering the identified (2%) and 5% damping ratios in order to observe the effect of damping ratio separately. Probability density functions in terms of interstory drift ratios were established in order to quantify the probability of failures under different ground motions. Results highlight that incorporation of system identification and model updating techniques into seismic performance assessment is crucial. Results also show the significant sensitivity of higher modes to the changes in structural parameters during updating procedure of tall buildings and excitation of higher modes due to seismic motions. In addition, recorded seismic response of the building demonstrated the dynamic excitation (vibration amplitude) of higher modes may be higher than the one of fundamental mode.

ÖZET

SİSTEM TANIMLAMANIN YÜKSEK BİR BİNANIN SİSMİK PERFORMANS DEĞERLENDİRMESİ ÜZERİNDEKİ ETKİSİ

Bu çalışmada, 26 katlı çekirdek duvarlı yüksek bir bina data toplama sistemi ile instrümente edilmiştir. Modal parametreler Frekans Uzayına Ayrıştırma (FUA) ile tanımlanmıştır ve detaylı bir Sonlu Elemanlar Model'i (SEM) yapının gerçek dinamik davranışını temsil etmesi için tanımlanan modal parametreler doğrultusunda güncellenmiştir. Detaylı bir SEM'in güncellenmesi zemin yatak katsayılarını temsil eden yaylar, ve plaklar aracılığı ile sürtünme kuvveti sağlayan sismik derzler gibi yapısal parametrelerdeki belirsizlikleri minimize etmektedir. Zaman tanım aralığında doğrusal olmayan analizler 5% sönümlenme oranı ile güncellenmiş ve güncellenmemiş SEM'lerle yapılmıştır. Ayrıca bu analizler, tanımlanan sönümlenme oranının etkisini incelemek amacı ile tanımlanan sönümlenme oranı (2%) ve 5% sönümlenme oranları ile güncellenen model kullanılarak da gerçekleştirilmiştir. Farklı deprem girdileri altında hasar görme olasılığı dağılımı fonksiyonları kat ötelenmesi cinsinden elde edilmiştir. Sonuçlar göstermiştirki sistem tanımlama ve model güncelleme tekniklerinin sismik performans değerlendirme metodları ile incelenmesi önemlidir. Sonuçlar ayrıca yüksek modların modal parametrelerinin modal güncellemesi sırasında değişen yapısal parametrelere önemli ölçüde duyarlı olduğunu göstermiştir. Yapıdan alınan deprem kayıtları ise yüksek modların dinamik tepkilerinin birinci moddan fazla olabileceği olasılığını göstermiştir.

TABLE OF CONTENTS

ACKNOWLEDGEMENTS . . . iii
ABSTRACT . . . iv
ÖZET . . . v
LIST OF FIGURES . . . viii
LIST OF TABLES . . . xiv
LIST OF SYMBOLS . . . xv
LIST OF ACRONYMS/ABBREVIATIONS . . . xvi
1. INTRODUCTION . . . 1
1.1. Overview . . . 1
1.2. Literature Review . . . 2
1.2.1. Literature Review on Structural Health Monitoring . . . 3
1.2.2. Literature Review on Damping . . . 12
1.2.3. Literature Review on Higher Modes . . . 17
1.3. Objective . . . 23
1.4. Scope . . . 24
2. INSTRUMENTED BUILDING . . . 26
2.1. Building Information . . . 26
2.2. Building Instrumentation . . . 27
3. SYSTEM IDENTIFICATION . . . 31
3.1. Frequency Domain Decomposition Method . . . 31
3.2. System Identification of the Structure . . . 32
3.3. Automatic Analysis of the Recorded Data . . . 34
3.4. Real-time Monitoring Module . . . 37
3.5. Identification under Different Wind Loads . . . 39
4. FEM OF THE STRUCTURE AND THE UPDATING PROCEDURE . . . 41
4.1. Finite Element Model and Primary Updating Procedure . . . 41
4.2. Sensitive Updating Procedure . . . 45
5. SELECTION OF GROUND MOTIONS . . . 49

6. DEVELOPMENT OF THE NONLINEAR FEM 55
7. EFFECT OF IDENTIFICATION ON SEISMIC PERFORMANCE ASSESSMENT OF THE TALL BUILDING 63
7.1. Effect of the identified modal shapes and frequencies 63
7.1.1. Explanation of Seismic Demand Results of the Updated and the Non-updated FEM's 68
7.2. Effect of the Identified Viscous Damping Ratio 77
8. CONCLUSIONS AND FUTURE WORK 83
8.1. Conclusions 83
8.2. Future Work 85

LIST OF FIGURES

Figure 2.1. The building monitored in the study. 26

Figure 2.2. The location of the complex in Istanbul. 27

Figure 2.3. The data recorder and the sensors at 17th floor. 28

Figure 2.4. The plan of the building and the instrumentation configuration. . 28

Figure 2.5. Typical floor plan of the tower and the sensors. 29

Figure 2.6. The vibration data in time domain in x direction recorded from all the instrumented floors. 30

Figure 3.1. The vibration data in time domain in x direction recorded from the 17th and 26th floors. 32

Figure 3.2. Cross-power spectral density matrix. 33

Figure 3.3. The impulse response function. 34

Figure 3.4. Schema of automatic analysis of the vibration data. 35

Figure 3.5. The steps of “real-time monitoring” module. 37

Figure 3.6. Real-time Monitoring Module. 39

Figure 3.7. Building acceleration responses at different wind speeds. 40

Figure 4.1. The part considered in the study and the structural elements. . . . 42

Figure 4.2. The part considered in the study and the structural elements. . . . 42

Figure 4.3. The finite element model in 3-D. 44

Figure 4.4. Zoomed view of the basement section of the FEM. 45

Figure 4.5. Schema of the Matlab code which performs the automatic FEM Updating Procedure. 46

Figure 4.6. Experimental, updated and non-updated mode shapes. 48

Figure 5.1. ASCE 41-13 design based uniform hazard spectrum. 49

Figure 5.2. Spectral acceleration map of Istanbul at the period of 0.2 s. 51

Figure 5.3. Spectral acceleration map of Istanbul at the period of 1 s. 51

Figure 5.4. The Marmara segment of the North Anatolian Fault and the location of the tall building. 52

Figure 5.5. The spectra of selected ground motions, their mean and the design spectrum. 53

Figure 6.1. Cross -section and Moment – Curvature graph of the shear wall side of the beams that connects the shear wall to the outher colums at basement section. 56

Figure 6.2. Cross -section and Moment – Curvature graph of the column side of the beams that connects the shear wall to the outher colums at basement section. 56

Figure 6.3. Cross-section and Moment – Curvature graphs of the column side of the beams that connects the shear wall to the outher colums at tower section. 56

Figure 6.4. Cross -section and Moment – Curvature graphs of the shear wall side of the beams that connects the shear wall to the outher colums at tower section. 57

Figure 6.5. Cross -section and P-M diagrahm of the colums at top storey of the tower. 57

Figure 6.6. The cross-section and P-M diagrahm of the colums at the base of basement section. 57

Figure 6.7. The cross-sections and P-M diagrahms of one of the shear walls at the top of the tower section. 58

Figure 6.8. The cross-sections and P-M diagrahms of one of the shear walls at the base of the basement section. 58

Figure 6.9. The modelling parameters and acceptence criterias in terms of plastic rotations for the beams (ASCE 41-13). 59

Figure 6.10. The modelling parameters and acceptence criterias in terms of plastic rotations for the columns (ASCE 41-13). 60

Figure 6.11. The modelling parameters and acceptence criterias in terms of plastic rotations for the shear walls (ASCE 41-13). 61

Figure 7.1. The damage levels of the Updated and Non-updated FEM's with 5% viscous damping ratio under the ground motion no 1. 64

Figure 7.2. The interstory drift ratios of the Updated and Non-updated FEM's with 5% viscous damping ratio under the ground motion no 1. . . 65

Figure 7.3. The damage levels of the Updated and Non-updated FEM's with 5% viscous damping ratio under the ground motion no 8. 65

Figure 7.4. The interstory drift ratios of the Updated and Non-updated FEM's with 5% viscous damping ratio under the ground motion no 8. . . 66

Figure 7.5. The mean interstory drift ratios of the Updated and Non-updated FEM's. 66

Figure 7.6. Probability density functions of the Updated and Non-updated FEM's. 67

Figure 7.7. Moments imposed by the first three modes of the updated and the non-updated FEM's. 68

Figure 7.8. Modal Shapes of the non-updated and the updated FEM's. 70

Figure 7.9. Modal Static Forces of the non-updated and the updated FEM's. . 70

Figure 7.10. Building acceleration response acquired from non-updated FEM's under input motions no. 5 71

Figure 7.11. Building acceleration response acquired from non-updated FEM's under input motions no 8 71

Figure 7.12. Source location of the earthquakes 72

Figure 7.13. Acceleration response of instrumented stories in time domain in one direction under Marmara Earthquake. 73

Figure 7.14. Acceleration response of instrumented stories in time domain in one direction under Romania Earthquake. 73

Figure 7.15. Acceleration response of instrumented stories in time domain in one direction under Yalova Earthquake. 74

Figure 7.16. Acceleration response of instrumented stories in time domain in one direction under Sakarya Earthquake. 74

Figure 7.17. Acceleration response of building to Marmara Earthquake and the frequency content of the seismic input recorded at the base of the building 75

Figure 7.18. Acceleration response of building to Romania Earthquake and the frequency content of the seismic input recorded at the base of the building. 75

Figure 7.19. Acceleration response of building to Yalova Earthquake and the frequency content of the seismic input recorded at the base of the building. 76

Figure 7.20. Acceleration response of building to Sakarya Earthquake and the frequency content of the seismic input recorded at the base of the building. 76

Figure 7.21. The damage levels of the updated FEM's with 2% and 5% viscous damping ratios under the ground motion no 9. 79

Figure 7.22. Interstory drift ratios of the updated FEM's with 2% and 5% viscous damping ratios under the ground motion no 9. 80

Figure 7.23. The damage levels of the updated FEM's with 2% and 5% viscous damping ratios under the ground motion no 7. 80

Figure 7.24. Interstory drift ratios of the updated FEM's with 2% and 5% viscous damping ratios under the ground motion no 7. 81

Figure 7.25. Mean Interstory drift ratios of the updated FEM's with 2% and 5% viscous damping ratios. 81

Figure 7.26. Probability density functions of the updated FEM's with 2% and 5% viscous damping ratios. 82

LIST OF TABLES

Table 4.1. The observed changes in the fundamental frequency with respect to the changes in the model 43

Table 4.2. Identified, non-updated and updated modal frequencies. 48

Table 5.1. Properties of the selected ground motions. 54

Table 7.1. Properties of the recorded earthquakes. 72

Table 8.1. Probabilities of exceeding the treshold interstory drift ratios for the updated and the non-updated FEM's 84

Table 8.2. Probabilities of exceeding the treshold interstory drift ratios for the updated FEM's with the identified and code based viscous damping ratios. 84

LIST OF SYMBOLS

$\left[C\right]$	Damping matrix
$C50$	50 Mpa-concrete class
E	Acceleration in SS direction
f	Frequency
g	Gravational Acceleration
GPa	Gigapaskal
h	Weightening coefficient for MAC value
H	Thickness
Hz	Heartz
k	Weightening coefficient for modal frequency
$\left[K\right]$	Stiffness matrix
kN	Kilonewton
m	Meter
$\left[M\right]$	Mass matrix
p	Material Mass Density
R	Reduction factor
Sa	Spectral acceleration
S_{xs}	Spectral acceleration corresponding to the period of 0.2sec
S_{x1}	Spectral acceleration corresponding to the period of 1sec
sec	Second
T	Natural period of the structure
ζ	Modal Damping ratio
α	Rayleigh damping coefficient
β	Rayleigh damping coefficient
ω_i	Natural frequency of the ith mode

LIST OF ACRONYMS/ABBREVIATIONS

ACI	American Concrete Institute
ARMA	Linear time invariant systems
ASCE	American Society of Civil Engineers
ATC	Applied Technology Council
DBE	Design basis earthquake
EFDD	Enhanced frequency domain decomposition
FEM	Finite element model
FEMA	Federal Emergency Management Agency
HTML	Hyper Text Makeup Language
LATBSDC	Los Angles Tall Building Structural Design Council
MAC	Modal Assurance Criteria
MCE	Maximum considered earthquake
MDLAC	Multiple Damage Location Assurance Criterion
MDOF	Multi degree of freedom system
MEMS	Micro electro mechanical systems
MPA	Modal pushover analysis
NEES	Network for Earthquake Engineering Simulation
NIST	National Institute of Standards and Technology
NLTH	Nonlinear time history
PDF	Portable Document Format
PEER	Pacific Earthquake Engineering Research
PGA	Peak Ground Acceleration
PSD	Power Spectral Density
RSA	Response Spectrum Analysis
RSS	Rich Site Summary
SDOF	Single degree of freedom system
SEI	Structural Engineering Institute
SHM	Structural health monitoring

SRSS	Square root of the sum of the squares
SSI	Stochastic Subspace Identification
TDG	Teknik Destek Grubu
UBC	Uniform Building Code
UCLA	University of California, Los Angles
SCSD	University of California, San Diego
UMRHA	Uncoupled modal response history analysis

1. INTRODUCTION

1.1. Overview

In recent decades, tall buildings have been the dominant means of accommodation and places of business in metropolises where economy and population grow fast. Due to lack of adequate construction sites and expensive land prices, the demand for tall buildings are increasing day by day. Thanks to the recent technological and technical advances in the construction and design stages of tall buildings, this demand for tall buildings can be met easily nowadays. In addition, tall buildings have become the symbols of metropolitan cities such as New York, Tokyo and Istanbul, and they create the skyline views of such cities.

Compared to ordinary buildings, tall buildings result in a bigger impact on the economy due to several reasons. First of all, they are more densely populated than the mid and low rise buildings. Therefore, any damage in such buildings may result in serious problems. Many people may lose their homes, even worse, they may lose their lives. Secondly, many of these buildings are utilized as places of business by banks, telecommunication providers and holdings. If tall buildings remain nonfunctional for a long time after any calamity, the economy of a country may encounter severe problems.

Because of the reasons above, safety and resiliency of such buildings should be known prior to any damage. "Resiliency" is a new term and it has been recently prevalent among the researchers. This terms refers to capability of cities to meet the challenges of any disaster such as floods, storms, explosions and earthquakes right after a disaster. Therefore, because of the fact that tall buildings are the major components of cities, and the fact that they are vulnerable to many catastrophic events, many researchers have begun carrying out studies about tall buildings with the aim of making them resilient.

Within the scope of resiliency of tall buildings, structural and earthquake engineers have been conducting studies in order to estimate the seismic performance of tall buildings precisely. The accurate estimation of the damage level is very crucial because tall buildings are desired to experience minimum damage due to their important aspects mentioned before. Mathematical models, (FEM's) are the most common tool to simulate the seismic responses of structures. However, due to many uncertainties in the structural parameters, many assumptions are made in FEM's. In contrast to the limited knowledge about such uncertainties, SHM provides real information about the dynamic characteristics of structures. Therefore, many researchers and structural engineering companies have adopted SHM techniques in order to obtain real dynamic parameters of structures. Upon obtaining the real dynamic parameters, FEM's are updated to mimic the real dynamic characteristics of structures. As a result, more reliable seismic simulations are carried out. In addition, the damage localization and intensity of structures may be estimated after any seismic event.

The tall building that has been investigated in this study is located in Istanbul and it serves as housing, places of business and shopping mall. Istanbul is one of the biggest metropolitan cities of the world and it is prone to seismic actions. Therefore, the tall building is very suitable for this study because of the reasons mentioned above. In order to demonstrate the importance of FEM Updating Procedure of the building based on the identified modal parameters, the probability density functions in terms of inter-story drift ratios are conducted both for the updated and the non-updated FEM. The reason to choose inter-story ratio is the fact that it is a global damage indicator. The results show the effect of identification on seismic performance assessment of a tall building. In addition, the results demonstrate that incorporation of probabilistic methods is crucial in estimating the damage level of a tall building after a seismic event.

1.2. Literature Review

In recent decades, tall buildings have been the significant sources of accommodation and places of business in metropolises where economy and population grow

fast. Compared to ordinary buildings, tall buildings are more densely populated, resulting in a bigger impact on the economy. Therefore, safety of such buildings should be known prior to an earthquake and any damage due to earthquakes should be detected in seismically prone areas, such as San Francisco, Tokyo and Istanbul. To meet such necessities, The Tall Building Initiative, a consortium of interested parties which develops guidelines through a series of research studies and workshops, has been active especially in California. The major purpose of the Tall Buildings Initiative is to establish a clear definition of performance objectives. These objectives involve procedures such as selecting and scaling earthquake ground motions, nonlinear modelling approaches and criteria for determining whether calculated demands are in acceptable ranges "(Moehle, 2007)".

1.2.1. Literature Review on Structural Health Monitoring

SHM techniques enable engineers to understand the real dynamic characteristics of buildings. In these techniques, vibration data (mostly acceleration) recorded under ambient conditions or during seismic events is processed in time or frequency domain and consequently the actual dynamic characteristics such as modal frequencies, shapes and damping ratios are obtained. Based on the identified model parameters, FEM's are updated. The updating procedure can be global in which the dynamic characteristics of an entire structure are updated or it can be in a local scale. In addition, The responses of structures to dynamic excitations may be captured by the virtue of SHM. Moreover, "health" of a structure can be investigated from the measurements.

Several studies demonstrate that dynamic characteristics generated from FEM's and vibration data exhibit remarkable differences. One of the main reasons of these differences is the assumptions made in development of FEM's. These assumptions are inevitable due to the uncertainties in structural parameters. By the virtue of SHM, the differences between the modal parameters of FEM's and the identified modal parameters can be minimized and more reliable seismic assessments at design stage become possible through FEM updating procedures. Therefore, SHM has made significant contributions to verification and enhancement of design assumptions, generation of more

reliable Finite Element Models (FEM's) and detection of damage. Consequently, SHM has gained remarkable attention worldwide and has been a common technique used among researcher and engineering companies.

Brownjohn *et al.* (2000) compared the dynamic parameters of six different FEM modelling approaches of a tall building frame-wall structural system with the identified dynamic parameters. The most remarkable results were that the detailed modelling of the shear wall gave the most realistic results of torsional rigidity, and that the framing system had the strongest influence on lateral stiffness for fundamental translational modes. In addition, a simple stick FEM led to acceptable results for the first translational modes.

Lord *et al.* (2003) used Artemis modal analysis software in order to extract the real modal parameters of a fifteen and a forty-eight storey reinforced concrete buildings. The parameters to be updated are the young's modulus (E) and material mass density (p) of beams, columns, shear walls, floor slabs and cladding, the second moment of inertia of beams and columns in principal directions, and the thickness (H) of the cladding. The results from the updating of the first building showed that the final values of E and H of the cladding presented the greatest differences with their initial values. For the second structure, a sensitivity analysis was conducted and consequently it was found out that the overall stiffness of the building was most sensitive to the parameters of shear walls, slabs and cladding. The final updating procedure illustrated that, as expected from the preliminary analysis, the parameters whose final values exhibited the biggest difference with their initial values after the updating procedure belonged to shear walls and slabs.

Ventura *et al.* (2005) performed a similar study of Lord *et al.* (2005) and conducted a FEM Updating study of a 48-storey reinforced concrete shear core building by using a multi-functional computer-aided engineering program, FEMtools, which can update FEM's automatically. The modal parameters were extracted from the ambient records via Artemis modal analysis software. Firstly, a sensitivity analysis was conducted. The number of parameters of this analysis was 161 including the

similar parameters of the previous study. The result showed that the FEM was most sensitive to change in E and p (for shear walls, floor slabs and cladding) and in H for the cladding. At the end of sensitive analysis, the number of parameters to be updated was decreased to 26. The result of the final Updating Procedure illustrated that the FEM needed to be more flexible and a reduction in E of shear walls was necessary in order to mimic the dynamic properties obtained from the identification.

Skolnik *et al.* (2006) and Skolnik *et al.* (2007) identified the modal shapes and frequencies of the UCLA Factor Building, a 15-storey steel moment-resisting frame, by processing the recorded data which were obtained under ambient vibrations and during 2004 Parkfield earthquake (M=6). The Subspace state-space system identification (N4SID) (Van Overschee, 1994) was used for the identification. It was observed that the modal frequencies obtained from ambient vibrations were more than the ones identified from the low-amplitude earthquake excitation. This result was attributed to the fact that there was no stiffness contribution of non-structural elements under low-amplitude seismic events. Following the initial comparison of the modal parameters obtained from the FEM and the identification, a simple stick model with mass and stiffness properties, which represented the additional mass and stiffness contribution of non-structural elements, was superimposed into the FEM. Then, the FEM of the structure was updated based on the modal parameters identified from the seismic response of building to the Parkfield Earthquake. The reason that the modal parameters identified from the seismic response was used for the Updating Procedure, was that they represented the seismic response of the structure more accurately under any seismic shaking. At the last step, the updated model was exposed to the 1994 Northridge earthquake. The results of this simulation were found to be consistent with the 1994 post-earthquake damage evaluation report of the building.

ASCE-SEI Performance of Structures Tract formed a technical committee on "Structural Identification (St-Id) of Constructed Systems" in 2005. The one of the main goals of this committee is to develop guidelines for more reliable field-calibrated FEM's and identification (characterization) of existing structures so that the theory can be validated or improved by practice with the help of using different methods and

technologies. The committee determined six crucial steps. These are 1) Establishing the divers for structural identification, 2) A-Priori Modeling, 3) Experimentation, 4) Processing data for parameter identification and interpretation, 5) Evaluation of model errors and 6) Utilization for decision making. This report, by involving the 6th step, highlighted the importance of justification of the results so that most proper decisions can be made for the structures which are monitored. (Catbas *et al.*,2010)

FEM Updating procedures may also be utilized for condition assessment of civil structures because of the fact that they provide a very efficient, nondestructive global damage identification methodology. In this methodology, two updating processes are carried out. In the first one, the initial FEM is updated in order to a represent the undamaged structure. The updated FEM at the end of this stage is called as the reference state. In the second step, the reference model is updated in order to generate a model that mimics the experimental modal properties of the damaged state. In the study of Teughels and De Roeck (2004), this methodology was applied to the Z24 Bridge in Switzerland, a concrete bridge with three spans. The damage was introduced to the structure by lowering one of the intermediate piers, leading to decreases in bending and torsion stiffness of the bridge girder. A nonlinear least squares method was performed in order to obtain the modal properties of the damaged structure. The final FEM successfully minimized the discrepancies between the experimental and the simulated characteristics of the bridge.

Moaveni *et al.* (2012) performed a similar study. A two-third-scale, 3- storey, 2-bay, infilled reinforced concrete frame was tested on the UCSD–NEES shake table with the aim of examining the seismic performance assessment of this type of construction. The damage was induced on the structure progressively through scaled historical earthquake records of increasing magnitudes. System identification of the structure was carried out by processing the ambient vibration records, which were collected after each damage level using a deterministic-stochastic subspace identification method. The non-damaged and damaged FEM's were updated by a sensitivity-based finite-element model updating strategy for the detection, localization and quantification of damage as a loss of effective local stiffness. The results showed that this method could

reliably identify the location and severity of damage caused by the seismic shakings during the tests.

A significant benchmark study for SHM applications is a full-scale seven-storey reinforced concrete shear wall building structure which was tested on the UCSD-NEES shake table. The tests were adjusted to damage the building progressively by using several historical seismic motions. At each stage of the damage, dynamic tests were conducted in order to identify the modal parameters of the structure. In the study of Moaveni (2009) and Moaveni (2011), a sensitivity-based FEM updating approach was adopted with the aim of identifying damage levels based on the identified modal parameters at each damage state. Because of the fact that the uncertainty in both of the system identification and the damage identification results may be crucial, in the study of Moaveni *et al.*, (2014), an uncertainty analysis on these system and damage identification results were performed. In order to carry out a systematic and comprehensive uncertainty analysis of damage identification results, information about exact magnitude and location of damage and exact modal parameters were required. This information was not available from an experimental case. The identified modal parameters of the damaged structure were generated numerically using a three-dimensional FEM with different levels of damage simulated along the height of the structure. The uncertainty in modal parameters, spatial density of measurements and mesh size of the FEM were determined as variability in inputs. The systematic investigation demonstrated that the reliability of the damage identification results obtained through FEM updating depended not only on the level of uncertainty in the identified modal parameters, but also on the decisions in the design of experiments such as spatial density of measurements and modeling errors.

Koh and Dyke (2007) utilized multiple damage location assurance criterion (MDLAC), which combined a correlation-based technique. This criterion is based on changes in frequencies of structures. In the study, also other methods such as least-squares, frequency-error, and sensitivity-based correlation method (MDLAC) which exploit the correlation of natural frequencies and mode shapes, were included. A cantilevered beam model was used for a comparative study for such methods. Then, a

cable-stayed bridge model was used for simulation of localized damage and for the demonstration of the effectiveness of the utilized method.

Catbas *et al.* (2012) demonstrated a cost-effective method in terms of sensor, data acquisition and analysis for damage detection. In this method, correlation coefficients between strain time histories at different locations are obtained. If, for a location, there is any differences in correlation coefficients calculated by using the strain measurements from the intact and damaged structure, damage location is detected. The methodology was validated by using a laboratory test structure and a real-life bridge.

Seismic responses of structures have also been examined and valuable information about soil-structure interaction, nonlinear behavior of structural elements, and interaction of structural and non-structural elements were obtained by analyzing the vibration records collected during seismic events.

Safak (1991) utilized a discrete-time method by using multi inputs and single output in order to identify the dynamic characteristics of a 60-storey tall building exposed to Loma Prieta earthquake. Determination of identification parameters for minimum errors, model validation and digital signal filtering approaches were introduced. Also, a significant rocking effect was observed and the importance of soil-structure interaction on dynamic response was emphasized. The high magnitude of the frequencies around the fundamental frequency in the spectrum of vertical sensors was attributed to the nonlinearities in the foundation soil and the rocking motions.

Safak (1992) analyzed a 30-story, three-winged building exposed to the Loma Prieta earthquake by using the same identification method in the previous study. It was observed that free-field vibration measurements during the earthquake were disrupted by the movements of the structure, causing the involvement of the frequencies of the structure in the vibration record. It was also observed that the building underwent nonlinear behavior. Torsionally coupled modes were extracted from the three-dimensional time history plots of the structure and their contribution was found to be

significant. In both studies, the differences of frequencies (elongation of first periods of buildings) obtained from ambient vibration and the seismic motion measurements were attributed to the soil-structure interaction and the nonlinear behavior of the soil.

Celebi (1993) investigated the seismic responses of five different buildings located at San Francisco Bay area to a Loma Prieta and ambient excitations. The elongations of first-mode periods during the seismic event were observed in this study as well. The slip of steel connections and the interaction of structural and non-structural elements were considered as the source of the period elongation in addition to the sources mentioned in previous studies.

Naeim (1998) also evaluated the recorded vibration motions from many different type of buildings that were obtained during 1994 Northridge Earthquake. Several remarkable conclusions were made as following: The periods of buildings estimated by building codes were consistently less than the identified periods. The base shears that many buildings experienced were larger than the design base shears. However, all the buildings performed much better in global sense than the expected because of the fact that the overall interstory drift ratios of buildings were less than the expected ones obtained from ordinary design procedures. Even though the base shears experienced during the earthquake didn't correlate well with the design code base shears, the observed and code based overall drift ratios correlated well. For the tall buildings, 2nd and 3rd modes had more contribution to the overall response than the fundamental mode. It was noted that the application of the lateral story force profiles as suggested by static lateral force procedures might have significantly underestimated the seismic demands. Indeed, the examination of the story forces at the instant of maximum base shears demonstrated that the forces were underestimated for tall buildings when the code based lateral force procedures were adopted. In addition, the significant elongations of the period of the buildings were not observed at undamaged structures. On the other hand, the periods of damaged buildings elongated considerably.

Boroschok *et al.* (2000) studied the records collected from a 22-stories high structural wall building during the ambient and earthquake excitations. The modal

frequencies, shapes and the seismic response of the building were identified through parametric and nonparametric techniques. A strong coupling of translational modes and very low damping values were observed during medium intensity seismic events and ambient excitations. An analytical model based on the procedures of design practice was also developed and it was observed that there was a good agreement between the modal parameters obtained from the FEM and ambient records. However, the recorded seismic responses didn't match very well with the ones simulated through FEM. The reason was attributed to the several factors such as the difficulties in modeling the lateral coupling of the building and the uncertainty in damping.

Kohler *et al.* (2005) and Celebi (2006) performed very similar studies. Kohler *et al.* (2005) acquired the dynamic properties of the moment-resisting steel-frame UCLA Factor building while and Celebi (2006) conducted the identification study on a 20-storey steel-framed Atwood Building in Alaska. In both of the studies, the vibration data were collected during low-magnitude seismic shakings and under ambient conditions. Similar results with the ones of the previous studies were obtained and the reasons of these results were discussed.

Immediate evaluation of a building after a seismic event is significant. Therefore, Celebi et. al. (2004) developed a real time monitoring system. The system enabled a client or a consultant engineer to assess the building condition by a software which could display the inter-story drifts as damage indicator in order to determine the safety level of a structure. It was shown that this system could be utilized for continuous monitoring of aging and damage detection.

In the research of Lemnitzer et. al. (2014), the aftershock responses of four reinforced concrete structures in Chile, one of which exhibited severe structural damage such as column buckling and shear wall cracking, were investigated. The measurements from one of the instrumented shear walls highlighted that the shear wall underwent five times more shear displacements than flexural displacements. By constructing several FEM's with reduction factors of FEMA 356, it was observed that the model of the damaged building captured the seismic behavior and fundamental period of the

building precisely. In this model, the stiffness contribution of cracked elements was reduced by 80% and the stiffness contribution of heavily damaged elements was not taken into account,

Furthermore, SHM techniques can be utilized for seismic risk assessments and reliability estimations due to their capability of eliminating the uncertainties in structural parameters. Vulnerability curves, which demonstrate the failure probability of a structure under seismic motions, may be established analytically or experimentally.

Boutin *et al.* (2005) adopted the Timeshenko shear beam model in order to represent the dynamic behavior of the existing buildings. Two buildings were studied for the implementation of this method. Modal parameters obtained from the ambient surveys were used for generating the Timeshenko beam models of these buildings. The main advantage of this beam model was that the internal strains could be obtained so that the tensile strain of concrete could be determined as damage criterion. The association of this approach could be utilized for the seismic vulnerability studies.

Catbas *et al.* (2008) studied the reliability of the longest cantilever truss bridge in the United States. The main goal was to minimize the uncertainties in reliability estimation. For this purpose, the bridge was monitored continuously for a year. The strains induced by temperature was found to be ten times higher than the maximum traffic-induced strains. Therefore, the observed temperature effects were included in the reliability estimation and the reliability of the bridge was estimated lower with the incorporation of temperature effect.

Soyoz *et al.* (2009) demonstrated the significance of FEM Updating Procedures by investigating the damage states of the updated and non-updated FEM's of a three-bent concrete bridge model. The bridge was exposed to different damage levels on a shake table by a sequence of earthquake motions with increasing intensities. Structural parameters were identified from vibration measurements after each damaging seismic shaking. In the first step, the non-updated FEM included the structural parameters that were generated based on the Monte Carlo simulation. Then, the updated FEM

was constructed by updating structural parameters in the previous step based on the identification results. NLTH were carried out with both models and the ductility of columns were chosen as damage indicator. In the scope of this paper, it was found out that the system estimated using the updated structural parameters had lower reliability than the one estimated using the non-updated structural parameters.

Liel *et al.* (2009) suggested a new method called as Approximate Second Order Second Method in order to quantify the effect of uncertainty in FEM's. Six case study frame structures with different heights and ductility capacities were studied in this study. It was concluded that this method outperformed the response surface methods in literature such as Monte Carlo and First Order Second Moment methods because of the fact that it captured the critical effects of modeling uncertainties better and it required less computational time.

Michael *et al.* (2012) utilized modal parameters obtained from ambient vibration surveys of three existing building in a moderate seismic-prone region. These parameters were adopted in order to generate two simple models that could represent the seismic response of structures and classify interstory drifts ratios according to the limits of slight damage levels. The first model was a multi-degree freedom system incorporating the higher modes while the second one was a single-degree of freedom model considering the fundamental modes of the structures. At the final step, the vulnerability curves were established with the aim of decreasing variability of the slight damage fragility curves. However, this method could be feasible only for moderate seismic-prone regions because of the fact that the damage levels were considered only for the elastic ranges which represent the slight damage states.

1.2.2. Literature Review on Damping

Another remarkable feature of SHM is to provide ability to identify the damping value, which has a major impact on the level of seismic responses. Since damping ratio of the structures depends on numerous factors, it is not possible to know the exact viscous damping ratio of a structure unless it is determined by vibration-based

system identification techniques. The accurate representation of viscous damping is very important for tall buildings even though seismic assessment of these structures is carried out by nonlinear time history (NLTH) analyses where the energy dissipation in nonlinear range is explicitly modelled by hysteretic behavior. Modelling and selection of viscous damping in the linear range of structural members are chosen according to seismic codes and guidelines.

In literature, Leger and Dassault (1992) conducted a parametric study on the effect of the modelling of viscous damping on seismic-energy dissipation of MDOF structures. Structures with different heights, which represented a linear variation of strength and stiffness over their heights, were analyzed. The average ductility demand, the average number of yield excursions, the ratio of hysteretic energy to input energy, and the maximum rate of hysteretic energy dissipation were chosen as parameters in order to characterize the nonlinear seismic response. The study presented several damping models such as models with mass and initial stiffness ($M1_{a,b0}$), with initial stiffness ($M1_{b0}$), with mass and tangent stiffness whose coefficients were computed with the initial elastic frequencies ($M2_{a,b}$), with tangent stiffness whose coefficient was computed with the initial elastic frequencies ($M2_b$), with mass and tangent stiffness whose coefficients were computed with the tangent frequencies ($M3_{at,bt}$), and with tangent stiffness whose coefficient was computed with the tangent frequencies ($M3_{bt}$). Damping models were compared with each other for three type of structures. The results showed that the ($M2_b$) and ($M3_{bt}$) performed well for structures with fundamental periods of less than 0.5s. ($M2_{a,b}$) and ($M3_{at,bt}$) performed well for structures whose fundamental periods were between 0.5s and 1.5s. An important remark was that the seismic responses of buildings whose periods were higher than the 1.5 were not affected by the choice of damping model.

Bernal (1994) demonstrated that the massless degree of freedoms or the degree of freedoms with small inertias gave rise to spurious damping forces. The reason was determined as the loss of damping orthogonality which is required during the numeric solution of non-linear analysis. A Four story frame, a single story frame and two degree of freedom system with translational and rotational degree of freedoms were utilized

in the study. Numerical results were adopted in order to examine the quantitative significance of the spurious damping forces on the seismic response.

Priestley *et al.* (2005) analyzed the performance of different damping models with the effects of different hysteretic rules by using a SDOF oscillator. According to the study, the results were very sensitive to the choice of damping models. Also, the tangent-stiffness proportional viscous damping modeled the seismic response more realistically. In addition, the results were found to be dependent on the initial period and hysteresis rules.

Hall (2006) suggested that the mass proportional term of Rayleigh damping, which corresponds to a physical system and in which there are linear viscous dampers connecting the degrees of freedom of the structure to external supports, should have been eliminated. The numerical studies of a base-isolated structure, which performed rigid body motion, and gravity dam, which slid on its base, demonstrated that the mass proportional term could give rise to excessive unrealistic damping forces. The numerical analysis also showed that the Rayleigh damping models based on the initial stiffness term resulted in unrealistically high damping term when the structure softened because of the damage. In order to overcome this problem, a damping formulation, which excluded the mass proportional term and which included some constrains in order to limit the boundaries of stiffness proportional term, was suggested.

Petrini *et al.* (2008) compared the performance of three cases (no damping, initial stiffness damping, tangent stiffness damping) when they were utilized with different non-linear modelling choices such as plastic hinge and fiber models. For this purpose, the seismic response of a simple bridge pier was obtained in terms of displacements by conducting a shake table test. The obtained displacement time history result was compared with the simulated ones. Six comparisons as a combination of three damping cases and two nonlinear modelling choices were made. The comparisons demonstrated that the tangent stiffness viscous damping performed better when the plastic hinge model was used in the simulations. They also showed that, when the fiber-element model was utilized, the best simulation of seismic response was captured accurately

when no additional viscous damping was introduced to the simulation.

In the studies of Charney (2008), Erduran (2012) and Jehel at. al. (2014), similar conclusions with the studies above were made. Charney (2008) performed the analysis with a five storey frame while Erduran (2011) performed analysis with three and nine storey buildings. Erduran (2011) also pointed out that the damping model used in the inelastic analysis didn't considerably effected the interstory drift ratios of low-rise building because of the fact that all the damping models provided approximately the same damping ratio for the fundamental mode (considering that the seismic response of low-rise buildings are governed by the fundamental mode). Jehel *et al.* (2014) developed analytical formulas for the initial and tangent stiffness based Rayleigh Damping methods in order to provide information about shift of damping ratios due to stiffness degradations during time history analyses. It was concluded that the tangent stiffness Rayleigh damping method provided a much better control on damping forces during analysis.

Zaerian and Medina (2010), in order to avoid problems occurred because of Rayleigh Damping models, offered to model the structural elements with a combination of elastic elements and yielding springs without the stiffness-proportional damping. So, the structural elements which underwent non-linear behavior were represented by zero stiffness initial damping whereas the structural elements which didn't exhibit any nonlinear behavior were modelled with the stiffness proportional damping term in order to create damping energy dissipation even though they remained in the elastic ranges. Application of this method to a SDOF frame demonstrated the efficiency of the proposed method.

However, although appropriate modelling of viscous damping have examined widely in many researches, not much emphasis has been put on the selection of the viscous damping ratio. The major problem about viscous damping is that it is not possible to know the precise value of viscous damping ratio. Therefore, in several studies the damping measurements from buildings with different heights were presented and best fit lines were generated according to these measurements.

Goel and Chopra (1997) compiled and analyzed strong motion data recorded from 85 buildings that were exposed to eight different earthquakes in California, from the 1971 San Fernando earthquake to the 1994 Northridge earthquake. The buildings in the study ranged from 2 to 60 stories and included 27 reinforced concrete moment frames, 43 steel moment frames and 16 reinforced concrete shear wall buildings. The damping ratios of the buildings were identified and plotted on the graphs in terms of number of stories and roof drift demands. Whereas there was no clear trend between the identified damping ratios and drift demands, there was a clear trend between the height of the buildings and identified damping ratios. It is important to remark that, because of the fact that the buildings might have underwent nonlinear behaviors under seismic events, the identified damping ratios in this study might have been less if they would have been obtained during ambient conditions.

Stake *et al.* (2003) collected and compiled the vibration data obtained from 137 steel-framed buildings, 25 reinforced concrete buildings and 43 steel-framed reinforced concrete buildings in Japan. These buildings were subjected to low-amplitude vibrations tests such as the tests conducted by mechanical shaker, vibration control devices, man power, and pull and release methods. Some of them were subjected to low amplitude earthquake and wind excitations. It was found out that the damping ratios of buildings decreases as the height of the buildings increases. In addition, the effect of building characteristics such as height, building use and foundation type on the damping ratios were examined as well.

Smith and Willford (2007) introduced the damped outrigger concept for tall buildings, which could provide higher damping in order to reduce the dynamic responses of buildings to wind effects. Besides this concept, in order to emphasize the fact that tall buildings present lower damping ratios, the damping ratios in terms of building heights were compiled from several studies including Stake *et al.* (2003), Li *et al.* (2000), Li *et al.* (2003), Li *et al.* (2006), Jery *et al.* (1997), Jery *et al.* (1986) and Brownjohn *et al.* (1998). The results were demonstrated in a graph with the trend line in order to highlight the fact that increases in height of buildings leads to decreases in their damping ratios.

Smith *et al.* (2010) carried out a similar study. Identified damping ratios were plotted in terms of building heights and several important remarks were made. The scatter in the data was attributed to variability in the type and age of buildings, foundation type, amplitude of measurements and non-structural elements. Another remark was that there was a significant downward trend in average values of damping ratios as the height of buildings increases. In the study, the sources of damping, the methods of mitigating the uncertainty in damping and the supplementary damping systems were also discussed.

In the last three studies, the damping ratios of structures were extracted from the acceleration records collected during the low-amplitude measurements. Therefore, these damping values represents the damping of structures for the conditions in which the structures exhibited low-amplitude vibrations.

Nevertheless, it is not possible to infer a viscous damping ratio for a particular building from the findings of these studies due to the differences in building characteristics and the amplitude of the vibration records in these studies. In addition, several guidelines such as Los Angles Tall Building Structural Design Council (LATBSDC, 2005) and PEER ATC72-1 (2013) give suggestions about selection of viscous damping ratio in NLTH analyses. However, LATBSDC provide only an upper limit for the viscous damping ratio of tall buildings while PEER ATC72-1 summarizes the studies about viscous damping ratio.

1.2.3. Literature Review on Higher Modes

In this study, in addition to the demonstration of significance of selecting an appropriate viscous damping ratio for seismic performance assessments of tall buildings, the sensitivity of higher modes to the changes in structural parameters during model updating procedure were highlighted. Besides, four earthquake records collected from the monitored tall building show that the higher modes of the structure may be likely to be excited more than its fundamental mode under the expected ground motions.

In literature, a large number of researches also demonstrated that seismic demands imposed by higher modes are crucial. In the pioneering work of Blakeley *et al.* (1975), the effects of the higher modes on the maximum shears in cantilever walls were revealed when they were loaded to their flexural capacity with earthquake forces. It was demonstrated that the code lateral load distribution underestimated the shear loadings at flexural capacity along the height of the walls. The results of NLTH analysis of the cantilever shear wall structures with different heights illustrated that the plastic hinge regions had possibility to be extended above the base of a wall, up to half of a tall structure. As a conclusion, amplification factors were suggested in order to account for additional higher mode demands when the code specific lateral force methods were used for the seismic analysis of tall structures.

Iqbal and Drecho (1980) performed an analytical investigation by comparing the distribution of seismic forces along the height of several isolated reinforced concrete structural walls. The distributions were obtained with the specification in Uniform Building Code (UBC) and Applied Technology Council (ATC) and also with nonlinear time history analysis. Because of the fact that the code base methods underestimated the responses, modifications to the code force distributions were suggested. The numerical study of Keintzel (1990) on shear walls also concluded similar results and offered some formulations in order to include the effect of higher modes in seismic response.

Sangarayakul and Warnitchai (2004) developed two different methods, the direct method and the orthogonal filter method, in order to understand the contribution of higher modes to the total seismic responses of buildings. Both methods were based on the equivalent linear concept where a non-linear behavior was represented by a set of equivalent linear models. The theoretical relations for these methods were developed under the framework of complex modal analysis. Medium to high-rise buildings whose lateral-resisting systems were provided by slender RC walls and the gravity-load-carrying system were studied for the verification of higher mode effects and the proposed methods. The time history results of moment and shear forces at base and three different elevations which were obtained through the direct integration analysis

were compared with the ones obtained through the sum of contribution of each mode. The contribution of each mode was obtained by the proposed methods. The results demonstrated the proposed methods were validated with a good match. It was also observed that, the higher intensities of seismic motions resulted in higher range of inelastic responses. Another significant observation was that the fundamental mode started to exhibit inelastic response at an earlier stage than the second mode. This phenomenon gave rise to a significant increase in the contribution of second mode to the overall seismic response of the wall building because of the fact that the seismic force contribution of second mode was not restricted due to nonlinearity as much as the seismic contribution of the first mode.

In the study of Klemencic *et al.* (2007), higher mode effects were also observed when a 40 storey case study building assumed to be in downtown Los Angeles, California was investigated. The shear forces at the shear wall under the design basis earthquake (DBE) and the moments at the shear wall under the maximum considered earthquake (MCE) were obtained by linear and NLTH analysis. The results pointed out the significant contributions of higher modes due to the fact that the linear analysis underestimated the seismic demands along the height of the building even though the results of the linear analysis were amplified with some coefficients.

Panagiotou and Restrepo (2009) developed a dual-plastic hinge (DPH) concept in order to reduce the effects of higher modes in seismic response of high-rise buildings by allowing the generation of plastic hinge regions only at the mid-height and base of buildings. Lumped-mass Euler-Bernoulli cantilever beams were used to model case-study 10, 20 and 40 storey buildings. The buildings were design with ACI-318, Eurocode 8 and DPH concept. The failure of ACI-318 and Eurocode 8 in estimating the seismic demands of tall buildings were pointed out. The proposed DPH design approach was successful in controlling the formation of plastic hinges only at mid-height and base.

Munir and Warnitchai (2012) used a 40 storey building with gravity load-carrying system and a central reinforced concrete core wall in order to show the contribution

of higher modes and to refute the application of RSA (Response Spectrum Analysis) for tall buildings. For this purpose, UMRHA (Uncoupled Modal Response History Analysis) method, which was developed in the study of Chopra and Goel (2002), was adopted. The nonlinear analysis demonstrated that the conventional seismic design approach (RSA) significantly underestimated the base shear and the bending moment at the mid-height of the tall building. In order to gain insight into the reasons of this outcome, the modal contributions of modes were decomposed by UMRHA procedure and their hysteretic behaviors were generated by a cyclic MPA (modal pushover analysis). The modal decomposition results were considered reliable because of the fact the sum of all significant modes captured the true seismic demands over the entire height of the building. The results of MPA displayed that the fundamental mode presented the highest inelastic response and the level of inelastic response of second mode was less than the one of the fundamental mode. The results also showed that the third and fourth modes didn't represent any inelastic behavior at all. Therefore, it was concluded that the use of large R factor for all modes in RSA procedure could result in the underestimation of the seismic demands of higher modes.

C. A. Maniatakis *et al.* (2013) summarized and compared the several methods such as UMRHA, MPA, modified MPA (MMPA), N2 and extended N2 methods. MPA, MMPA, N2 and extended N2 methods were briefly explained as following: MPA and MMPA (Chopra *et al.*, 2004) methods are the simplification of the UMRHA method. N2 Method proposed by Fajfar and Fischinger (1988) are similar to MPA but only the first mode is taken into consideration. Kreslin and Fajfar (2012) improved this method (extended N2) by taking the higher modes into account. The authors also proposed a new method which was the modification of the Response Spectrum Analysis (RSA) which uses the same reduction factor (R) for each mode. The proposed method was called as mMRSA and applied different reduction factors for each mode. A nine storey moment resisting frame was investigated for the comparison of all of these methods and for the demonstration of the effect of higher modes. After the investigation, higher mode effects were found to be important even for the first mode dominated reinforced concrete frames, especially in terms of inertial forces and storey accelerations at all

floors and in terms of shear forces at higher storeys. Displacements and inter-storey drift ratios were found to be influenced less. The model reduction factors for each mode were found to be decreasing with the increasing mode order. Therefore, it was concluded that the RSA procedure underestimated the seismic demands. MMPA and the extended N2 methods were found to provide good results on the average, except for the inertial forces obtained by the extended N2 method. The proposed method performed well for both deformation and force quantities.

Moreover, a Full-Scale 7-storey Building Slice Test at UC-San Diago (M. Panagiotou, 2010) also revealed higher mode contributions. The building was tested in two stages. This study investigated the results of the first phase, in which the building had a load-bearing wall acting as the main lateral force-resisting element and in which the building was subjected to four historical California input ground motions. Base shear overstrength and base moment overstrength factors, which are the ratio of the measured and design based shear forces and base moments respectively, were found to be different than each other. The reason of this difference was found to be the lowering of the location of the lateral force resultant center which was occurred due to the higher modes, especially due to the second mode. In addition, the total acceleration profile along the height of the building at a time instant demonstrated that the response was governed by the second mode.

In sum, the studies above regarding the effect of higher mode forces concluded similar results. In addition to these experimental, numerical and analytical studies, the investigation of seismic responses of tall buildings by SHM techniques during seismic events confirmed the high possibility of excitation of higher modes, depending on the frequency content of the earthquake motions.

Şafak and Çelebi (1992), and Şafak and Çelebi (1991) observed the contribution of higher modes when the recorded seismic motions of the tall buildings were analyzed. It was found out that, during the earthquakes, the higher modes were triggered essentially but died out quickly, and that the free vibration response of the buildings after the earthquake oscillations was generated by first mode.

Brownjohn and Pan (2001) instrumented two tall buildings in Singapore with the purpose of identifying the characteristics and the effects of wind loads on the buildings. However, during the monitoring, it was observed that the largest accelerations in the buildings occurred because of the far fault earthquakes having magnitudes between 6 and 8. The examination of the recorded raw data and the building responses during the earthquakes revealed the significant excitation of the second mode. Furthermore, the contribution of each mode to the base shear was thanks to the availability of response records, mode shapes and building mass distribution of the buildings. As a result of the calculations, the largest contribution to the seismic forces was found to be made by the second mode.

In the study of Pu *et al.* (2012) the seismic responses of three tall buildings whose heights ranges from 85 to 130 meters were recorded under the East Japan Earthquake of magnitude 9 on March 11, 2011. The acceleration response in frequency domain of the 130 meter height building showed that the second and third modes of the building were excited more than the fundamental mode. The displacement time history responses were obtained as well. The displacement time history responses of the three buildings demonstrated that the response was dominated by the first mode whereas the acceleration time history responses of these buildings were governed by the second and third mode during the strong shaking and by the first mode right after the strong shaking stopped.

In the study of Kasai *et al.* (2012), the responses of tall buildings, which have passive control dampers, to the same earthquake were investigated in order to investigate the performance of buildings with passive dampers. Comments about the excitation of higher modes were made as well when the acceleration response of a 41-storey office building in frequency domain demonstrated that the second and third mode of the structure were excited more than the fundamental one. In addition, it was shown that the acceleration time histories were dominated by these higher modes.

However, in many similar studies, the influence of FEM updating on higher mode effects are usually omitted. Also, simplified FEM's are adopted and considerable

excitation (vibration amplitude) of higher modes during seismic events is not validated for the structures of interests. This study reveals the sensitivity of higher modes to the detailed modelling and importance of selecting an appropriate viscous damping ratio for tall buildings. Moreover, the sensitivity of higher modes to an expected earthquake at building side was validated by the evaluation of structural response to the recorded seismic events.

1.3. Objective

The prevalence of SHM applications has been increasing because of the fact that engineers and researchers have been aware of the essential benefits of SHM techniques. Therefore, many research and case study projects involving SHM techniques have been performed so far. In these studies, many different system identification methodologies such as Stochastic Subspace Identification (SSI), Linear Time Invariant Systems (ARMA) and EFFD, have been introduced and several FEM updating procedures have been carried out in order to show the importance of such procedures. In addition, valuable information about seismic responses of structures is presented. Moreover, SHM techniques have been utilized for seismic risk assessments due to its capability of eliminating the uncertainties in structural parameters. Modal based models from vibration surveys allowed for the generation of experimental vulnerability curves which demonstrate the failure of a structure under seismic motions.

In this study, in order to demonstrate the importance of FEM updating based on modal identification and proper selection of viscous damping ratio on the seismic performance of tall buildings, a twenty-six story, core-wall tall building in Istanbul was instrumented with thirteen accelerometers. A fine FEM of the building was generated based on design drawings and then updated based on the identified modal shapes and frequencies. In many studies, coarse FEM's are established and the material properties are changed to account for the uncertainties in overall stiffness of buildings in updating procedures. In this study, updating of a fine FEM allowed to minimize the uncertainties in other structural parameters such as effects of soil springs and seismic gaps with frictional plates which are usually omitted. Upon the updating procedure,

NLTH analyses were performed with the updated and the non-updated FEM with 5% damping ratio to observe the influence of the identified modal frequencies and shapes. Afterwards, NLTH analyses were carried out with updated FEM considering the identified (2%) and 5% damping ratios to observe the influence of the identified viscous damping. In order to observe the performance of the building in a possible earthquake caused by the North Anatolian Fault, probability density functions in terms of interstory drift ratios were established. And by setting a threshold value failure probabilities for the updated and non-updated models were obtained. This kind of probabilistic assessment of seismic performance of tall building with the integration of vibration-based identified modal values comprises a unique approach of this study. The investigation of the results of this study reveals the importance of the detailed modelling and selecting an appropriate viscous damping ratio for tall buildings. In addition, the investigation of the results of this study reveals the sensitivity of higher modes to the detailed modelling and to the changes in structural parameters during Updating Procedure. Moreover, the sensitivity of higher modes to an expected earthquake at building side is validated by the evaluation of structural response to the recorded seismic events.

1.4. Scope

This study is structured according to the order of the steps in the project. In chapter 1, an introduction about the importance of tall buildings and SHM, literature review on SHM applications and techniques, damping and higher mode contributions, the objectives of the study and the scope of the project are presented.

In chapter 2, the location and the characteristics of the instrumented building as well as the instrumentation configuration are demonstrated.

In chapter 3, the identification methodology, that is utilized to obtain the modal frequencies, shapes and damping ratio, is explained. An in-house developed Matlab code, which processes the recoded vibration data automatically, and the “Real-time Monitoring Module” embedded in the web page of the research group are introduced.

In chapter 4, the development of the FEM of the structure is described. The updating procedure and the selection of the structural parameters for this procedure are explained. The updated and the non-updated modal parameters are compared and the reasons of differences between these modal parameters are explained.

In chapter 5, the characteristics of the expected earthquake in Istanbul and the ground motion selection procedure for non-linear time history analysis are explained.

In chapter 6, the development of the non-linear FEM is briefly introduced and some section properties of the structure are demonstrated.

In chapter 7, first, the effect of identified modal frequencies and shapes by using the updated and the non-updated FEM with 5% viscous damping ratio is investigated. Then, the effect of identified modal damping ratio on the seismic performance assessment is investigated by using the updated FEM with the identified (2%) damping ratio and the 5% damping ratio. The probabilistic approach in order to compare the results is introduced. In addition, sensitivity of higher modes to the changes in model parameters during Updating Procedure and to the detailed modelling was emphasized. Moreover, significant excitation of higher modes under seismic motions was discussed.

Finally, the conclusion of the study and the recommendation for the future work are presented in chapter 8.

2. INSTRUMENTED BUILDING

2.1. Building Information

The building in this study, shown in Figure 2.1, is one of the four tall buildings of a complex in the financial district of Istanbul.



Figure 2.1. The building monitored in the study.

The building is surrounded by a large shopping mall and parking areas at the first and basement floors. Therefore, it is divided into three sections such as basement, shopping mall and residential sections. Residential section consists of storeys of the tall building above the shopping mall section. The structural system of the tall building is cast-in-situ reinforced concerete structure, consisting of two cores of structural walls in the center, and columns on the outer region. The structural plan and the height of the floors are the same for the residential floors whereas they exhibit differences in the shopping mall and basement floors. The location of the complex in Istanbul can be seen as shown in Figure 2.2.



Figure 2.2. The location of the complex in Istanbul.

2.2. Building Instrumentation

The building was instrumented with thirteen accelerometers in order to measure the vibrational responses of the building. For each instrumented story, accelerometers were placed in x and y directions at a position close to the centre. At the top storey, there is an additional accelerometer located away from the center in order to observe the torsional modes. The accelerometers are connected to the data recorder placed at the twelfth floor. The recorder that is utilized in this project is a 16-channel dynamic data acquisition system with a netbook connection and software. The netbook has been connected to internet in order to transfer the recorded vibration data to the office computer. The sensors consist of micro electro mechanical system (MEMS) that can perform between excitations ranging from -3g to +3g. The models of the recorder and the sensors are TDG Textbox 2010 and TDG Sensebox, respectively. Figure 2.3 demonstrates the data recorder and the sensors in the 17th floor while Figure 2.4 displays the building plan and the sensor confriguation.



Figure 2.3. The data recorder and the sensors at 17th floor.

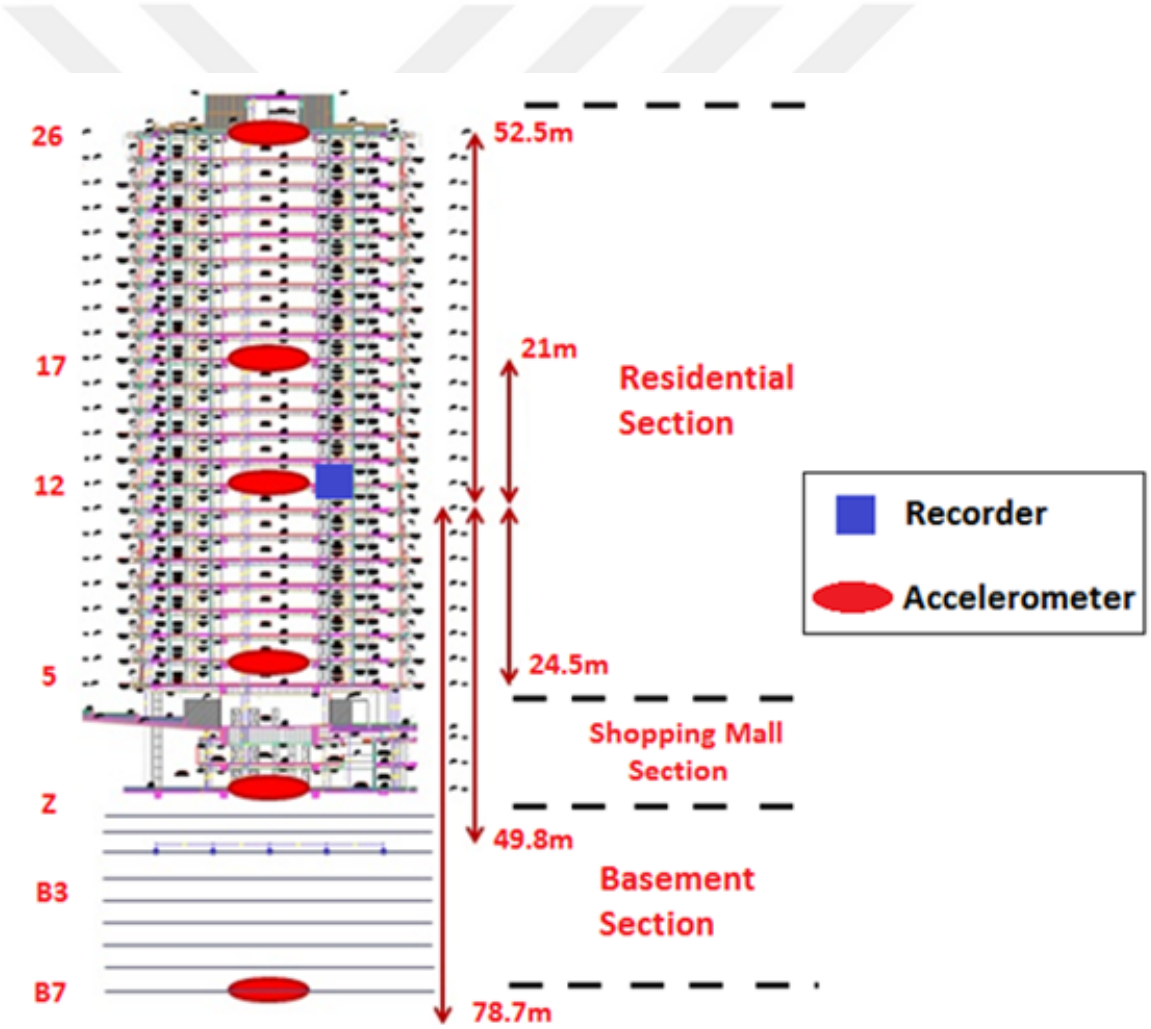

Figure 2.4. The plan of the building and the instrumentation configuration.

Figure 2.5 demonstrates the typical floor plan of the tower and the location of sensors in the centre of an instrumented floor. The outer columns are connected to the cores with beams. This floor plan of the tower section remains the same also at many floors of the shopping mall and basement sections. The plan only shows differences at the stories where the shopping mall section is connected to the tower section.

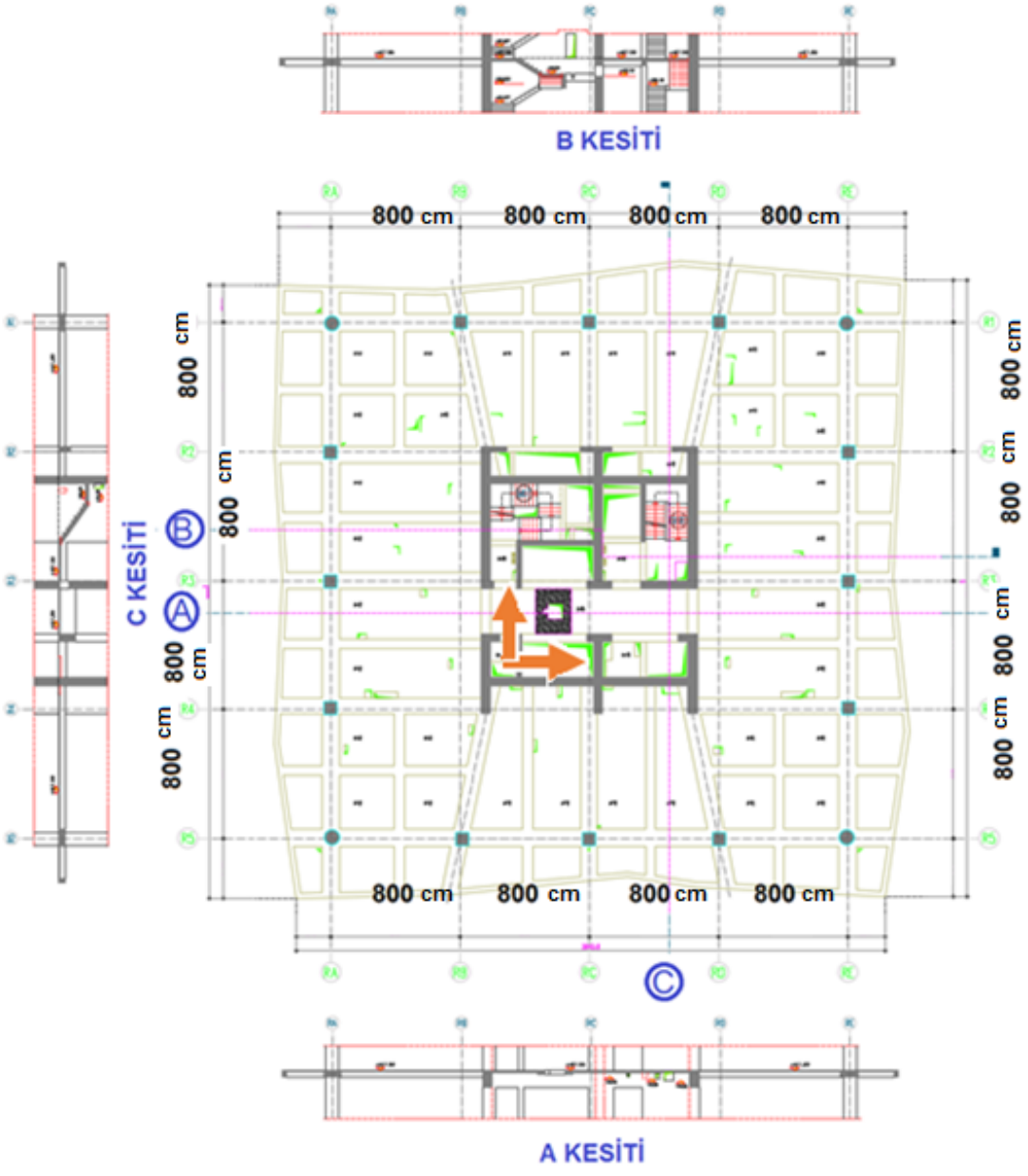

Figure 2.5. Typical floor plan of the tower and the sensors.

The vibration data in time domain in x direction recorded from all the instrumented floors are shown in Figure 2.6. It is clear that the amplitude of the excitations increase from the basement level to the top level.

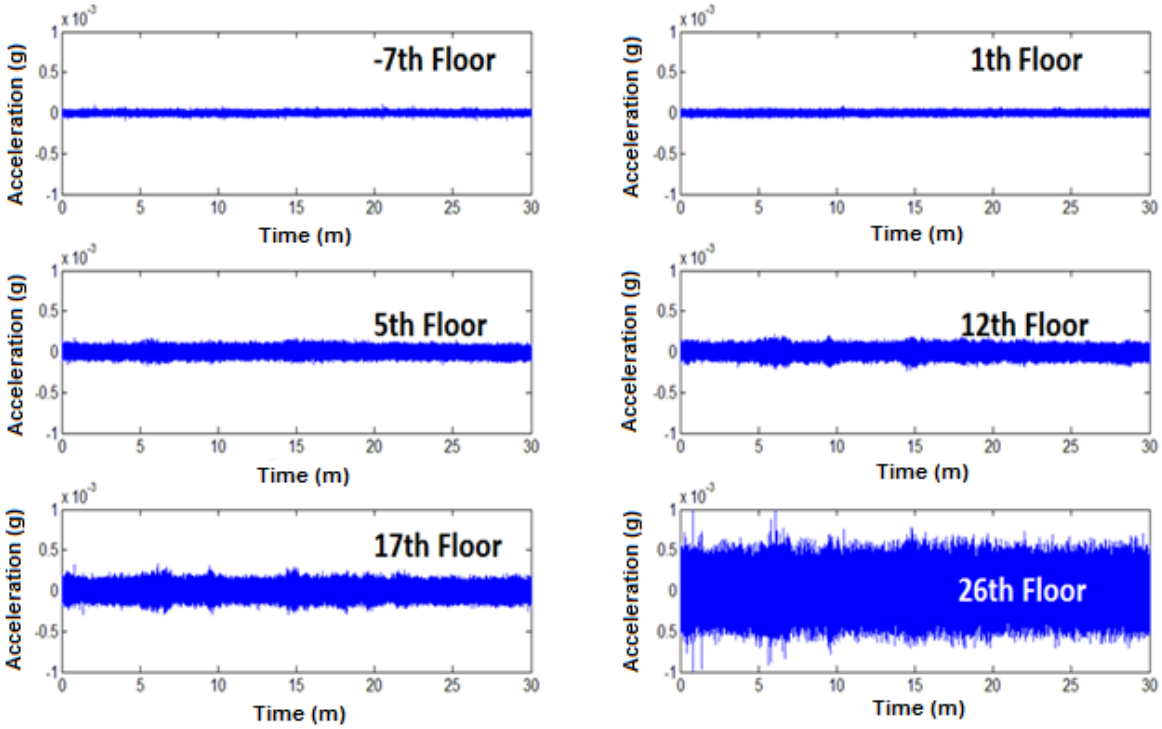

Figure 2.6. The vibration data in time domain in x direction recorded from all the instrumented floors.

3. SYSTEM IDENTIFICATION

3.1. Frequency Domain Decomposition Method

In this study, system identification was performed by the Enhanced Frequency Domain Decomposition (EFDD) method by Brincker *et al.* (2000). This method is an output-only method and capable of identifying close modes and damping ratios. In this method, square matrices whose indices are the cross-power spectral density of the vibration data from two sensors are obtained for each frequency. The singular value decomposition of those matrices at a prescribed frequency gives spectral values and mode shapes at that frequency. Decomposition of spectral density matrix is formulated in Equation 3.1.

$$G_{yy}(w)_{nxn} = H^{*}(w)_{nxm} G_{xx}(w)_{mxm} H^{T}(w)_{mxn} \tag{3.1}$$

where $G_{xx}(w)_{mxm}$ is the (m x m) power spectral density (PSD) matrix of the input, m is the number of inputs, $G_{yy}(w)_{nxn}$ is the (n x n) PSD matrix of the responses, n is the number of responses. $H(w)_{mxn}$ is the (m x n) frequency response function matrix and the over bar and superscript T denote the complex conjugate and transpose, respectively.

This method is applicable for cases where the PSD of the input is constant, i.e $G_{yy}(w)_{nxn} = C$. Such cases arise from broadband random input excitations such as white noise (ambient excitations). In this way, EFDD is developed for output only modal identification where only measurements of the response is available

The spectral values at a frequency give the response of the system in frequency domain. Therefore, even close modes can be detected by a fine discretization of frequency domain.

In Matlab, cross power spectral density of data from two different sensor are obtained using "csd" command whose resolution is 4096 data points and whose sampling frequency is 200 Hz (the sampling frequency of the recorder). A hanning window filter and averaging are applied for preventing aliasing and eliminating the noise.

3.2. System Identification of the Structure

Figure 3.1 displays the vibration data in time domain in x direction recorded from the 17th and 26th floors when there was some extra excitations to these floors due to construction work.

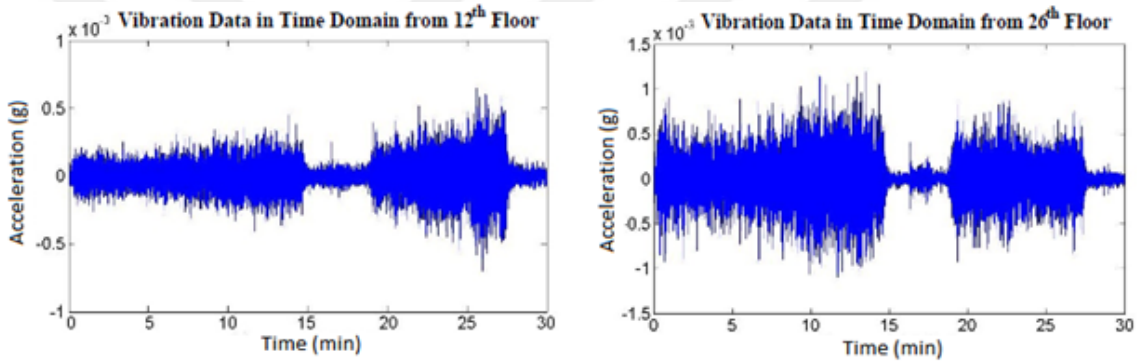

Figure 3.1. The vibration data in time domain in x direction recorded from the 17th and 26th floors.

Figure 3.2 shows the cross-power spectral density matrix where the peaks are the natural frequencies of the structure. The data in time domain was converted to frequency domain by using the EFDD method in order to find the modal parameters of the structure. From the figure, it is observed that the frequencies of the first, second, third, and fourth translational modes are 0.59, 2.15, 3.81, and 7.23 Hz, respectively in the x-direction as the result of modal identification. In order to check if there is changes in the identified modal parameters, data is collected and analyzed three times in day for last 2 years. However, no change in modal parameters has been observed during this time period.

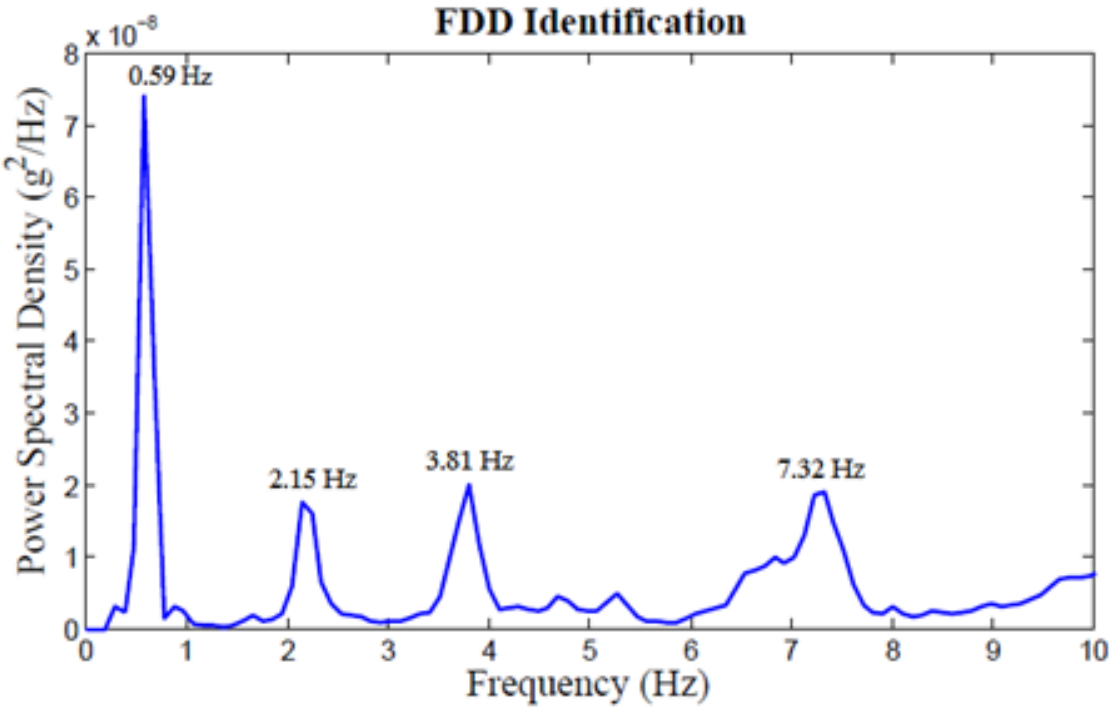

Figure 3.2. Cross-power spectral density matrix.

After obtaining the cross-power spectral density, the damping identification of the structure was performed. For this purpose, the impulse response function was generated by transforming the response of the first mode in frequency domain to time domain. The level of exponential decay in the impulse response function gives the damping ratio. Therefore, an exponential line was fitted to the peaks of each cycle in the impulse response and the damping ratio of the building was identified as 2% as shown in Figure 3.3. As the identified modal frequencies has been observed for a 2 year time period, the damping ratio has been observed as well. It is well-known that when the magnitude of the wind excitation increases, the level of damping increases. However, no clear correlation between the change in damping and magnitude of wind has been observed. Because of the fact that the damping identification has been always carried out under ambient vibrations and low-amplitude earthquakes, where the structural parameters remains in their linear ranges, the identified damping ratio is the viscous damping ratio of the structure.

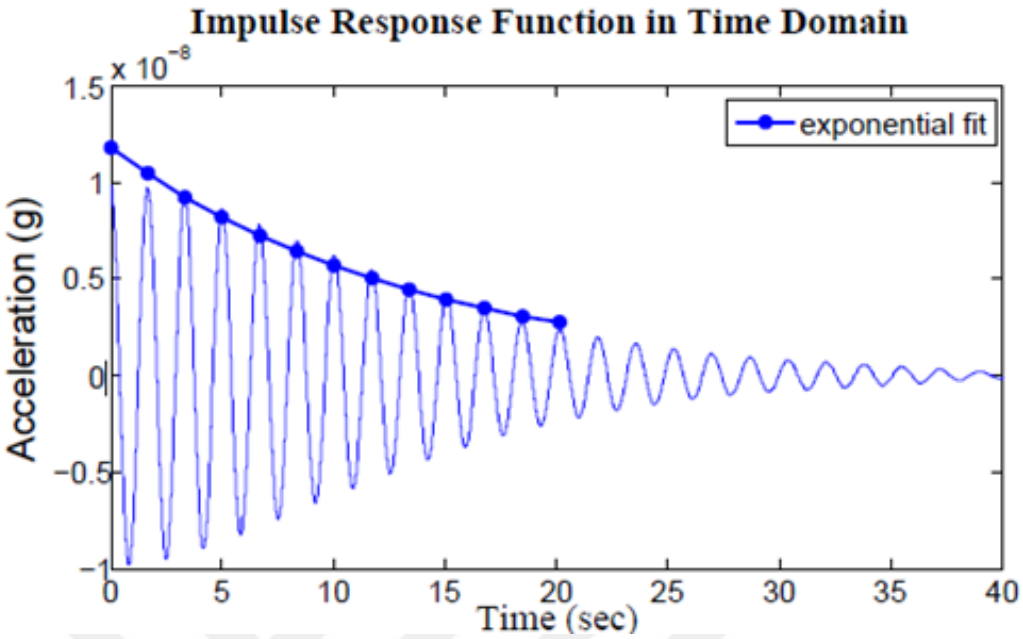

Figure 3.3. The impulse response function.

3.3. Automatic Analysis of the Recorded Data

The vibration data from the building has been carrying out for 2 years. Therefore, there has been a huge amount of data to be analyzed. Analyzing such amount of data is cumbersome and time consuming. Consequently, a Matlab code which can analyze the recorded data everyday automatically was developed.

The schema of automatic analysis of the vibration data is demonstrated in the Figure 3.4. The netbook is connected to the recorder and obtains the vibration data. This data is taken to the office computer by a synchronization software through the internet connection. The office computer stores the transferred data. By using the task scheduler of Windows operating system, the Matlab code is run by three times in a day automatically.

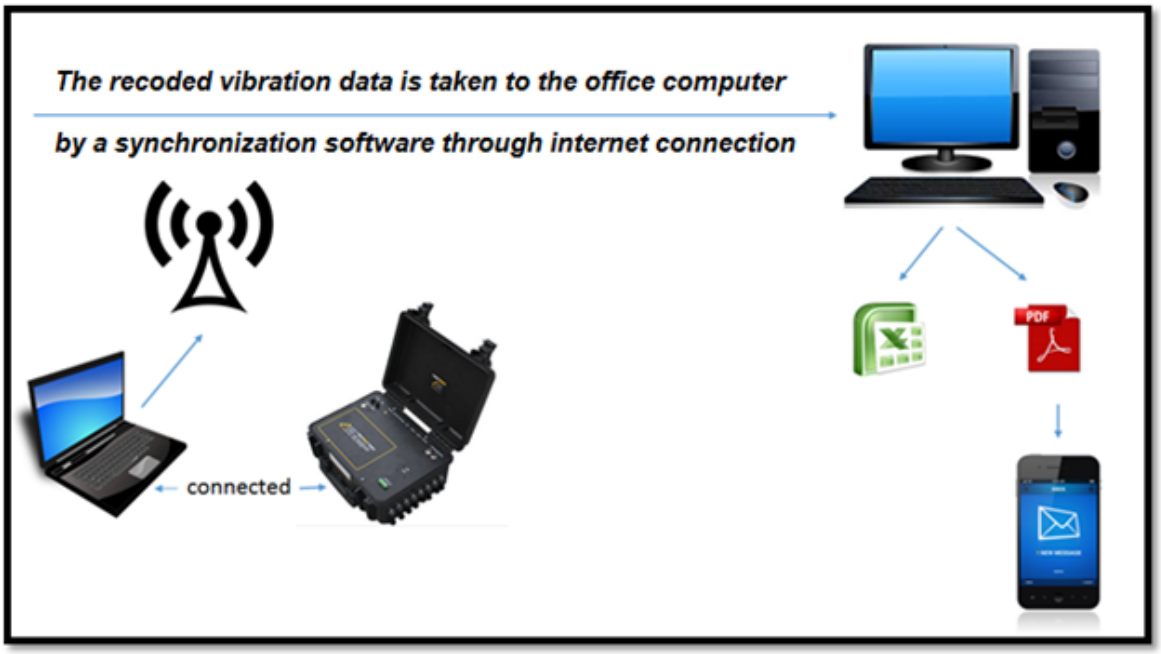

Figure 3.4. Schema of automatic analysis of the vibration data.

This code performs the EFDD algorithms in order to find the power spectral density graph, impulse response function graph and mode shapes of the building. The peaks in the spectral density graph are detected and the level of exponential decay in the impulse response function in time domain is calculated.

Besides obtaining the graphical and numerical results of the EFDD method, this code is capable of obtaining the weather information of the district, where the tall building is located, by connecting to the Yahoo Weather webpage. Process of obtaining the weather information from the webpage is as following:

(i) The code reaches and transfers the data from the RSS field (Really Simple Syndication) of Yahoo Weather. RSS field of a webpage contains the data in XML language, which is displayed on the webpage.

(ii) The data obtained from the step 1 is a very long string which includes all the information. The code parses this long string and put them in a structure type array.

(iii) The code finds the weather information of Zincirlikuyu District, the district where the tall building is located, in structure type arrays. Consequently, the weather information such as weather degree, wind speed, wind direction and humidity are obtained.

The Matlab code stores the data in two formats. The first format is the xlsx format (Microsoft Excel format). The numeric data is stored in this format so that it can be processed by Matlab in order to see if there are changes in the modal frequencies or damping ratio of the building over a time period. The second format is PDF format. In this format, the graphical results such as cross power spectral density, impulse response function and mode shapes are stored. The numerical values of peaks in the cross power spectral density, the identified damping ratio and the weather information are also placed into the graphs. The names of these files contain the date and the time of the data that is analyzed.

However, two reasons might inhibit the continuous functionality of the code. The first reason is that there may a problem at the data transfer from the building to the office computer so that the code can't find any data to analyze. The second problem may be that the office computer is shut down due to a problem so that the code can't be run. It is important to know that the code is working permanently so that the continuous analyze of the data is not disturbed. Therefore, two approaches were developed as a precaution to these possible problems as following;

(i) A small algorithm was placed in the beginning of the code. This algorithm sends an e-mail to the user in order to notify that the code can't find any data to process. So, when the user receives this e-mail, he or she may urge to fix the data transfer problem.
(ii) Even though there exists data for the code to analyze, an e-mail containing the pdf file is sent to the user automatically so that the user knows that the system is perfectly working. In addition the user is also capable of seeing the identification results instantaneously.

3.4. Real-time Monitoring Module

As a part of this project, it is considered crucial to display the recorded data in time domain from the tall building on the web-page of the research group so that the streaming of the data can be observed by any computer with an internet connection. Figure 3.5 demonstrates the steps of the real-time monitoring module. As it is seen in the figure, the data is published to the web. Then, the webpage takes the data and displays it in the "real-time monitoring" module.



Figure 3.5. The steps of "real-time monitoring" module.

The publication of the recorded data from the netbook in the tall building is accomplished by converting this netbook to a server. For this purpose, a software was installed on the netbook. However, this software requires a code in PHP language to publish the recorded data to the internet. For this purpose, a PHP code was generated. This code performs the following steps;

(i) Finds the directory of the recoded data and obtain the columns of the data. Each column contains the data collected from one of the accelerometers.

(ii) The mean of each column is subtracted from the indices of that column so that the mean of the data is zero.

(iii) Final data of each column is published to the web through using the IP address of the netbook. The web address of data in each column is in the form of "IP address of the computer/column?=X", where X is the number of the column.

In order to display the data in real-time continuously, a code in JavaScript language was embedded in the source code of the research group webpage. The source code of the webpage was developed in HTML language on Microsoft Visual Studio Software. The java script code performs the following steps;

(i) Takes the data of each column by using the IP address and the column number of the data.

(ii) Displays the data in 10 seconds intervals.

(iii) Pushes the data four times per second so that a continuous stream of the data is provided.

The real-time monitoring module also displays the wind speed and the degree of the weather by a weather gadget embedded in the source code of the module. Figure 3.6 displays the real time monitoring module.

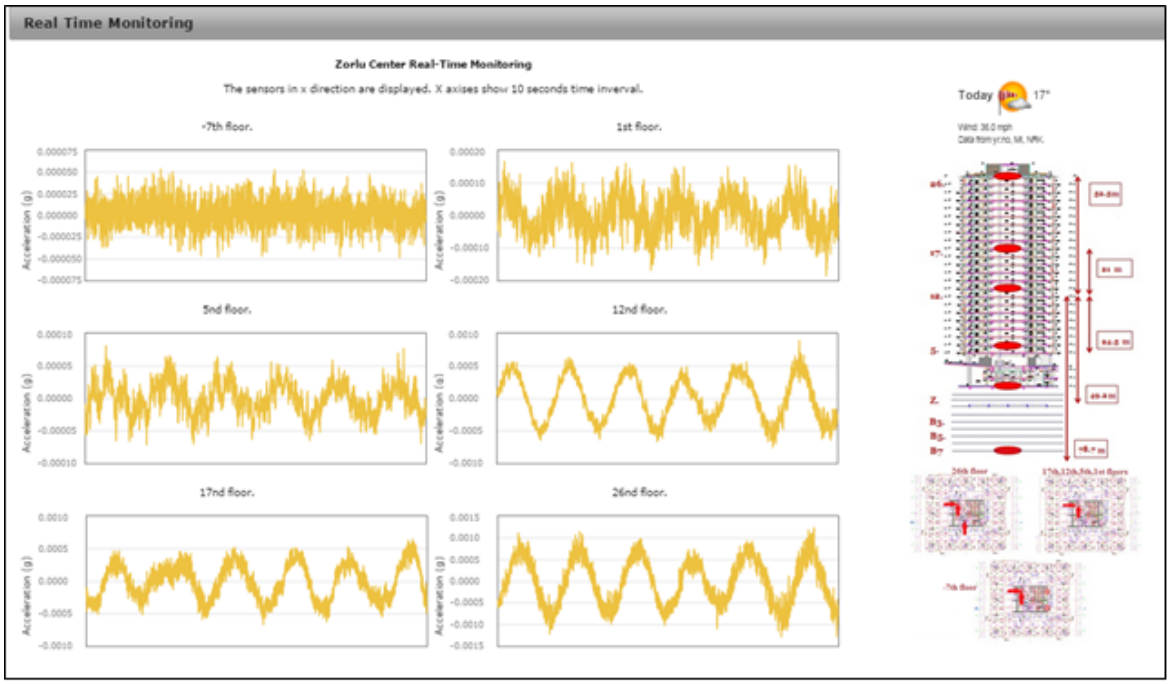

Figure 3.6. Real-time Monitoring Module.

3.5. Identification under Different Wind Loads

As explained in section 3.3, the wind speeds are recorded by the Matlab code which process the recorded vibration data automatically. It was observed that the fundamental mode of the building was excited much more than the higher modes of the building during strong winds. The reason is attributed to the fact that the wind profile generates an excitation force in the shape of the fundamental mode so that the fundamental mode is excited much more. Figure 3.7 demonstrates the building acceleration response on 2 different days. On the first day, the wind speed was moderate and the excitation of the first four mode of the building were clearly observed. On the other day, the wind speed was high and it is seen that the fundamental mode were excited so much that the excitation of higher modes are extremely low compared to the excitation of the fundamental mode.

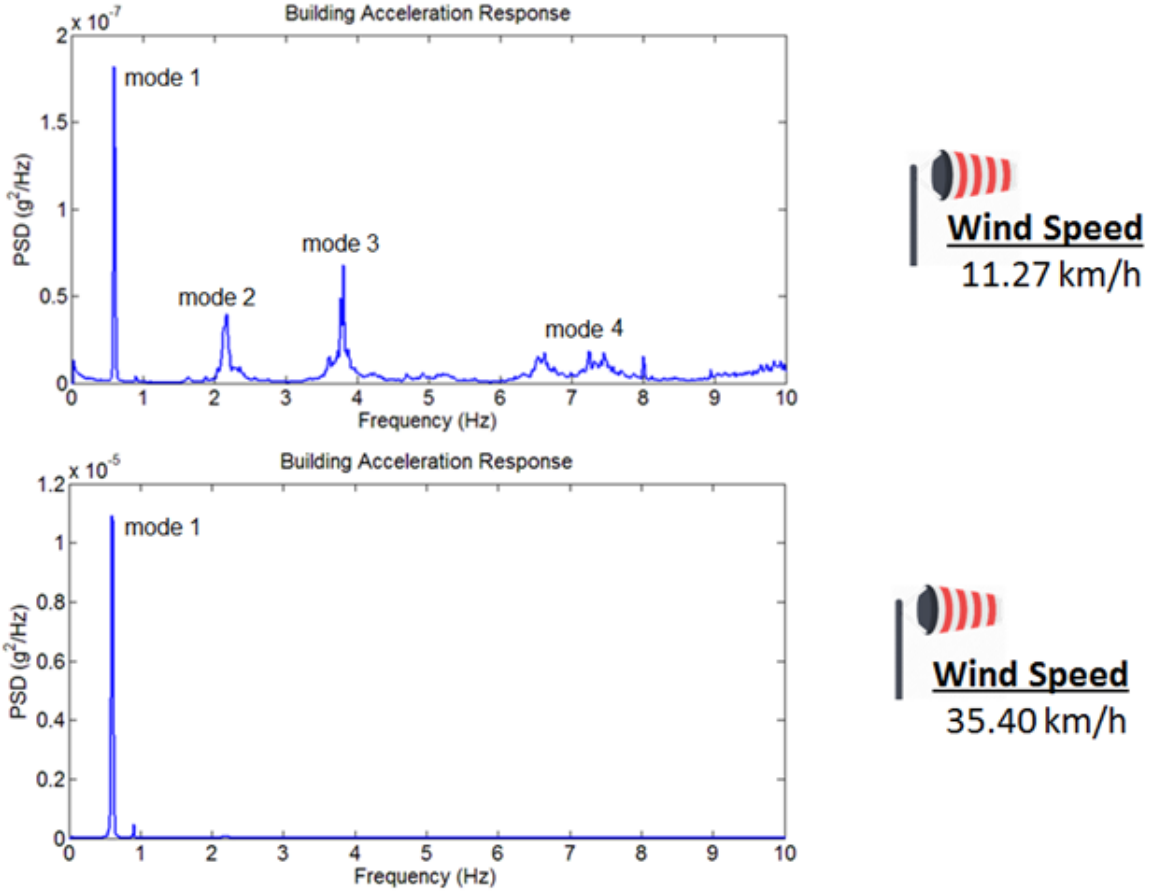

Figure 3.7. Building acceleration responses at different wind speeds.

4. FEM OF THE STRUCTURE AND THE UPDATING PROCEDURE

4.1. Finite Element Model and Primary Updating Procedure

FEM of the building was created in the SAP 2000 v16 software platform based on the design drawings and site investigations. The shear walls, columns and beams were modelled as frame elements which have six degree of freedoms. The slabs at each flor were explicitly modelled. Diaphragm constraint at each floor level was avoided in order not to affect the shear wall-shear frame interaction.

As explained before, the building consists of three different levels. Within these levels, the building has three sections. These sections are the basement level which is located under the ground level, shopping mall leveli which at ground leven, and residential sections which starts right over the shopping mall section. Residental sections consist of the tower part starting over the shopping mall part. The basement floors of the structure is located under the ground level. The basement floors around the building are separated from the basement floors of other buildings with seismic gaps at three sides. At one of these sides, there is gap which prevents any contact between the structural parts. At two of these three sides, there are steel plates placed in the seismic gaps. These steel plates provide friction in horizontal directions. This type of seismic gap with frictional plates is shown in Figure 4.1. As seen ih the figure, even though the structure is seperated from the sorrounding structure with gaps, the steel plates are in contact with each other. The other side of the building is separated with the soil strata with a concrete wall. The basement is connected to the foundation at the lowest level. The structural members of shopping mall section are very irregular and complex unlile the structural members in the tower section. Slender columns are used in the last storey of shopping mall section, where the residential section starts and shopping mall section ends.

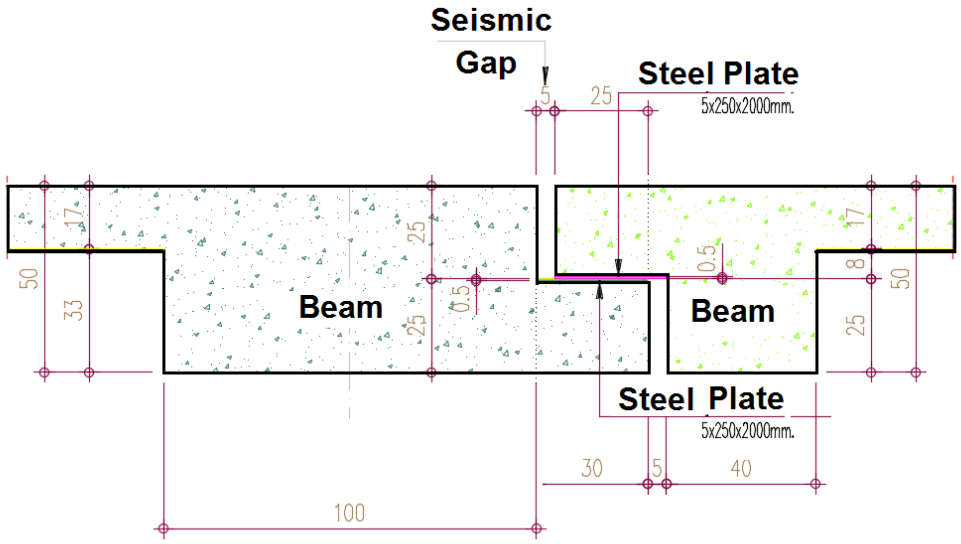

Figure 4.1. The part considered in the study and the structural elements.

The part of overall project considered in this study is marked with yellow region and the structural elements at the sides of the considered part are displayed in Figure 4.2. As the first step, the building with the surrounding shopping mall was modelled. Vertical springs were assigned at the base to simulate the foundation-structure fixity. The modulus of elasticity of C50 concrete was calculated in accordance with Turkish Standards 500 (TS500).

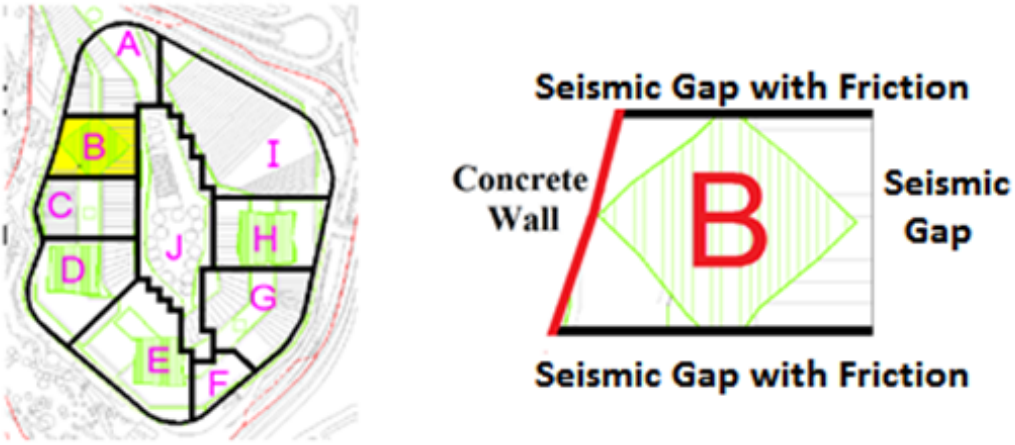

Figure 4.2. The part considered in the study and the structural elements.

Table 4.1. The observed changes in the fundamental frequency with respect to the changes in the model

The Tower and the Additional Structural Parameters	**Fundamental Frequency**
Tower + surrounding Structure	0.47 Hz
Tower + surrounding Structure + horizontal soil springs	0.50 Hz
Tower + surrounding Structure + horizontal soil springs + Seismic Gaps with frictional plates	0.56 Hz
Tower + surrounding structure + 3 times the initial value of horizontal soil springs + Seismic Gaps + 5 times the initial value of vertical soil springs + 1.15 times the initial flexural rigidity	0.59 Hz
Identification Results	0.59 Hz

To check the validity of the FEM, the fundamental frequency of the model was compared with the one obtained from the system identification. The comparison illustrated that the rigidity of the model was very low, leading to the conclusion that an increase in the detailing of the model was necessary. To observe the changes in the fundamental frequency with the increase in detailing, Table 4.1 was prepared. It can be seen that when the horizontal soil springs were assigned to the concrete wall, the fundamental frequency was increased due to the stiffness provided by soil strata. The coefficient of horizontal soil springs was calculated as 3.2 GN/m. This value was 2/3 of the coefficient of vertical springs which were calculated according to Boussinesq Theorem. Yet, the fundamental frequency was still low compared to the identified one.

Therefore, at this stage, the seismic gaps which provide friction by two steel plates were modeled in the FEM by link elements. Inclusion of seismic gaps that provides friction increased the stiffness and the fundamental frequency significantly. Therefore, the inclusion of seismic gaps with frictional plates in FEM, which is usually omitted, illustrates their remarkable effect on the dynamic characteristics of the structures. Figure 4.3 displays the final FEM while Figure 4.4 displays the zoomed view of the basement section where the seismic gaps with frictional plates and the soil springs were placed. As a result of the comparison of modal parameters obtained from the

identification and FEM, the FEM was considered to be updated by the placement of seismic gaps that provides friction. Therefore, the updating of FEM in this step is regarded as the Primary Updating Procedure.

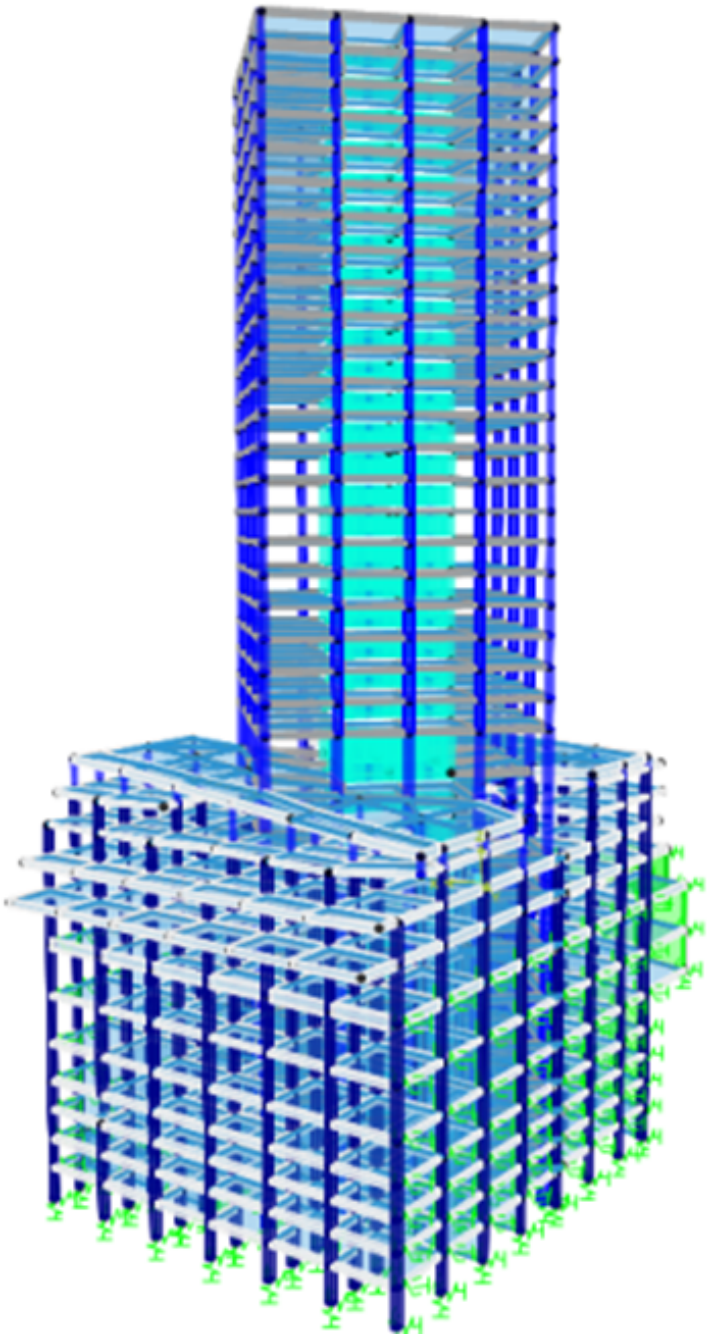

Figure 4.3. The finite element model in 3-D.

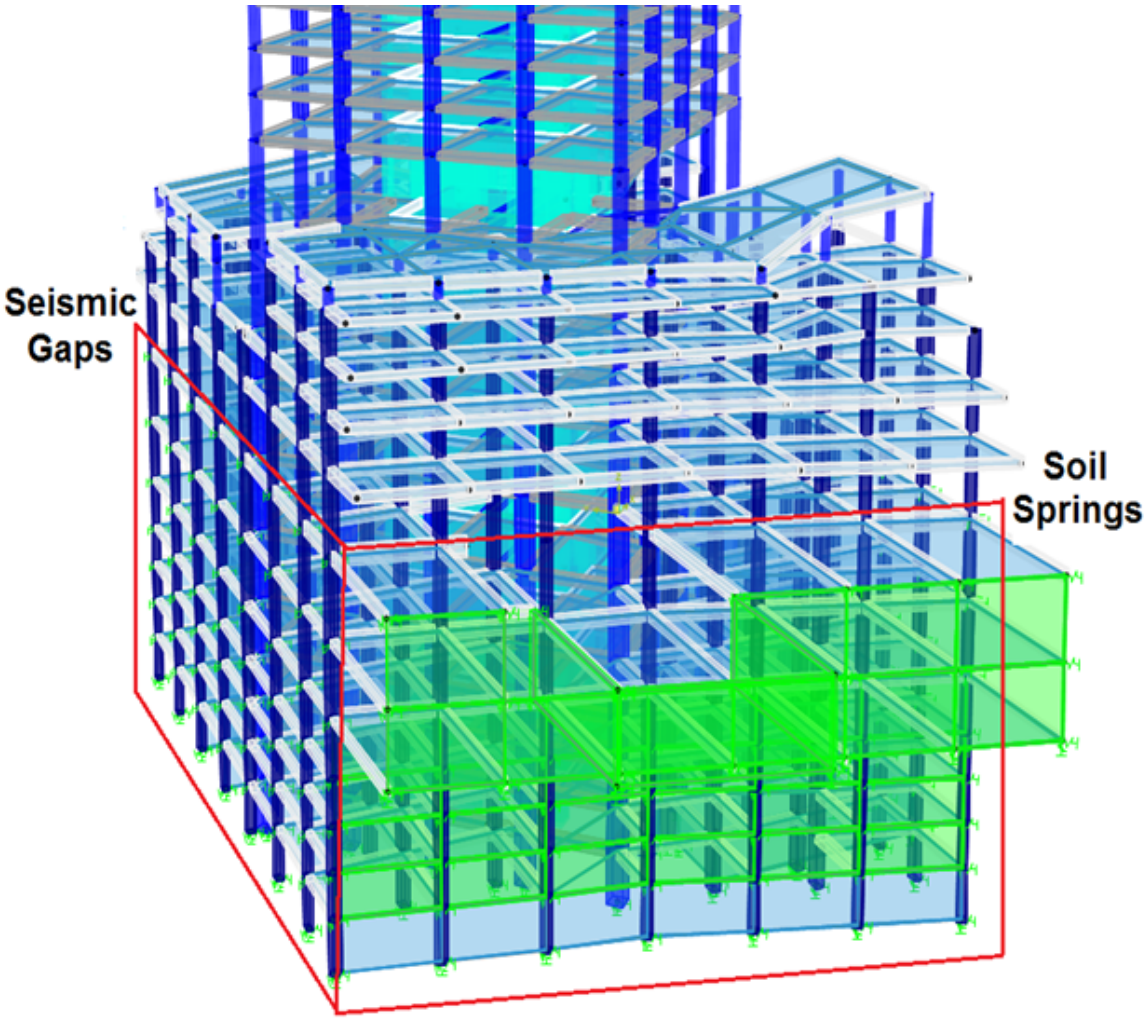

Figure 4.4. Zoomed view of the basement section of the FEM.

4.2. Sensitive Updating Procedure

As a next step, the coefficients of vertical and horizontal soil springs and the flexural rigidity of the tower section were chosen as variables to be updated with the aim of matching the modal frequencies and shapes of the FEM with the identified ones. The change of soil spring coefficients reflects the ambiguity in soil stiffness while the change of the flexural rigidity represents the overall stiffness of the structure. The flexural rigidity was chosen as a variable because it can't be determined precisely due to uncertainty in modulus of elasticity of concrete, stiffness contribution of partition walls and rigid end zones.

FEM updating procedure was performed based on minimizing the difference between experimental and analytical modal values. For this purpose, a Matlab code which can automatically update the initial FEM by changing the structural parameters within determined values was developed. The code compares modal outputs from each model with the identified modal parameters based on an error function to find the most optimal model. The schema of this code is displayed in Figure 4.5. Because of the fact that numerous combinations of parameters were changed automatically, this process is called as the Sensitivity Updating Procedure.

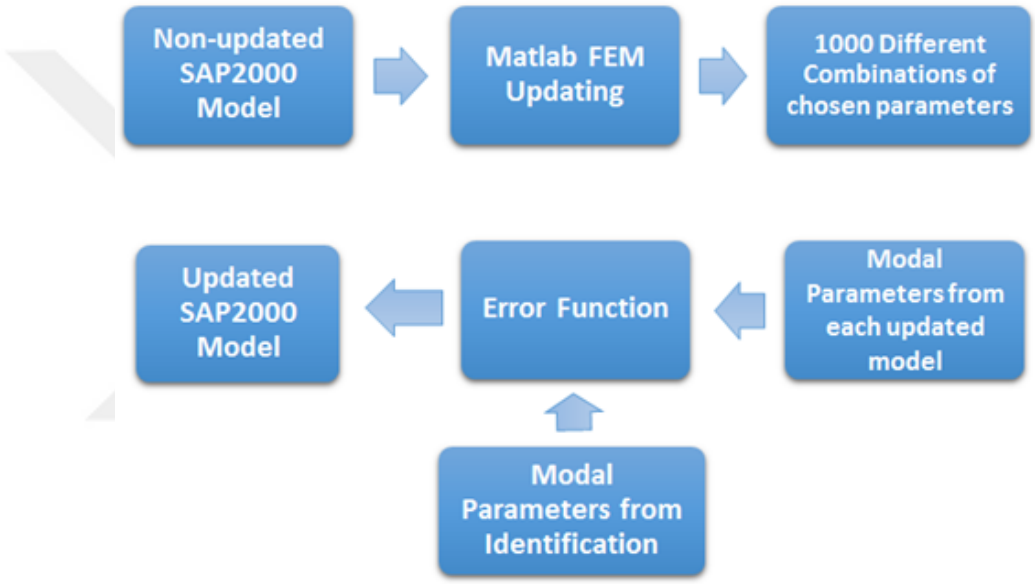

Figure 4.5. Schema of the Matlab code which performs the automatic FEM Updating Procedure.

Following the FEM Updating Procedure, modal frequencies and mode shapes which represent the ones generated from model identification were obtained. Equation 4.1 exhibits the objective function which quantifies the error between the simulations and the identification results.

$$E = (k_i.\left[(f_i^* - f_i)^2/f_i^*\right] + h_i.[1 - MAC_i]^2) \tag{4.1}$$

Where, i is mode number; k_i is the weighing coefficient for modal frequency; h_i is the

weighing coefficient for modal assurance criteria; f_i^* is the measured modal frequency of mode; f_i is the simulated modal frequency of mode; MAC_i is the modal assurance criteria for mode shape. The formulation of MAC value which compares the measured and simulated mode shapes is given in equation 4.2

$$MAC = \frac{|\varphi_*^T \varphi|}{(\varphi_*^T \varphi_*).(\varphi^T \varphi)} \tag{4.2}$$

Where φ is the measured mode shape and φ_* is the simulated mode.

In terms of MAC, the value 1 means that the mode shapes are matched precisely.

Because of the fact that the primary modes have higher effects on the dynamic behavior of the structures, the objective function involved weighing coefficients to define the contribution of different modes. Decoupling of modes in linear analyses demonstrated that the first three modes produce a large portion of the seismic forces. Therefore, the first three modes were adequate to be considered in the updating procedure. The weighing of coefficients were determined as 0.60, 0.25, 0.15 for comparison of the first, second and third modal parameters, respectively. These coefficients were chosen according to the modal participation factors of corresponding modes.

As a result of the minimization of the objective function, the vertical springs, horizontal springs and the flexural rigidity were increased as 4, 5 and 1.15 times of their initial values, respectively. These results point out that the stiffness imposed by soil strata and the overall stiffness of the tower are higher than their initial values which would be used in design practice. The final updated FEM consist of final values of the parameters updated in the Sensitivity Updating Procedure and the seismic gaps that provides friction, whose significant contribution was revealed at the first comparison of the modal parameters obtained from the system identification and the FEM. Table 4.2 compares the modal frequencies of the updated and the non-updated FEM's with the identified ones. Figure 4.6 illustrates the comparison of the mode shapes obtained from system identification, the non-updated FEM and the updated FEM.

Table 4.2. Identified, non-updated and updated modal frequencies.

Mode Number	Frequencies of Vibration		
	Modal Identification	**Updated FEM**	**Non-updated FEM**
1	0.59 Hz	0.59 Hz	0.50 Hz
2	2.15 Hz	2.03 Hz	1.77 Hz
3	0.59 Hz	3.18 Hz	2.62 Hz

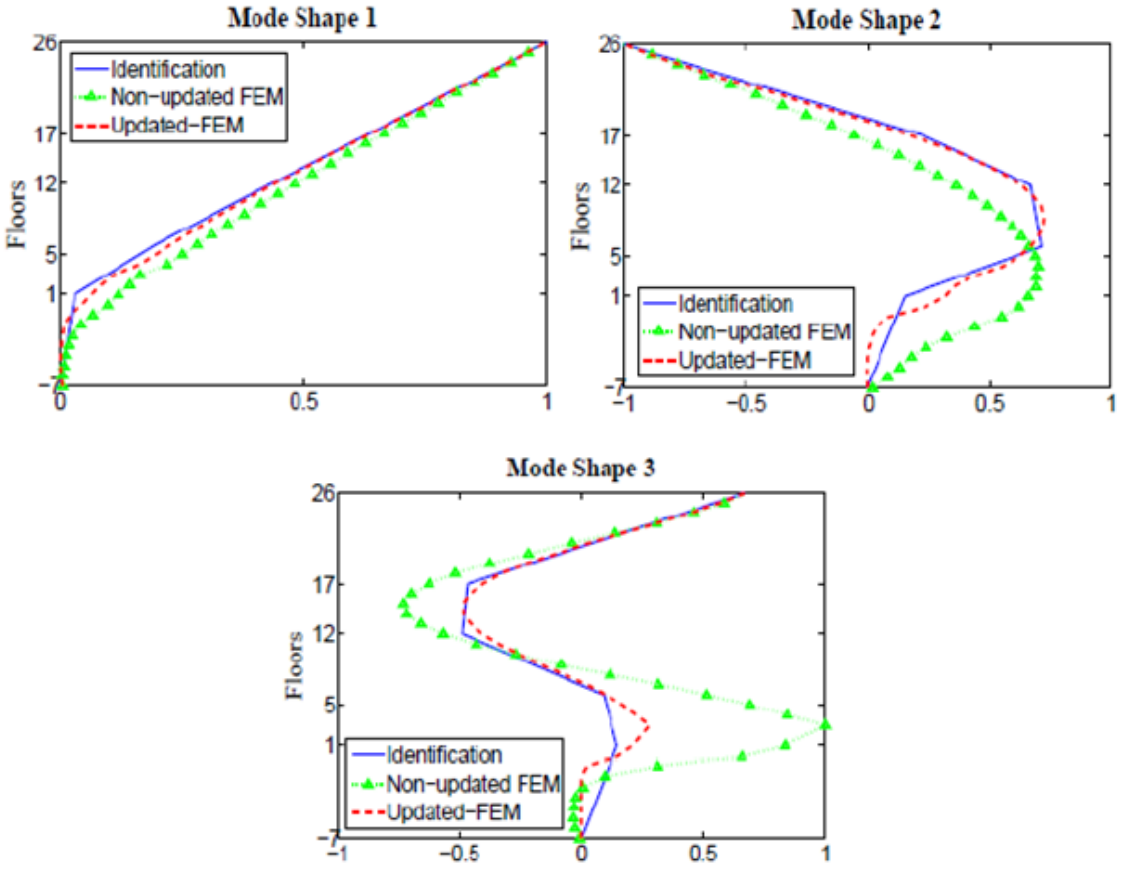

Figure 4.6. Experimental, updated and non-updated mode shapes.

5. SELECTION OF GROUND MOTIONS

To simulate the seismic demands on the building, a suite of 10 earthquake motions with their horizontal components were selected according to design-level earthquake via Peer Strong Motion Database NGA-West 2 Ground Motion Selection Tool. The horizontal components of the earthquake motions were combined by Square Roots of the Sum of the Squares (SRSS) method. The selection was conducted based on the ASCE 41-13 design based uniform hazard spectrum with 2% identified damping ratio, which was generated based on PGA maps of Istanbul Metropolitan Municipality. Figure 5.1 displays the ASCE 41-13 design based uniform hazard spectrum. The design spectrum was prepared for an earthquake scenario of 10% exceedance probability in 50 years.

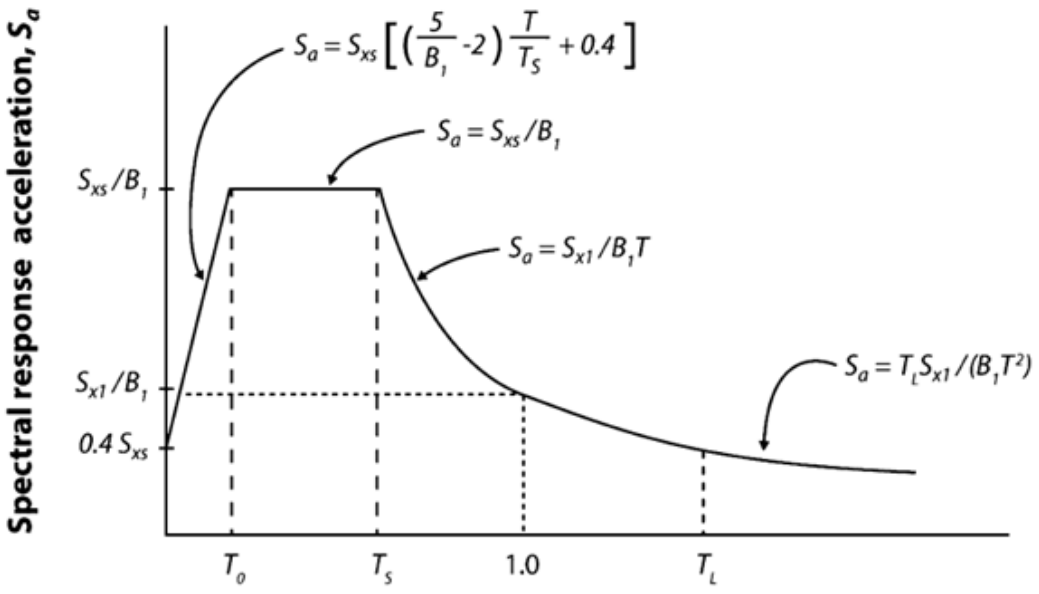

Figure 5.1. ASCE 41-13 design based uniform hazard spectrum.

The construction ranges of the spectrum are between 0 and T_o, T_o and T_s, T_s and 1s, 1s and T_L. T_L is the long period transition parameter and it should be obtained from published maps or site specific response analysis. To find the values of T_o, T_s

and T_L, the equations 5.1 and 5.2 are utilized.

$$T_s = S_{x1}/S_{xs} \tag{5.1}$$

$$T_0 = 0.2T_s \tag{5.2}$$

Where S_{x1} and S_{xs} are the spectral accelerations corresponding to the periods of 0.2 s and 1 s.

The spectral accelerations between different rages of periods are obtained by using the equations 5.3, 5.4, 5.5 and 5.6.

$$S_a = \left[(\frac{S}{B_1} - 2)\frac{T}{T_s} + 0.4\right] \quad for \quad 0 < T < T_0 \tag{5.3}$$

$$S_a = S_X S/B_1 \quad for \quad T_0 < T < T_S \tag{5.4}$$

$$S_a = S_{X1}/(B_1 T) \quad for \quad T_S < T < T_L \tag{5.5}$$

$$S_a = T_L S_{X1}/(B_1 T^2) \quad for \quad T > T_L \tag{5.6}$$

The values of the spectral accelerations according to the viscous damping ratio is adjusted by a coefficient B_1 which is obtained through equation 5.7

$$B_1 = 4/\left[5.6 - \ln(100\xi)\right] \tag{5.7}$$

Where ξ ıs the viscous damping ratio.

Figure 5.2 and Figure 5.3 demonstrate the spectral acceleration maps of Istanbul Metropolitan Municipality for an earthquake scenario of 10% exceedance probability in 50 years. The spectral accelerations at the building site at the periods of 0.2 s and 1 s, $4S_{x1}$ and S_{xs} , are obtained by using these maps. Because of the fact the location of the tall building is in between two different spectral acceleration boundaries, interpolation between these boundaries are performed in order to find the S_{x1} and S_{xs}. The building site is marked with a star on these maps.

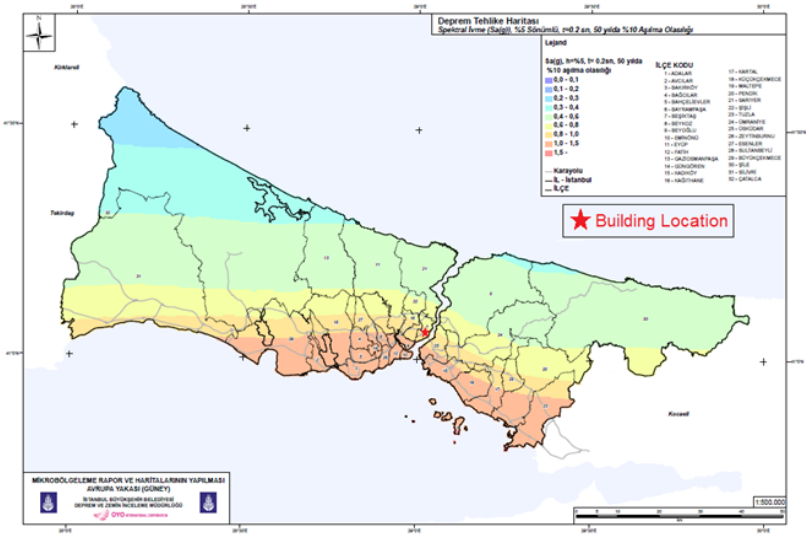

Figure 5.2. Spectral acceleration map of Istanbul at the period of 0.2 s.

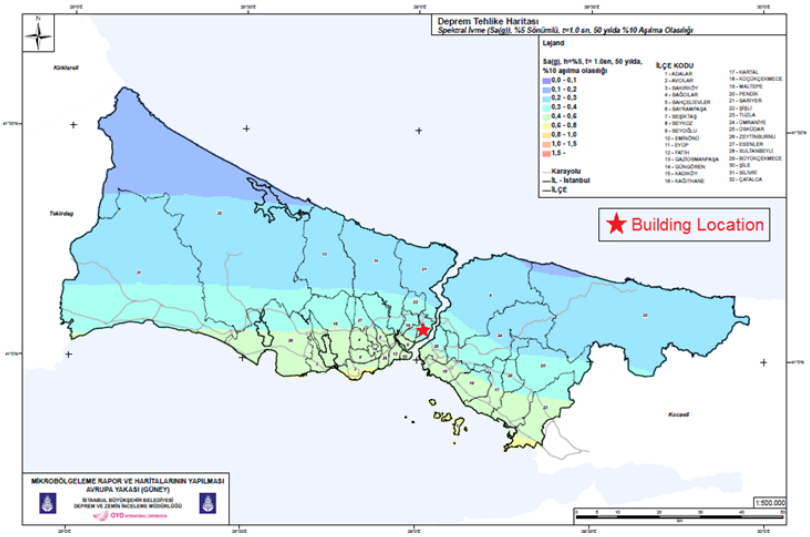

Figure 5.3. Spectral acceleration map of Istanbul at the period of 1 s.

The expected earthquake in Istanbul is estimated to be generated by the North Anatolian Fault, which is one of the most significant fault lines in Anatolia. This fault line is very active. Historical records demonstrates that many major and numerous minor seismic events occurred on this fault line. The last two devastating major earthquakes occurred in Kocaeli (M=7.4) and Duzce (M=7.2) in 1999. This fault line dives into Marmara Sea and continues to the west. The figure 5.4 shows the Marmara segment of the North Anatolian Fault and the location of the tall building. The distance between the fault line and the building is approximately 26 km. Therefore the ground motions were selected based on this distance. The records were also intended to represent the characteristics of the expected earthquake that is going to be generated by this fault line. These characteristics are 7.5 magnitude and strike-slip fault mechanism as suggested by Erdik *et al.* (2003). To produce a mean which is over the design spectrum in the range of 0.2 T and 1. 5T, where T is the fundamental period of the structure, the ground motions were scaled in reasonable scale factors in order to avoid excessive accelerations in short period ranges as suggested by National Institute of Standards and Technology (NIST).

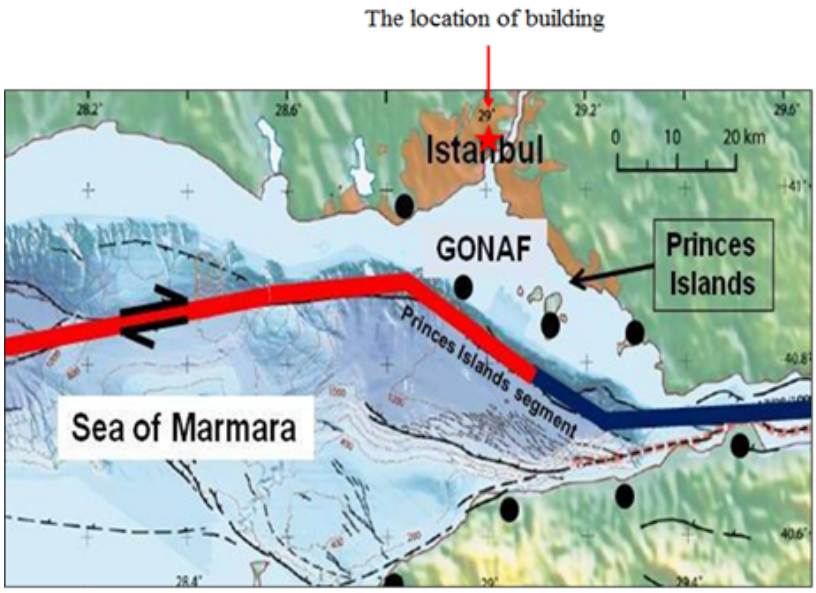

Figure 5.4. The Marmara segment of the North Anatolian Fault and the location of the tall building.

The pair of ground motions were applied in random directions to the building due to long distance of the building site to the earthquake fault as suggested in Huang (2009). According to this report, there is no schematic dependence on horizontal components of the ground motions when the distance between the building site and the fault is more than 15 km. Otherwise, the parallel and normal components of the ground motions should be applied to the FEM simulation in the same directions of the components of the expected ground motions that is generated by the fault line. Figure 5.5 shows the spectra of the selected ground motions, their mean and the design spectrum. The mean spectrum is more than the design spectrum in the period ranges of 0.2T and 1. 5T as explained before. 1.5T is specified in the code so that the softening of the first mode during the earhtquake excitation is taken into account. 0.2T is specified so that the higher modes of a structure is considered.

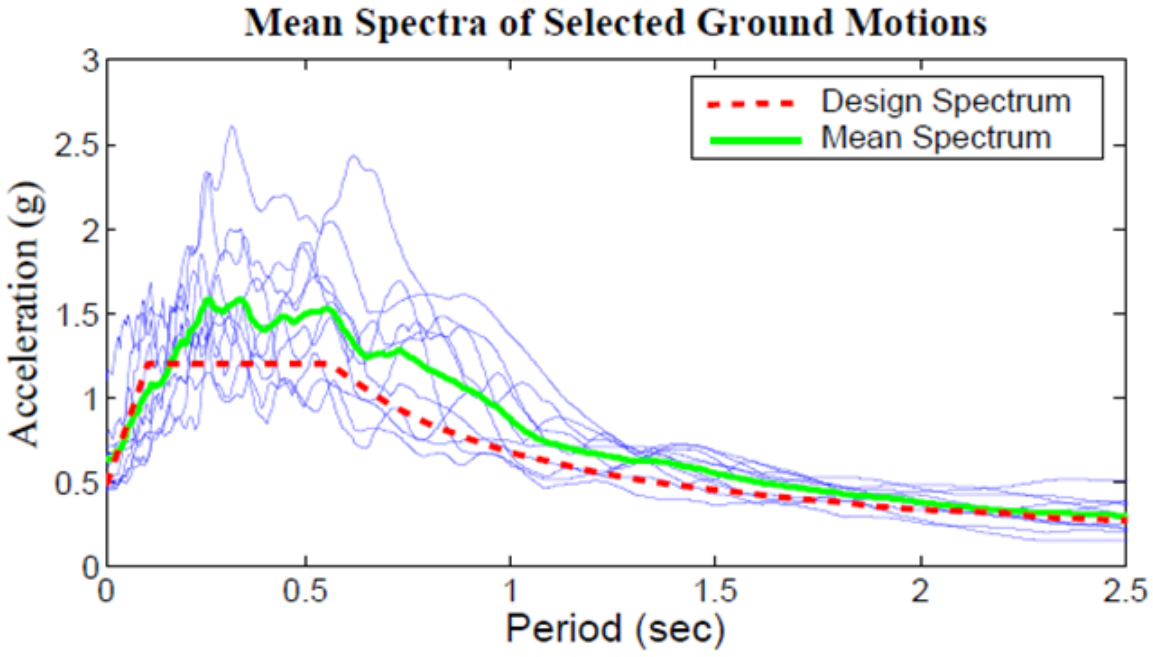

Figure 5.5. The spectra of selected ground motions, their mean and the design spectrum.

Table 5.1 demonstrates the name, station and year of the selected ground motions and their characteristics such as distance, PGA, magnitude, scale factor and mechanism. The distance between the site and earthquake location ranges between 12.02 km to 48.84 km. The PGA values of the selected seismic inputs ranges between 0.44 g to 0.76 g while magnitudes of these records ranges from 6.7 to 7.51. The maximum scale factor utilized is 2.15. As explained before, high scale factors should be avoided in order not to cause unrealistic spectral acceleration values in the considered period ranges. Ten seismic motions with their two horizontal components were considered to be adequate for the nonlinear time history analysis of the structure in terms of probabilistic approach and computation time.

Table 5.1. Properties of the selected ground motions.

No	**Name/Station/Year**	**Distance (km)**	**PGA**	**Magnitude**	**Scale Factor**	**Mechanicsm**
1	Hector Mine / Amboy / 1999	41.81	0.49	7.13	2.08	Strike-Slip
2	Landers / Indio - Jackson Road /1992	48.84	0.75	7.28	2	Strike-Slip
3	El Mayor / El Centro - Imperial & Ross /2010	19.39	0.69	7.2	1.1	Strike-Slip
4	Duzce / Bolu / 1999	12.02	1	7.14	1	Strike-Slip
5	Kocaeli / Duzce / 1999	13.6	0.45	7.51	1	Strike-Slip
6	Northridge / Castaic-Old Ridge Route / 1994	17.64	0.76	6.7	1	Reverse
7	Darfield, New Zealand / Kaiapoi North School / 2010	30.53	0.7	7	1.5	Strike-Slip
8	Darfield, New Zealand / Pages Road Pumping Station/ 2010	24.55	0.45	7	1.53	Strike-Slip
9	Darfield, New Zealand / Christchurch Resthaven / 2010	19.48	0.44	7	1.53	Strike-Slip
10	Darfield / SPFS / 2010	29.86	0.56	7	2.18	Strike-Slip

6. DEVELOPMENT OF THE NONLINEAR FEM

To include the nonlinear behaviors of structural members in SAP 2000 analytical model, plastic hinges were assigned at both ends of the structural members. Two type of plastic hinges were used in the analytical model. These hinges provide the nonlinearity when the moment capacity of the hinges are exceeded. P-M2-M3 type hinges, which represent the coupling behavior of structural members under bidirectional seismic inputs, were used in the column and shear walls while M3 type of hinges were assigned to beams. The moment capacity and moment-curvature relationships of structural elements were obtained through the cross sectional analyses program called XTRACT. Structural drawings of the building were utilized in order to design the cross sections of the structure members on XTRACT software. Becuase of the fact that the structure is very large, and that the structural members at the shopping mall section are complex and irregular, the number of different beam sections is 34, the number of different columns sections is 16 and the number of different shear wall sections is 8, in the building. Figure 6.1 demonstrates the cross-section and Moment – Curvature graph of the shear wall side of the beams that connects the shear wall to the outher colums at tower section. Figure 6.2 demonstres the cross-section and Moment – Curvature graph of the column side of the beams that connects the shear wall to the outher colums at tower section. Figure 6.3 demonstrates the cross-section and Moment – Curvature graphs of the shear wall side of the beams that connects the shear wall to the outher colums at basement section. Figure 6.4 demonstrates the cross-section and Moment – Curvature graphs of the column side of the beams that connects the shear wall to the outher colums at basement section. Figure 6.5 displays the cross-section and P-M diagrahm of the colums at top storey of the tower while Figure 6.6 displays the cross-section and P-M diagrahm of the colums at the base of basement section. Figure 6.7 and 6.8 demonstrate the cross-sections and P-M diagrahms of one of the shear walls at the top of the tower section and at the base of the basement section, respectively.

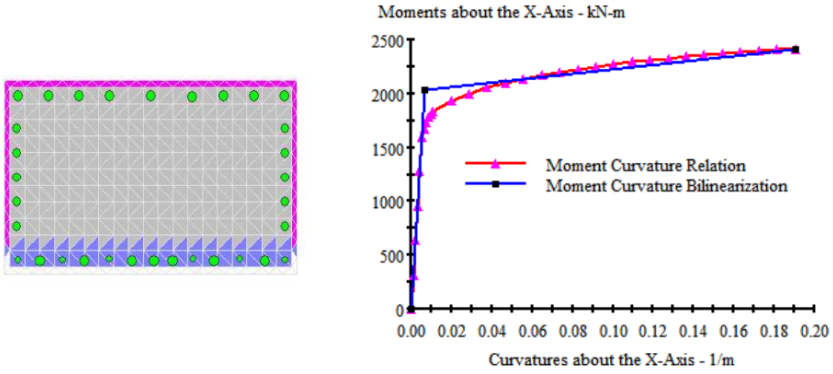

Figure 6.1. Cross -section and Moment – Curvature graph of the shear wall side of the beams that connects the shear wall to the outher colums at basement section.

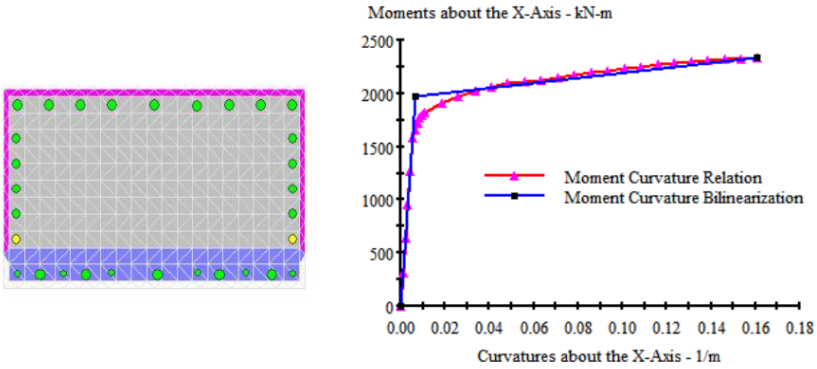

Figure 6.2. Cross -section and Moment – Curvature graph of the column side of the beams that connects the shear wall to the outher colums at basement section.

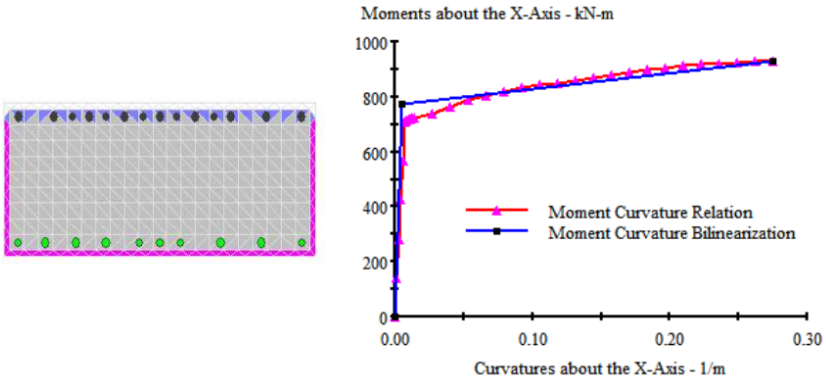

Figure 6.3. Cross-section and Moment – Curvature graphs of the column side of the beams that connects the shear wall to the outher columns at tower section.

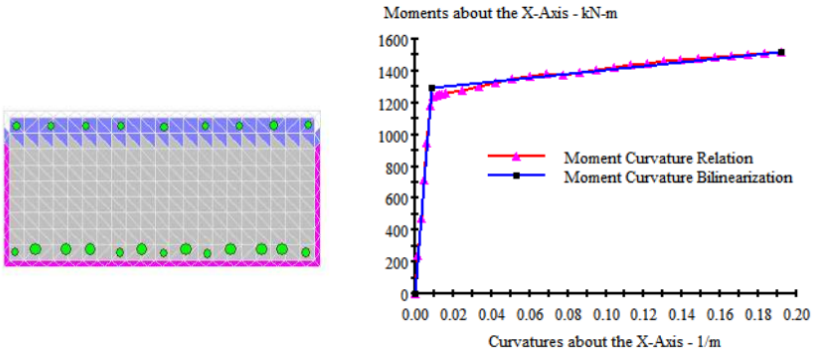

Figure 6.4. Cross -section and Moment – Curvature graphs of the shear wall side of the beams that connects the shear wall to the outher colums at tower section.

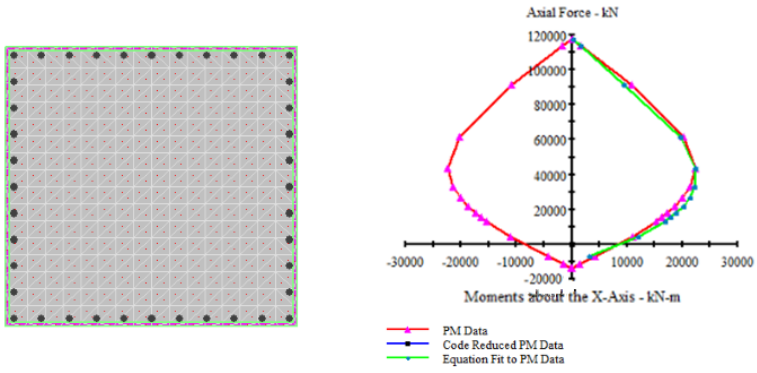

Figure 6.5. Cross -section and P-M diagrahm of the colums at top storey of the tower.

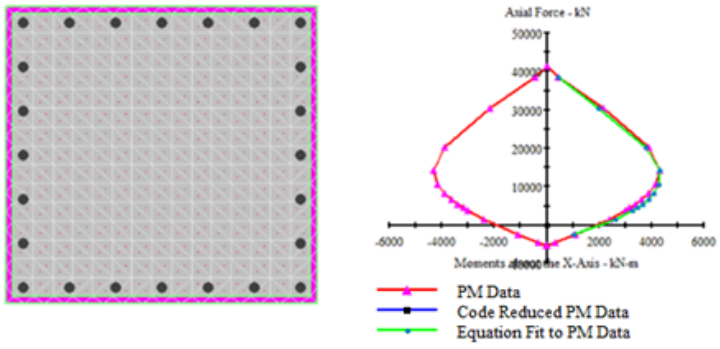

Figure 6.6. The cross-section and P-M diagrahm of the colums at the base of basement section.

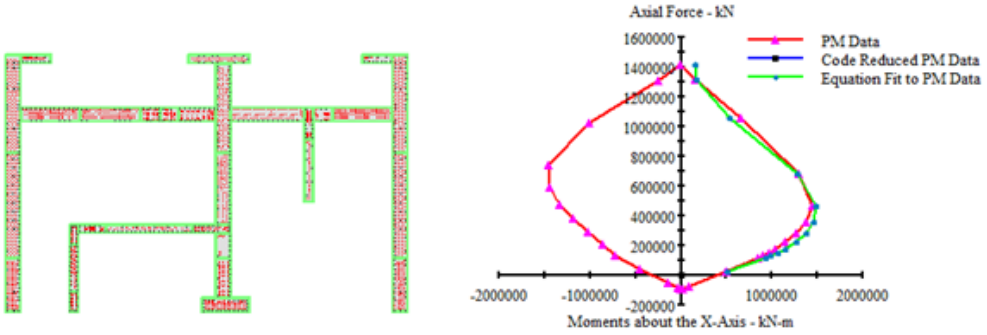

Figure 6.7. The cross-sections and P-M diagrahms of one of the shear walls at the top of the tower section.

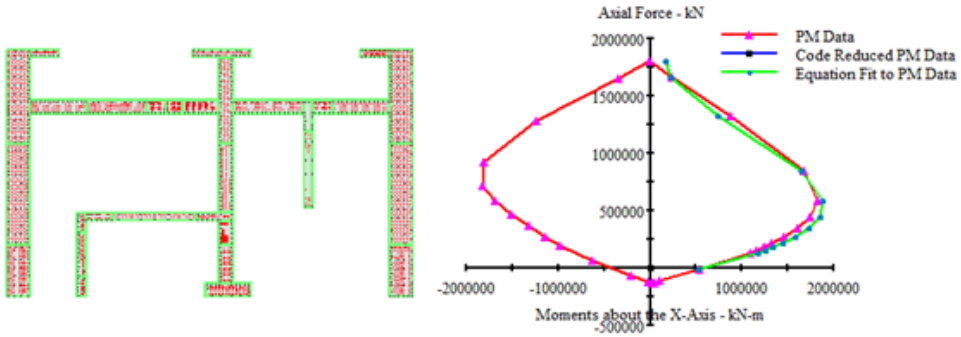

Figure 6.8. The cross-sections and P-M diagrahms of one of the shear walls at the base of the basement section.

From the figures above, It is apparent that the moment capacities of the colums and shear walls at bottom stories are much higher than the moment capacities of the columns and shear walls at the higher stories. This situation is also valid for the beams. The beams at the basement stories carry the loads transferred from the slabs, which were design the carry vehicle loads. Therefore, the section capacities of these beams are much higher than the ones at the tower section.

The performance acceptance criterias of the structural members such as columns, shear walls and beams were determined based on plastic rotation limits according to ASCE 41-13 Standards. Priliminary linear time history analysis with the strongest ground motion was conducted in order to acquire the maximum moments and shear forces on the structural members. So, the necessary conditions located at the left sides of the tables were calculated in order to find the plastic rotation limits of members. Figure 6.9, 6.10 and 6.11 demonstrates the modelling parameters and acceptence criterias in terms of plastic rotations of ASCE 41.13 for the beams, columns and shear walls, respectively.

Table 10-7. Modeling Parameters and Numerical Acceptance Criteria for Nonlinear Procedures—Reinforced Concrete Beams

			Modeling Parameters[a]			Acceptance Criteria[a]		
			Plastic Rotations Angle (radians)		Residual Strength Ratio	Plastic Rotations Angle (radians)		
						Performance Level		
Conditions			a	b	c	IO	LS	CP
Condition i. Beams controlled by flexure[b]								
$\frac{\rho-\rho'}{\rho_{bal}}$	Transverse reinforcement[c]	$\frac{V}{b_w d\sqrt{f'_c}}$ [d]						
≤0.0	C	≤3 (0.25)	0.025	0.05	0.2	0.010	0.025	0.05
≤0.0	C	≥6 (0.5)	0.02	0.04	0.2	0.005	0.02	0.04
≥0.5	C	≤3 (0.25)	0.02	0.03	0.2	0.005	0.02	0.03
≥0.5	C	≥6 (0.5)	0.015	0.02	0.2	0.005	0.015	0.02
≤0.0	NC	≤3 (0.25)	0.02	0.03	0.2	0.005	0.02	0.03
≤0.0	NC	≥6 (0.5)	0.01	0.015	0.2	0.0015	0.01	0.015
≥0.5	NC	≤3 (0.25)	0.01	0.015	0.2	0.005	0.01	0.015
≥0.5	NC	≥6 (0.5)	0.005	0.01	0.2	0.0015	0.005	0.01
Condition ii. Beams controlled by shear[b]								
Stirrup spacing ≤ $d/2$			0.0030	0.02	0.2	0.0015	0.01	0.02
Stirrup spacing > $d/2$			0.0030	0.01	0.2	0.0015	0.005	0.01
Condition iii. Beams controlled by inadequate development or splicing along the span[b]								
Stirrup spacing ≤ $d/2$			0.0030	0.02	0.0	0.0015	0.01	0.02
Stirrup spacing > $d/2$			0.0030	0.01	0.0	0.0015	0.005	0.01
Condition iv. Beams controlled by inadequate embedment into beam–column joint[b]			0.015	0.03	0.2	0.01	0.02	0.03

NOTE: f'_c in lb/in.^{2} (MPa) units.
[a]Values between those listed in the table should be determined by linear interpolation.
[b]Where more than one of conditions i, ii, iii, and iv occur for a given component, use the minimum appropriate numerical value from the table.
[c]"C" and "NC" are abbreviations for conforming and nonconforming transverse reinforcement, respectively. Transverse reinforcement is conforming if, within the flexural plastic hinge region, hoops are spaced at ≤ $d/3$, and if, for components of moderate and high ductility demand, the strength provided by the hoops (V_s) is at least 3/4 of the design shear. Otherwise, the transverse reinforcement is considered nonconforming.
[d]V is the design shear force from NSP or NDP.

Figure 6.9. The modelling parameters and acceptence criterias in terms of plastic rotations for the beams (ASCE 41-13).

Table 10-8. Modeling Parameters and Numerical Acceptance Criteria for Nonlinear Procedures—Reinforced Concrete Columns

Conditions			Modeling Parameters[a]			Acceptance Criteria[a]		
			Plastic Rotations Angle (radians)		Residual Strength Ratio	Plastic Rotations Angle (radians)		
						Performance Level		
			a	b	c	IO	LS	CP
Condition i.[b]								
$\frac{P}{A_g f_c'}$[c]	$\rho = \frac{A_v}{b_w s}$							
≤0.1	≥0.006		0.035	0.060	0.2	0.005	0.045	0.060
≥0.6	≥0.006		0.010	0.010	0.0	0.003	0.009	0.010
≤0.1	=0.002		0.027	0.034	0.2	0.005	0.027	0.034
≥0.6	=0.002		0.005	0.005	0.0	0.002	0.004	0.005
Condition ii.[b]								
$\frac{P}{A_g f_c'}$[c]	$\rho = \frac{A_v}{b_w s}$	$\frac{V}{b_w d\sqrt{f_c'}}$[d]						
≤0.1	≥0.006	≤3 (0.25)	0.032	0.060	0.2	0.005	0.045	0.060
≤0.1	≥0.006	≥6 (0.5)	0.025	0.060	0.2	0.005	0.045	0.060
≥0.6	≥0.006	≤3 (0.25)	0.010	0.010	0.0	0.003	0.009	0.010
≥0.6	≥0.006	≥6 (0.5)	0.008	0.008	0.0	0.003	0.007	0.008
≤0.1	≤0.0005	≤3 (0.25)	0.012	0.012	0.2	0.005	0.010	0.012
≤0.1	≤0.0005	≥6 (0.5)	0.006	0.006	0.2	0.004	0.005	0.006
≥0.6	≤0.0005	≤3 (0.25)	0.004	0.004	0.0	0.002	0.003	0.004
≥0.6	≤0.0005	≥6 (0.5)	0.0	0.0	0.0	0.0	0.0	0.0
Condition iii.[b]								
$\frac{P}{A_g f_c'}$[c]	$\rho = \frac{A_v}{b_w s}$							
≤0.1	≥0.006		0.0	0.060	0.0	0.0	0.045	0.060
≥0.6	≥0.006		0.0	0.008	0.0	0.0	0.007	0.008
≤0.1	≤0.0005		0.0	0.006	0.0	0.0	0.005	0.006
≥0.6	≤0.0005		0.0	0.0	0.0	0.0	0.0	0.0
Condition iv. Columns controlled by inadequate development or splicing along the clear height[b]								
$\frac{P}{A_g f_c'}$[c]	$\rho = \frac{A_v}{b_w s}$							
≤0.1	≥0.006		0.0	0.060	0.4	0.0	0.045	0.060
≥0.6	≥0.006		0.0	0.008	0.4	0.0	0.007	0.008
≤0.1	≤0.0005		0.0	0.006	0.2	0.0	0.005	0.006
≥0.6	≤0.0005		0.0	0.0	0.0	0.0	0.0	0.0

NOTE: f_c' is in lb/in.^{2} (MPa) units.
[a]Values between those listed in the table should be determined by linear interpolation.
[b]Refer to Section 10.4.2.2.2 for definition of conditions i, ii, and iii. Columns are considered to be controlled by inadequate development or splices where the calculated steel stress at the splice exceeds the steel stress specified by Eq. (10-2). Where more than one of conditions i, ii, iii, and iv occurs for a given component, use the minimum appropriate numerical value from the table.
[c]Where $P > 0.7A_g f_c'$, the plastic rotation angles should be taken as zero for all performance levels unless the column has transverse reinforcement consisting of hoops with 135-degree hooks spaced at ≤ $d/3$ and the strength provided by the hoops (V_s) is at least 3/4 of the design shear. Axial load P should be based on the maximum expected axial loads caused by gravity and earthquake loads.
[d]V is the design shear force from NSP or NDP.

Figure 6.10. The modelling parameters and acceptence criterias in terms of plastic rotations for the columns (ASCE 41-13).

The evaluation of the performance of the structural members on plastic rotation instead of the strains give rises simplicity in the evaluation. For this purpose, performance evaluation based on plastic rotation was preferred.

Table 10-19. Modeling Parameters and Numerical Acceptance Criteria for Nonlinear Procedures—R/C Shear Walls and Associated Components Controlled by Flexure

Conditions			Plastic Hinge Rotation (radians)		Residual Strength Ratio	Acceptable Plastic Hinge Rotation[a] (radians)		
						Performance Level		
			a	*b*	*c*	IO	LS	CP
i. Shear walls and wall segments								
$\frac{(A_s - A_s')f_y + P}{t_w l_w f_c'}$	$\frac{V}{t_w l_w \sqrt{f_c'}}$	Confined Boundary[b]	0.015					
≤0.1	≤4	Yes	0.010	0.020	0.75	0.005	0.015	0.020
≤0.1	≥6	Yes	0.009	0.015	0.40	0.004	0.010	0.015
≥0.25	≤4	Yes	0.005	0.012	0.60	0.003	0.009	0.012
≥0.25	≥6	Yes	0.008	0.010	0.30	0.0015	0.005	0.010
≤0.1	≤4	No	0.006	0.015	0.60	0.002	0.008	0.015
≤0.1	≥6	No	0.003	0.010	0.30	0.002	0.006	0.010
≥0.25	≤4	No	0.002	0.005	0.25	0.001	0.003	0.005
≥0.25	≥6	No	0.002	0.004	0.20	0.001	0.002	0.004
ii. Shear wall coupling beams[c]								
Longitudinal reinforcement and transverse reinforcement[d]	$\frac{V}{t_w l_w \sqrt{f_c'}}$			0.050				
Conventional longitudinal reinforcement with conforming transverse reinforcement	≤3		0.025	0.040	0.75	0.010	0.025	0.050
	≥6		0.020	0.035	0.50	0.005	0.020	0.040
Conventional longitudinal reinforcement with nonconforming transverse reinforcement	≤3		0.020	0.025	0.50	0.006	0.020	0.035
	≥6		0.010	0.050	0.25	0.005	0.010	0.025
Diagonal reinforcement	NA		0.030	0.050	0.80	0.006	0.030	0.050

[a]Linear interpolation between values listed in the table shall be permitted.
[b]A boundary element shall be considered confined where transverse reinforcement exceeds 75% of the requirements given in ACI 318 and spacing of transverse reinforcement does not exceed $8d_b$. It shall be permitted to take modeling parameters and acceptance criteria as 80% of confined values where boundary elements have at least 50% of the requirements given in ACI 318 and spacing of transverse reinforcement does not exceed $8d_b$. Otherwise, boundary elements shall be considered not confined.
[c]For coupling beams spanning <8 ft 0 in., with bottom reinforcement continuous into the supporting walls, acceptance criteria values shall be permitted to be doubled for LS and CP performance.
[d]Conventional longitudinal reinforcement consists of top and bottom steel parallel to the longitudinal axis of the coupling beam. Conforming transverse reinforcement consists of (a) closed stirrups over the entire length of the coupling beam at a spacing ≤ $d/3$, and (b) strength of closed stirrups $V_s \geq 3/4$ of required shear strength of the coupling beam.

Figure 6.11. The modelling parameters and acceptence criterias in terms of plastic rotations for the shear walls (ASCE 41-13).

The nonlinearity in the sorrounding parts of tower in basement and shopping mall sections is not modelled for sake of simplicitly. This simplification is considered not to provoke a significant effect on the results because of the following reasons. Firstly, the basement levels don't experience large shaking due to very high stiffness cause by the soil and seismic gaps which provide friction. Secondly, the seismic behavior of the tower part is considered in this study and the sorrounding structure along shopping mall floors doesn't impose any significant sitffness and mass contribution to the tower section.

NLTH analysis requires damping matrix as well as it requires mass and stiffness matrices because of the fact that the matrices are solved by numeric integration

methods at NLTH analysis. Rayleigh Damping is the most well-known method that is utilized to generate the mass matrix. Equation 6.1, 6.2 and 6.3 demonstrate the generation of damping matrix by Rayleigh Damping method. As it is seen, the damping matrix is a linear combination of the initial mass and stiffness matrices. Therefore, the mass matrix should include mass of each degree of freedom in order to yield reasonable results at each time step. (Chopra, 1995)

$$C = a.M + \beta.K \tag{6.1}$$

Where C is the damping matrix, M is the mass matrix and K is the stiffness matrix.

The coefficients a and β involve the damping ratio parameter such as

$$a = \zeta \frac{2.w_i.w_j}{w_i + w_j} \tag{6.2}$$

$$\beta = \zeta \frac{2}{w_i + w_j} \tag{6.3}$$

Where w_i and w_j are the natural frequencies of the ith and j^{th} modes.

Lager and Dassault (1992) demonstrated that the selection of different damping models doesn't have a considerable effect on the seismic responses of buildings whose fundamental period is higher than 1.5 seconds. Therefore, because of the fact that the fundamental period of the tall building in this study is 1.7 seconds, the utilization of Rayleigh Damping with the initial stiffness and mass matrices in the NLTH analysis is considered not to impose any disturbance on the results of the seismic responses of the building.

7. EFFECT OF IDENTIFICATION ON SEISMIC PERFORMANCE ASSESSMENT OF THE TALL BUILDING

In this section, the effect of identified modal frequencies and shapes by using the updated and the non-updated FEM with 5% viscous damping ratio is investigated. Then, the effect of identified modal damping ratio on the seismic performance assessment is investigated by using the updated FEM with the identified (2%) damping ratio and the 5% damping ratio. Probability density functions in terms of interstory drift ratios are established in order to quantify the probability of exciting prescribed damage levels.

7.1. Effect of the identified modal shapes and frequencies

In order to compare the effect of identified modal shapes and frequencies on seismic performance assessment of a tall building, NLTH analyses were carried out with the updated and non-updated FEM's with 5% viscous damping ratio. The same viscous damping ratio (5%) is assigned to both FEM's in order to compare only the effect of the updating procedure mentioned in Chapter 4. Figure 7.1 and 7.3 illustrate the damage states of the non-updated and the updated FEM's under the ground motion number 1 and 8, respectively. It can be seen in these figures that some columns of the non-updated FEM experience higher damage states at the 5th floor, where the shopping mall ends and the residential section starts. In addition, the number of damaged beams at the basement and shopping mall sections of the non-updated FEM is found to be more than the number of the damaged beams of the updated FEM. It is also seen that more beams are damaged at the upper floors of the residential section in the non-updated FEM. The damage states under other ground motions give similar results as well.

In this study, the interstory drift ratio was chosen as damage indicator of the building studied. The selection of interstory drift as damage indicator provides a quick assessment of the seismic performance of the building. Figure 7.2 and Figure 7.4 demonstrate the interstory drift ratios of the updated and the non-updated FEM's under the ground motion number 1 and 8, respectively. Figure 7.5 displays the mean interstory drift ratios of both FEM's. The figures demonstrate that the rate of increase in the drift ratios is high in the shopping mall section and gradually decreases along the building. However, the differences between them immediately start at the base and continue along the height. Such differences indicate the non-updated FEM experiences higher seismic demands than the updated one.

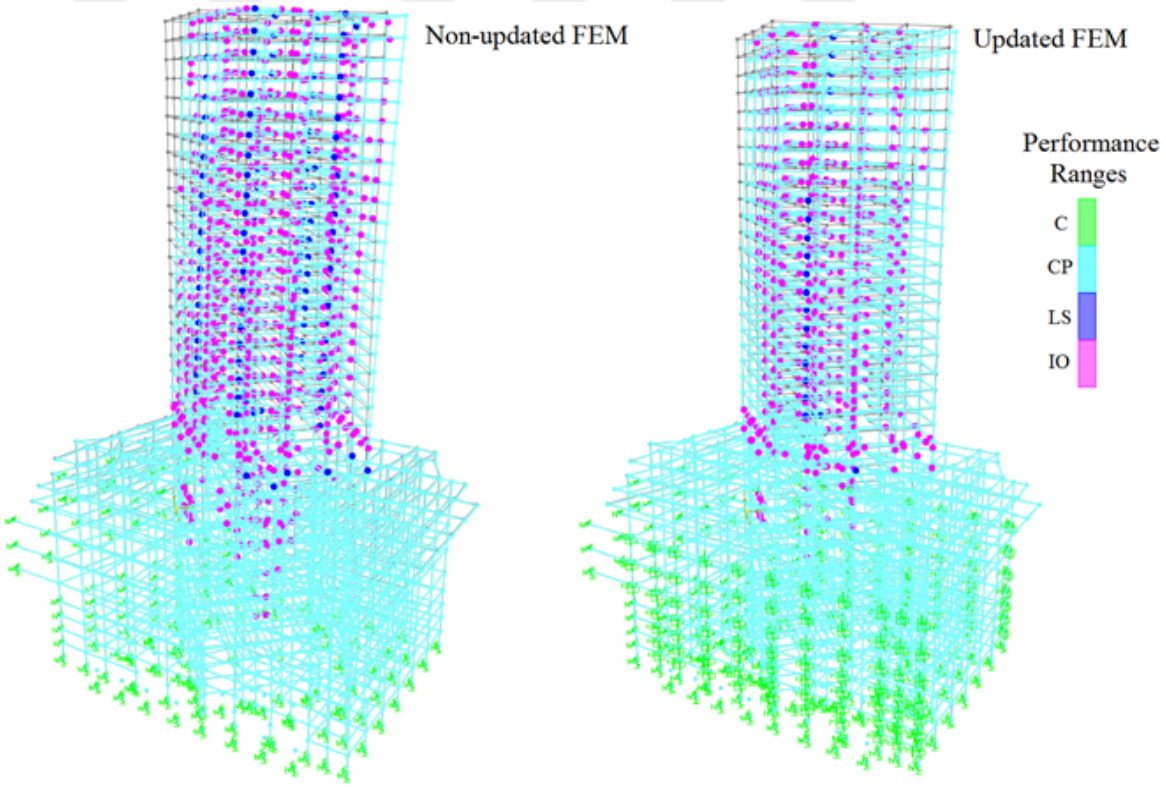

Figure 7.1. The damage levels of the Updated and Non-updated FEM's with 5% viscous damping ratio under the ground motion no 1.

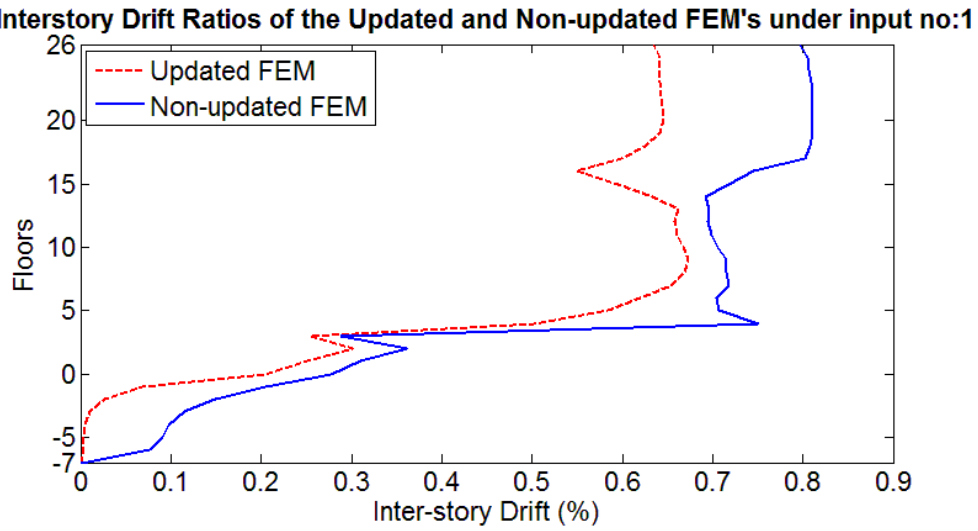

Figure 7.2. The interstory drift ratios of the Updated and Non-updated FEM's with 5% viscous damping ratio under the ground motion no 1.

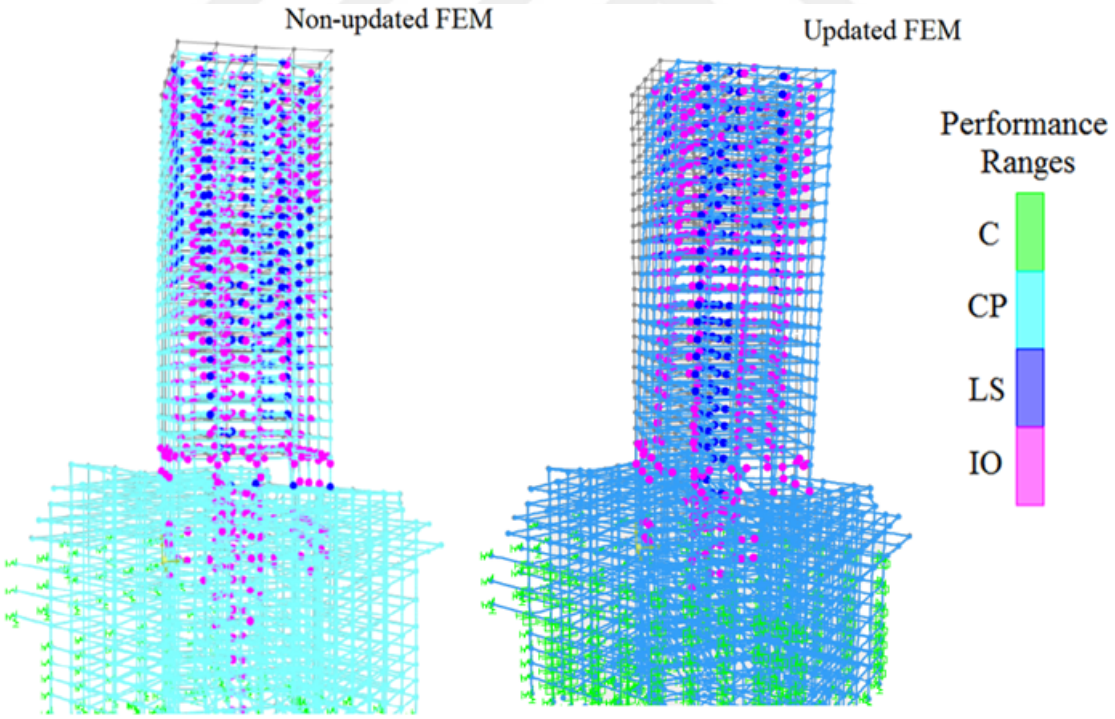

Figure 7.3. The damage levels of the Updated and Non-updated FEM's with 5% viscous damping ratio under the ground motion no 8.

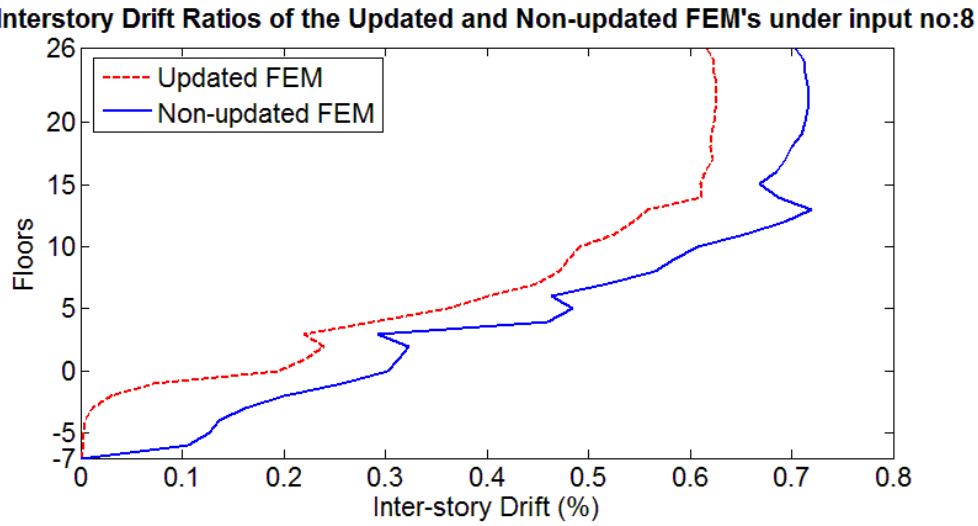

Figure 7.4. The interstory drift ratios of the Updated and Non-updated FEM's with 5% viscous damping ratio under the ground motion no 8.

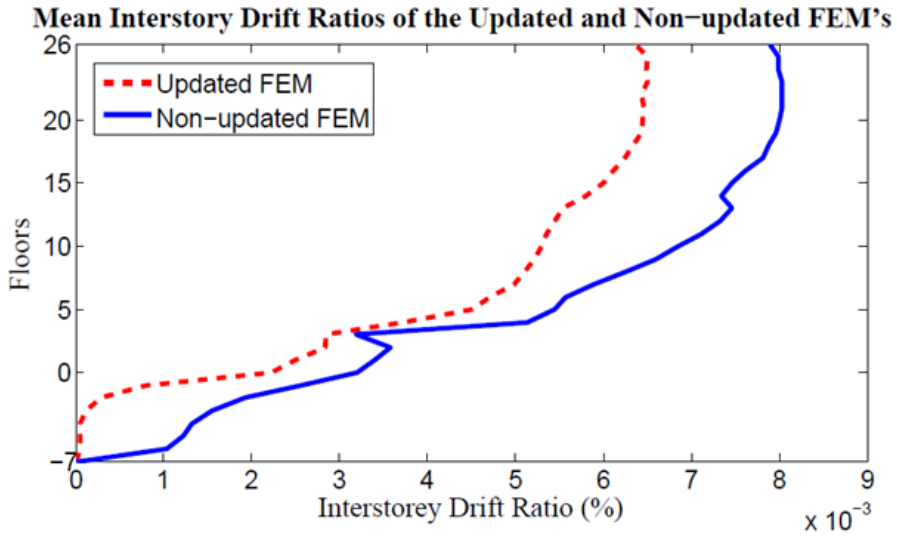

Figure 7.5. The mean interstory drift ratios of the Updated and Non-updated FEM's.

In order to quantify the probability of failure under the selected input motions, probability density functions in terms of interstory drift ratios were established for both FEM's in order to compare the differences of these functions depicted in Figure 7.6, 1% drift ratio can be chosen as threshold because the Turkish Earthquake Code states that 1% interstory drift ratio is the limit value between immediate occupancy

and life safety damage states. The probability of exceeding this value is 16% for the non-updated FEM while it is 10% for the updated FEM.

Even if the probability density functions demonstrate that the level of damage is not destructive and the building in interest remains mostly in the immediate occupancy damage level, the cost of repairment may be too much or the building owner may want to sustain the full functionality of his or her investment right after any seismic event. Therefore, even if the damage is not severe, anticipating the real seismic demands on the structures plays a crucial role in the performance of structures. To emphasize this fact, a threshold value may be set on 0.5% interstory drift ratio. The probability of exceeding this value is 55% for the non-updated FEM while it is 44% for the non-updated FEM.

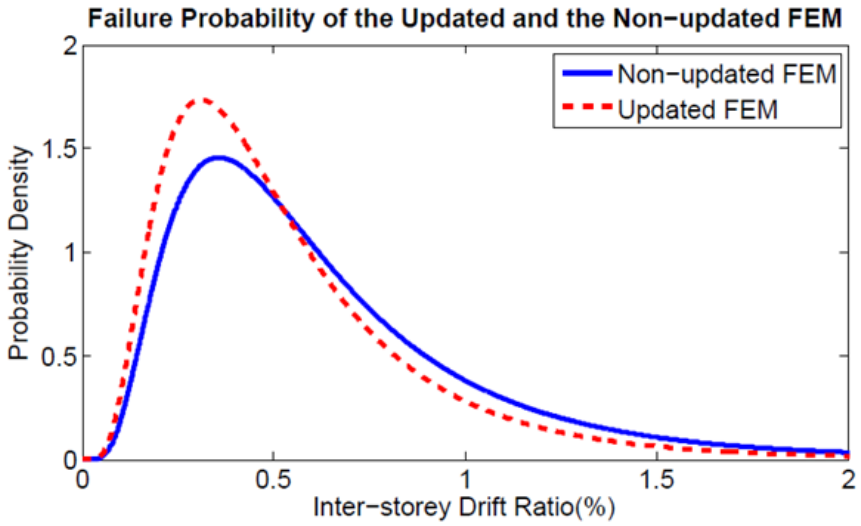

Figure 7.6. Probability density functions of the Updated and Non-updated FEM's.

As expected, probability density functions demonstrate that the level of damage is not destructive and the building remains mostly in the immediate occupancy damage level; however, probability that building will be at this level is different for updated and non-updated models.

7.1.1. Explanation of Seismic Demand Results of the Updated and the Non-updated FEM's

In order to investigate the reason of the differences in interstory drift ratios, the mean moments imposed by the first three modes of the updated and the non-updated FEM's were decomposed and illustrated in Figure 7.7. For this purpose, linear time history analysis method was adopted due to its simplicity in model decoupling.

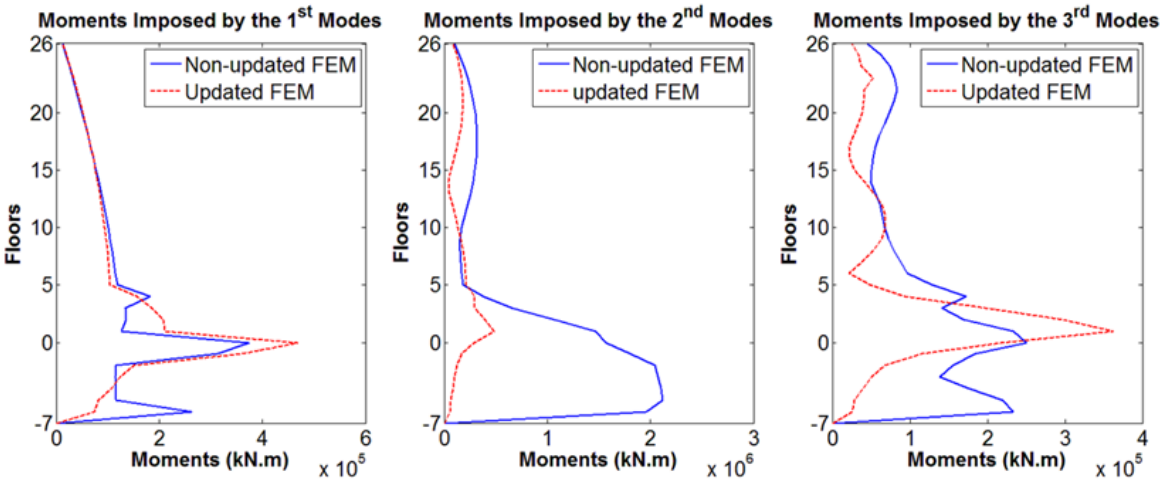

Figure 7.7. Moments imposed by the first three modes of the updated and the non-updated FEM's.

The comparison of results show that the magnitude of moments caused by first mode of the updated FEM is almost the same as the one caused by the first mode of the non-updated FEM at all stories. The magnitude of moments at base caused by the second mode of the non-updated FEM is approximately four times more than the one caused by the second mode of the updated FEM. At the upper parts, the non-updated FEM produces 1.5 times higher moments. For the third more, the non-updated FEM has higher moments than the updated FEM along the basement stories.

The increases in the magnitude of moments at basement stories induced by the second mode of the non-updated FEM explain the reason that the differences in the interstorey drift ratios immediately start at base levels. The higher magnitude of

moments at ground level, which arises from the second mode of the non-updated FEM, and the slightly higher magnitude of moments at tower section stories, which arises from the second and third modes of the non-updated FEM, explain the reason that the difference in the interstory drift ratios continue along the height of the structure.

In order to examine the cause of significant increases in the magnitude of moments imposed by higher modes, the modal shapes and the static forces of the first three modes of FEM's are displayed in the Figure 7.8 and Figure 7.9, respectively. It is seen in Figure 7.8 that the second and third mode shapes of the non-updated FEM at basement floors is much more than the one of the updated FEM. The reason is that the stiffness of basement floors in the non-updated FEM is lower due to lack of seismic gaps with frictional plates. As it is seen in Figure 7.9, this difference leads to higher static forces at the base caused by the 2nd and 3rd modes of the non-updated FEM. The moments imposed by the 3rd mode of the non-updated FEM is less than the ones of the updated FEM only at ground floors. This reason is attributed to the fact that the seismic forces are accumulated at ground levels due to big differences in the stiffness of the basement and ground floors. The slight increases in the static forces of second and third modes explain the higher moments in the upper parts. In addition to static forces, modal accelerations of the non-updated FEM under input motion no 5 and 8 are also displayed in Figure 7.10 and Figure 7.11, respectively. The results under all ground motions are similar for both FEM's. Therefore, only the results of the non-updated FEM under two ground motions are represented here. The results demonstrate that the power spectral density of second mode is higher than the power spectral density of other modes in FEM simulations. Therefore, when the high static force of second mode of the non-updated FEM is combined with its high power spectral density, the second mode has the most significant contribution on total seismic response and responsible for the increases in base moments and the moments at upper parts as well.

However, the moments caused by the second mode of the updated FEM is also significant. They are almost as high as the moments caused by the first mode due to high accelerations of second mode. Therefore, because of the fact that significant

excitation of higher modes are possible for the tall building, and that static forces of higher modes are sensitive to changes in stiffness variations, the effect of FEM Updating Procedure is crucial on higher mode contributions, consequently, on overall seismic demands of tall buildings.

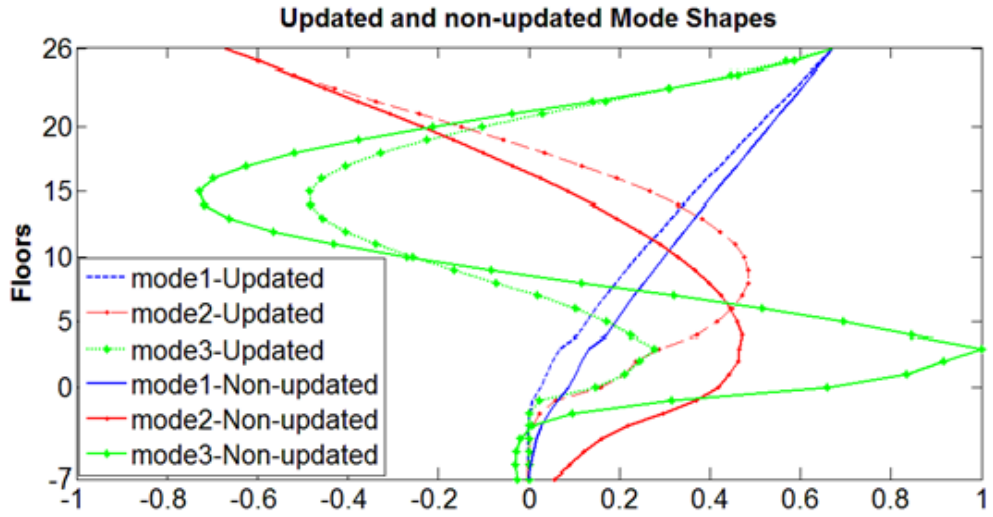

Figure 7.8. Modal Shapes of the non-updated and the updated FEM's.

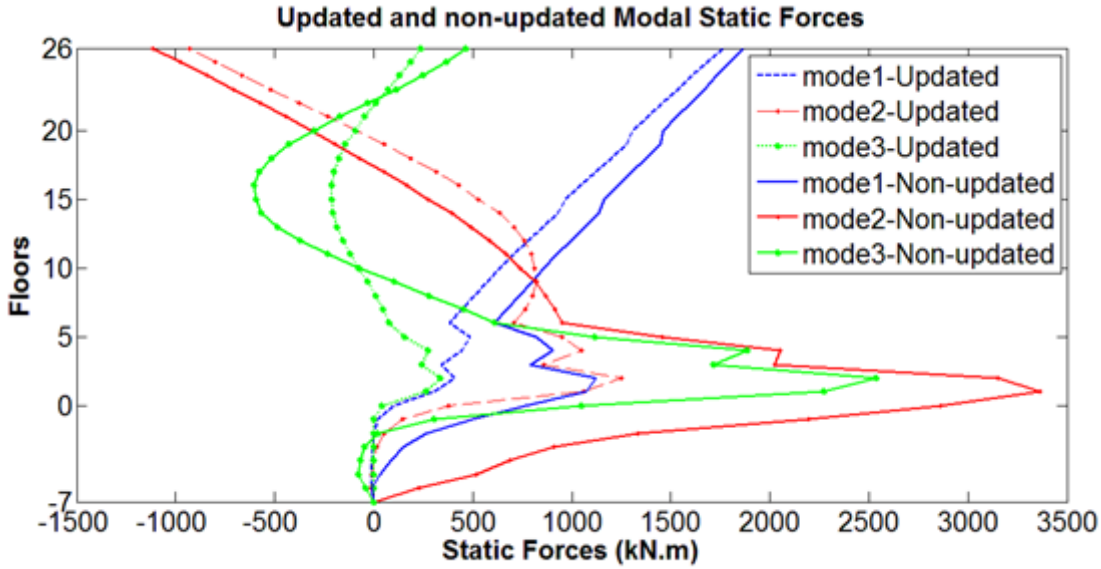

Figure 7.9. Modal Static Forces of the non-updated and the updated FEM's.

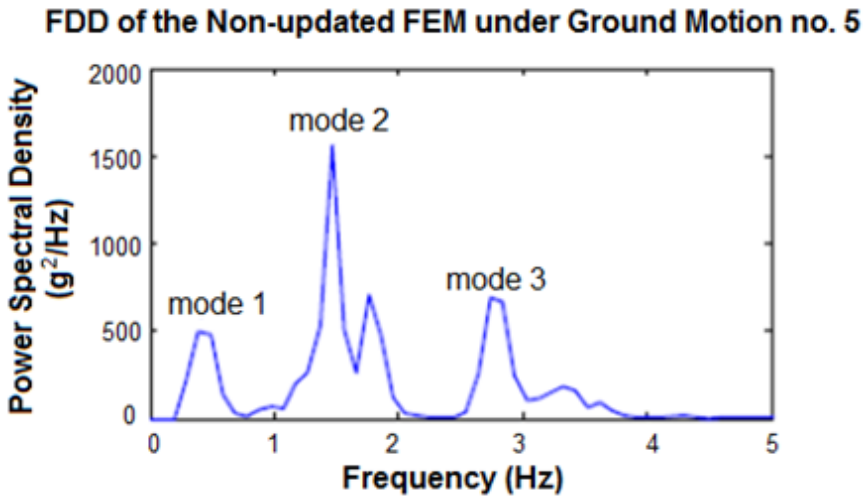

Figure 7.10. Building acceleration response acquired from non-updated FEM's under input motions no. 5

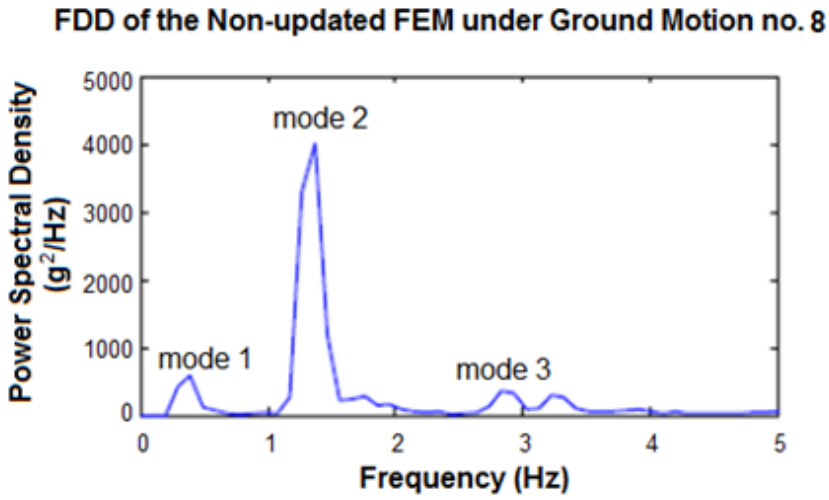

Figure 7.11. Building acceleration response acquired from non-updated FEM's under input motions no 8

Furthermore, in order to verify that the expected ground motions at the building site are likely to cause excitation of higher modes as the ones used in FEM simulations, the response of the tall building to four small magnitude earthquakes are analyzed. Table 7.1 gives information about these recorded earthquakes. Figure 7.12 demonstrates the location of the earthquakes. Figures 7.13, 7.14, 7.15 and 7.16 display the

acceleration response of instrumented stories in time domain in one direction under Marmara, Romania, Yalova and Sakarya earthquakes, respectively.

Table 7.1. Properties of the recorded earthquakes.

No	Location	Distance (km)	Magnitude	Base Acceleration (g)	Roof Acceleration (g)
1	Yalova	48	4	0.0006	0.0016
2	Sakarya	120	4.5	0.0011	0.0055
3	Marmara	67	3.2	0.0015	0.0026
4	Romania	522	5.5	0.0006	0.0024

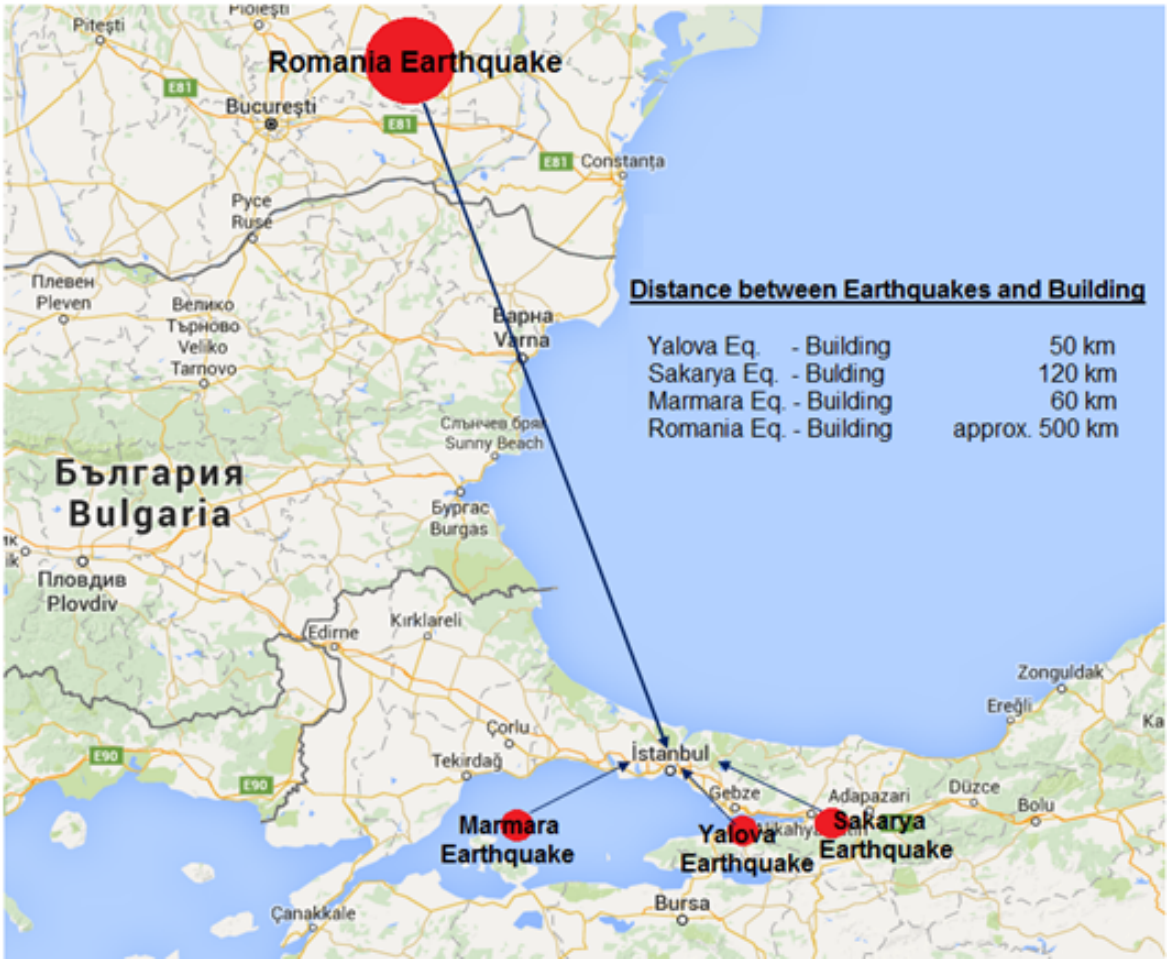

Figure 7.12. Source location of the earthquakes

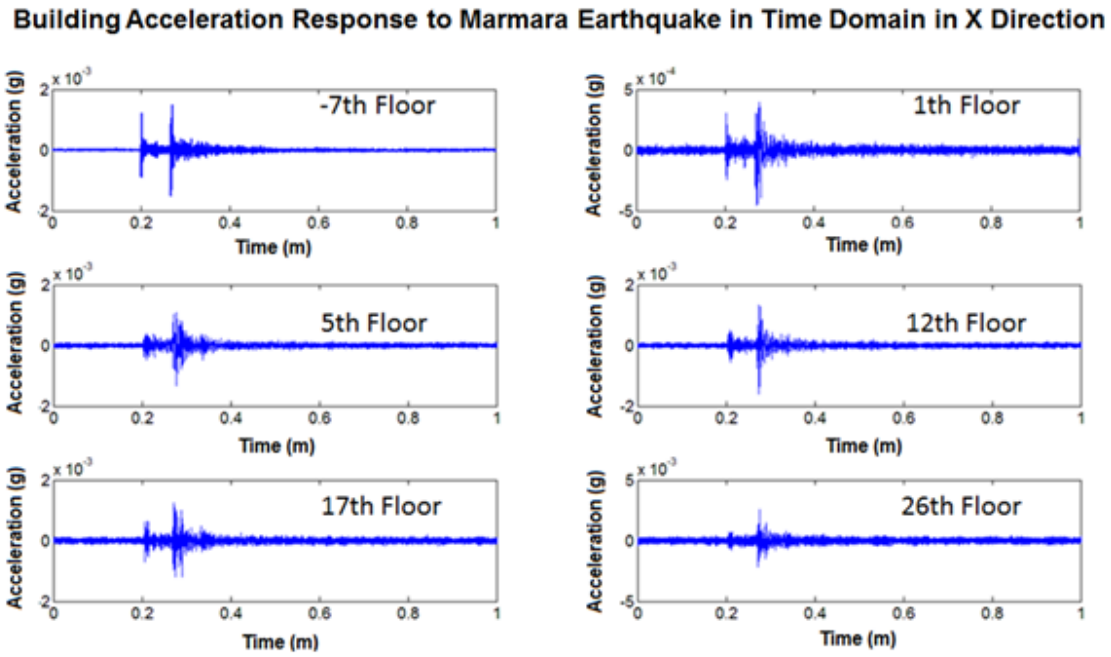

Figure 7.13. Acceleration response of instrumented stories in time domain in one direction under Marmara Earthquake.

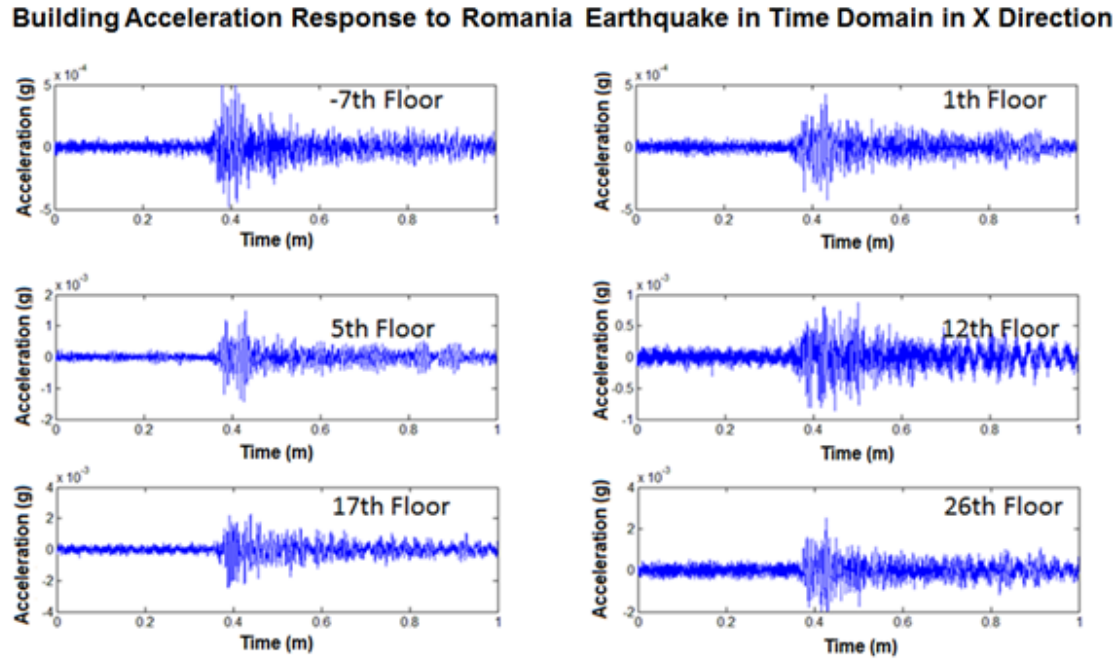

Figure 7.14. Acceleration response of instrumented stories in time domain in one direction under Romania Earthquake.

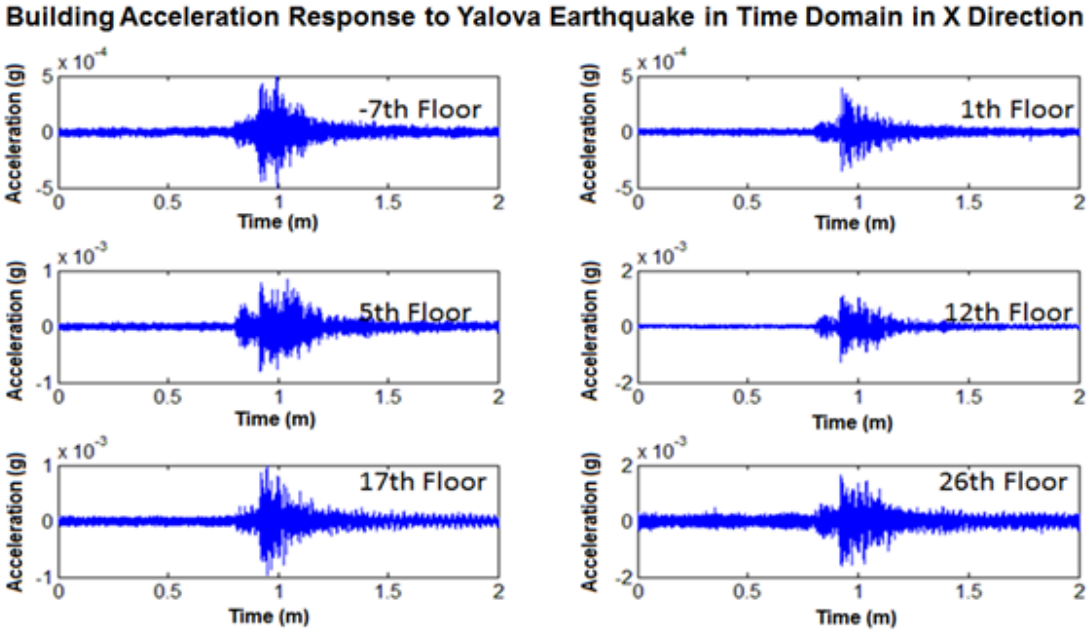

Figure 7.15. Acceleration response of instrumented stories in time domain in one direction under Yalova Earthquake.

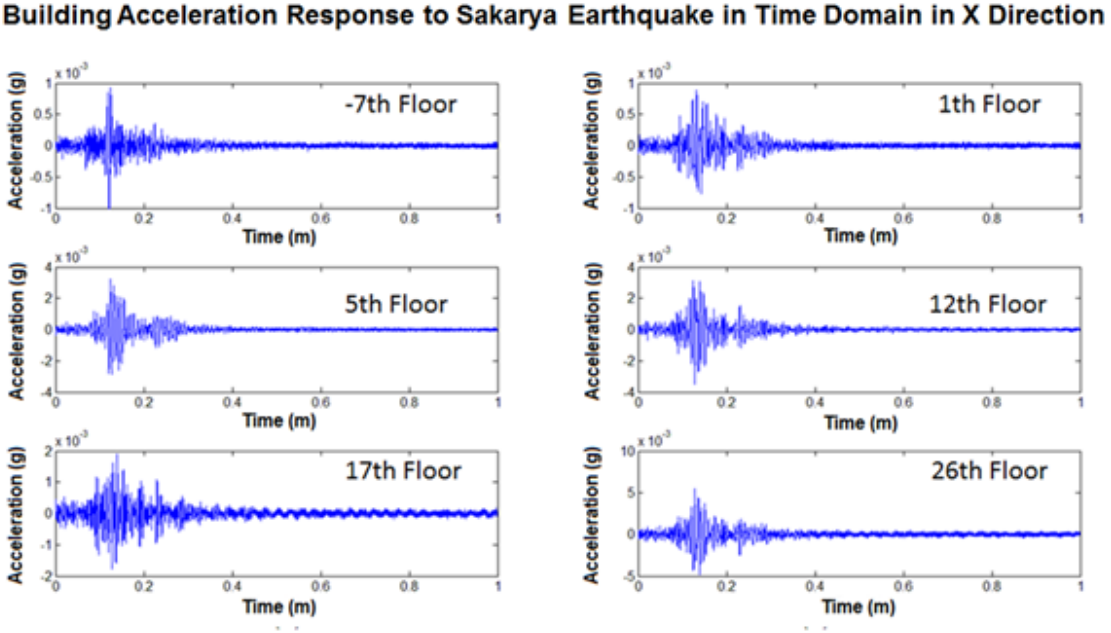

Figure 7.16. Acceleration response of instrumented stories in time domain in one direction under Sakarya Earthquake.

Figures 7.17, 7.18, 7.19 and 7.20 shows the acceleration response of building to Marmara, Romania, Yalova and Sakarya earthquakes and the frequency content of the seismic inputs recorded at the base of the building, respectively. These figures illustrate that the Romania, Yalova and Sakarya Earthquakes excited the 2nd and the 3rd modes the most whereas the Marmara Earthquake excited the 4th mode the most.

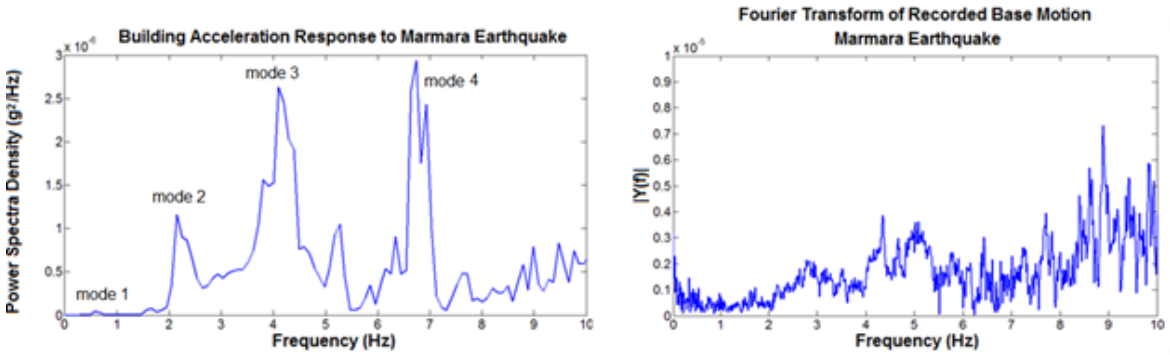

Figure 7.17. Acceleration response of building to Marmara Earthquake and the frequency content of the seismic input recorded at the base of the building

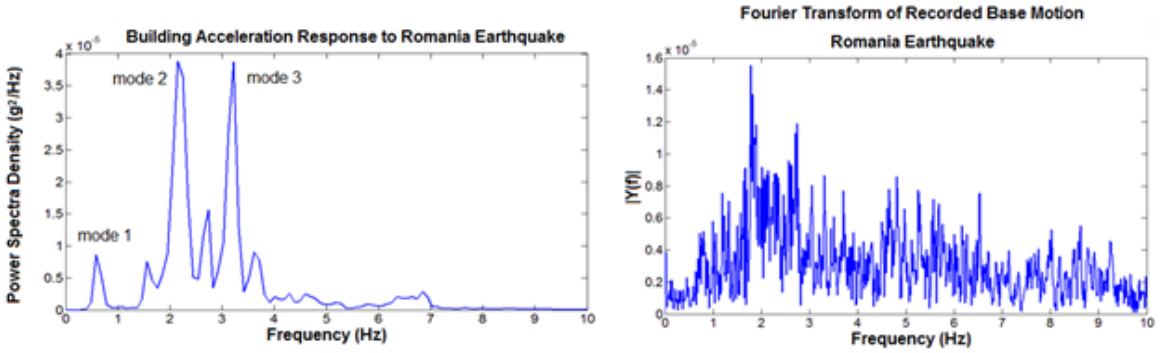

Figure 7.18. Acceleration response of building to Romania Earthquake and the frequency content of the seismic input recorded at the base of the building.

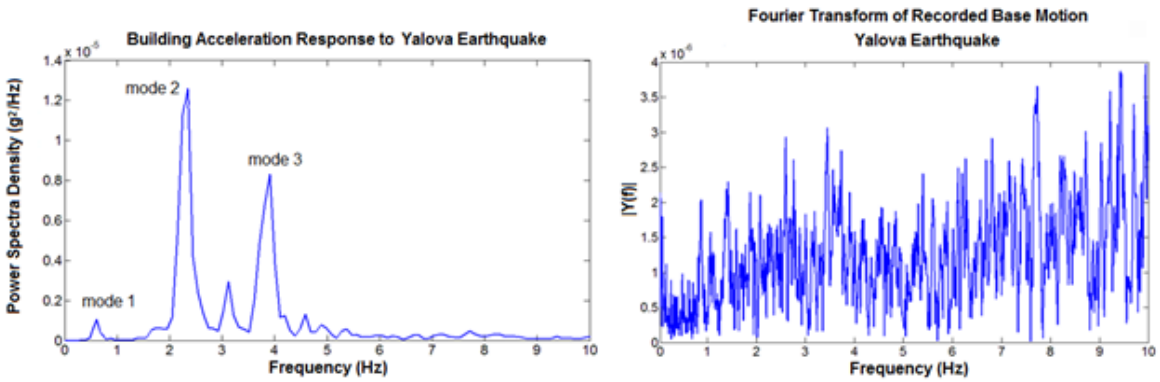

Figure 7.19. Acceleration response of building to Yalova Earthquake and the frequency content of the seismic input recorded at the base of the building.

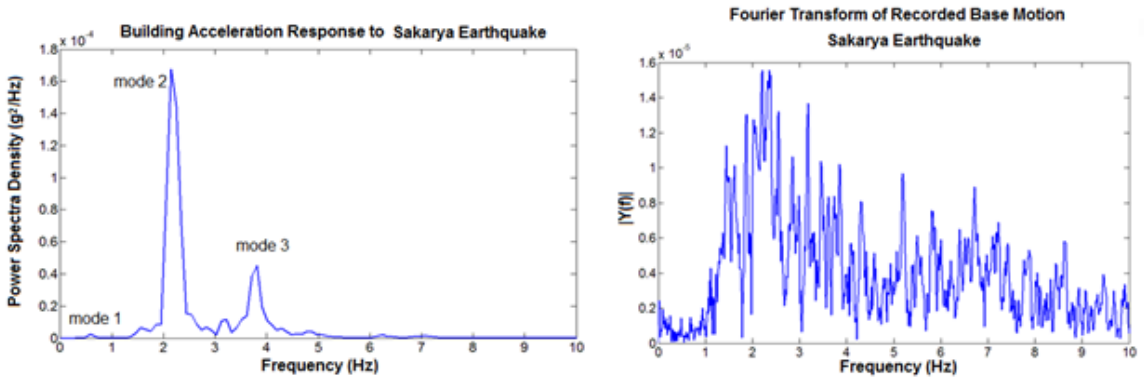

Figure 7.20. Acceleration response of building to Sakarya Earthquake and the frequency content of the seismic input recorded at the base of the building.

In literature, a large number of researches also demonstrated that seismic demands imposed by higher modes crucial. In the pioneering work of Blakeley *et al.* (1975), the significant contribution of higher modes is revealed and amplification factors are suggested to account for additional higher mode demands. The experimental study of Iqbal *et al.* (1980) and the numerical study of Keintzel (1990) concluded similar results. The analytical examinations in studies conducted by Sangarayakul and Warnitchai (2004), Munir and Warnitchai (2012), M. Panagiotou *et al.* (2009), Klemencic *et al.* (2007), C. A. Maniatakis *et al.* (2013) agreed in the fact that current seismic codes underestimate the seismic demands induced by higher modes. A

Full-Scale 7-storey Building Slice Test at UC-San Diago (M. Panagiotou, 2010) also revealed higher mode contributions. In addition to these experimental, numerical and analytical studies, the system identification of seismic responses of tall buildings during seismic events confirmed the high possibility of excitation of higher modes, depending on the frequency content of the earthquake motions (Kasai *et al.*, 2012; Pu *et al.*, 2012; Şafak and Çelebi, 1992; Şafak and Çelebi, 1991; Brownjohn and Pan, 2001).

However, in many studies, the influence of FEM updating on higher mode effects are usually omitted. Also, simplified FEM's are adopted and excitation of higher modes during seismic events is not validated for the structures of interests. In this study, besides the excitation of higher modes in the FEM simulation, four earthquake records collected from the monitored tall building verify that the higher modes of the structure is likely to be excited more than its fundamental mode under the expected ground motions.

7.2. Effect of the Identified Viscous Damping Ratio

In the seismic assessment of structures by analytical models, NLTH analyses has been the common tool due to its advantages in providing a better understanding of local and overall damage state and seismic behavior of structures. However, the accuracy of NLTH analyses results is quite sensitive to modelling choices. Therefore, there are still investigations going on regarding modelling of viscous damping. Even though the energy dissipation in the nonlinear range of structural elements are explicitly modeled by hysteretic damping, a level of viscous damping should be introduced in the analytical model in order to consider the damping in the first phases of response, or in elements which stays in the linear range. For this purpose, Rayleigh Damping has been a widely popular method due to its convenience of establishing the damping matrix, which is required in the solution of nonlinear analyses. However, the proper construction of damping matrix by this method has been a popular research topic because of the fact that the unforeseen consequences of this method can cause overestimation of damping forces.

A brief summary of researches related to the damping mentioned in chapter one is presented here: Bernall (1985) demonstrated that the massless degree of freedoms give rise to spurious damping forces. Leger and Dassault (1992), Hall (2006), Prestley and Grand (2005), Petrini *et al.* (2008), Charney (2008) and Erduran (2012) pointed out that using tangent stiffness in Rayleigh damping can induce unrealistically high forces because of not eliminating the viscous damping forces in the nonlinear phases of structural elements. Zaerian and Medina (2010) offered to model the structural elements with combination of elastic elements and yielding springs without stiffness-proportional damping. To provide information about shift of damping ratios due to stiffness degradations during time history analyses, Jehel *et al.* (2014) developed equations for initial and tangent stiffness based Rayleigh Damping.

However, although appropriate modelling of viscous damping have examined widely in many researches, not much emphasis is put on the selection of the viscous damping ratio. The major problem about viscous damping is that it is not possible to know the precise value of viscous damping ratio. Therefore, in several studies, (Goel *et al.*, 1997; Smith and Willford, 2007; Smith *et al.*, 2010), the damping measurements from buildings with different heights are presented and best fit lines are obtained according to these measurements. However, the results from those studies differ from each other due to source of damping and characteristic of structures such as type of foundation, amount of partition walls, construction materials and design type. Therefore, it is difficult to infer a specific viscous damping ratio for a particular building from the outcomes of these studies. Some guidelines such as LATBSDC (2014) and PEER ATC72-1 (2013) give suggestions about selection of viscous damping in NLTH analyses. However, LATBSDC only provide an upper limit for the viscous damping ratio of tall buildings while PEER ATC72-1 summarizes the studies about viscous damping ratio.

In order to compare the effect of the identified viscous damping on seismic performance assessment of a tall building, nonlinear time history analyses were carried out with the updated FEM's which have the identified viscous damping ratio (2%) and 5% viscous damping ratio. The 5% damping ratio was chosen due to the fact that

it is the highest damping ratio suggested in seismic codes, including Turkish Seismic Code. Figure 7.21 and Figure 7.23 highlight the damage states of these two FEM's under the ground motion no 7 and 9, respectively. It is seen in these figures that the columns of the updated FEM with the identified viscous damping ratio experience higher damage states at the 5th floor, where the shopping mall sections ends and the residential section starts. It is also seen that more beams are damaged at the first floors of residential section in the updated FEM with the identified viscous damping ratio. The damage states under other ground motions give similar results as well.

In this study, the interstory drift ratio was chosen as damage indicator of the building. Figure 7.22 and Figure 7.24 show the interstory drift ratios of the updated FEM's with the identified damping ratio (2%) and the 5% viscous damping ratio under the ground motion number 7 and 9, respectively. Figure 7.25 displays the mean interstory drift ratios of both models. The distributions of these figures show that the rate of increase in interstory drift ratios is highest in the shopping mall section and decreases gradually along the height. However, the FEM with 2% viscous damping ratio exhibits more interstory drifts after the 5th floor.

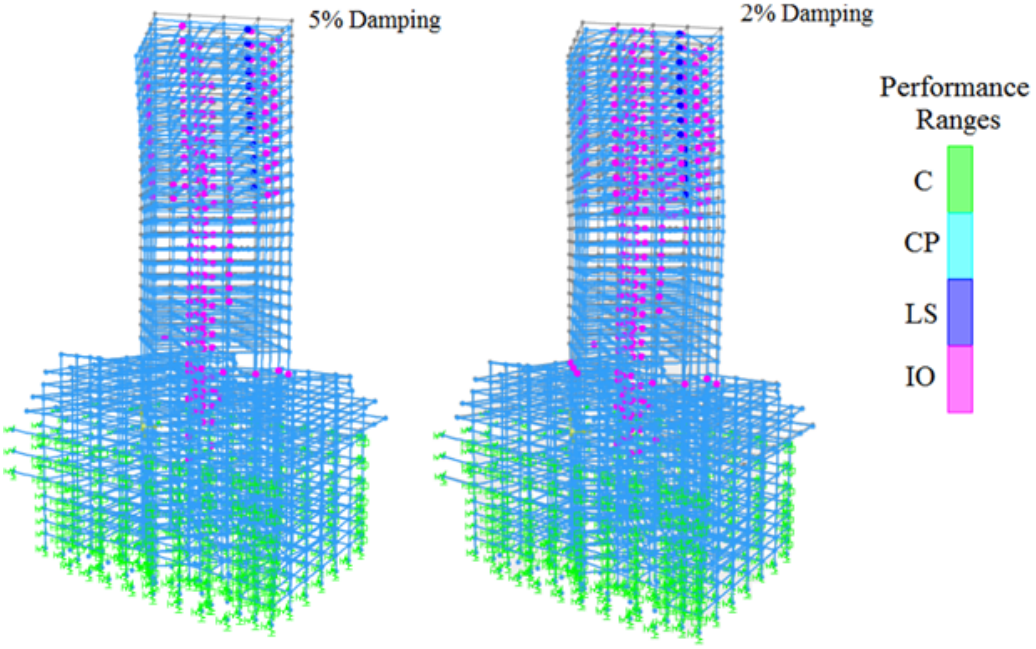

Figure 7.21. The damage levels of the updated FEM's with 2% and 5% viscous damping ratios under the ground motion no 9.

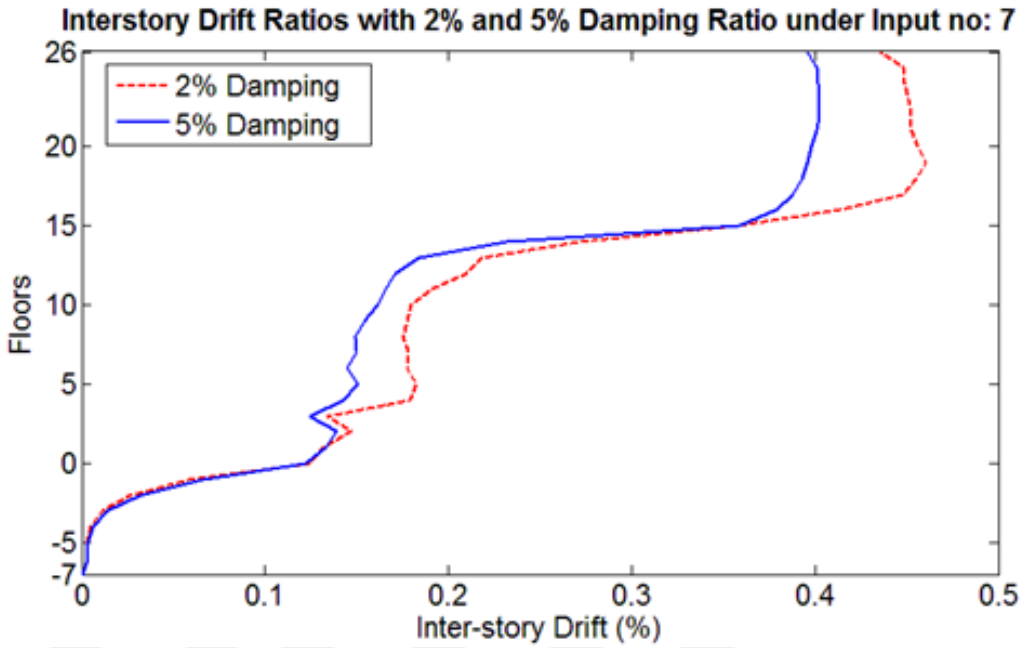

Figure 7.22. Interstory drift ratios of the updated FEM's with 2% and 5% viscous damping ratios under the ground motion no 9.

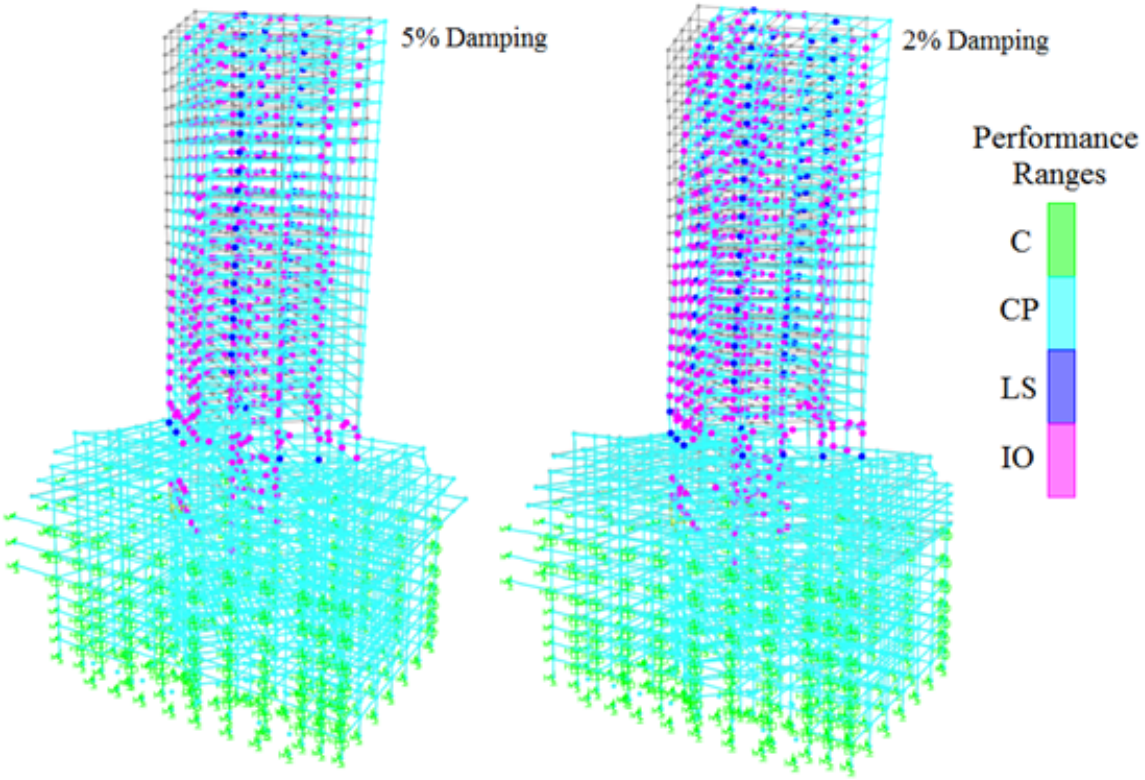

Figure 7.23. The damage levels of the updated FEM's with 2% and 5% viscous damping ratios under the ground motion no 7.

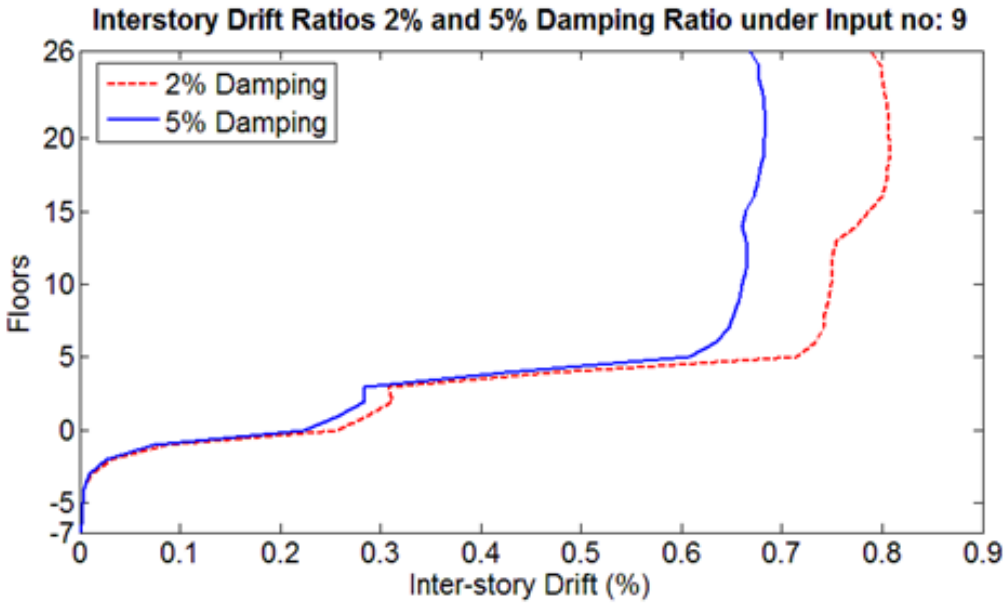

Figure 7.24. Interstory drift ratios of the updated FEM's with 2% and 5% viscous damping ratios under the ground motion no 7.

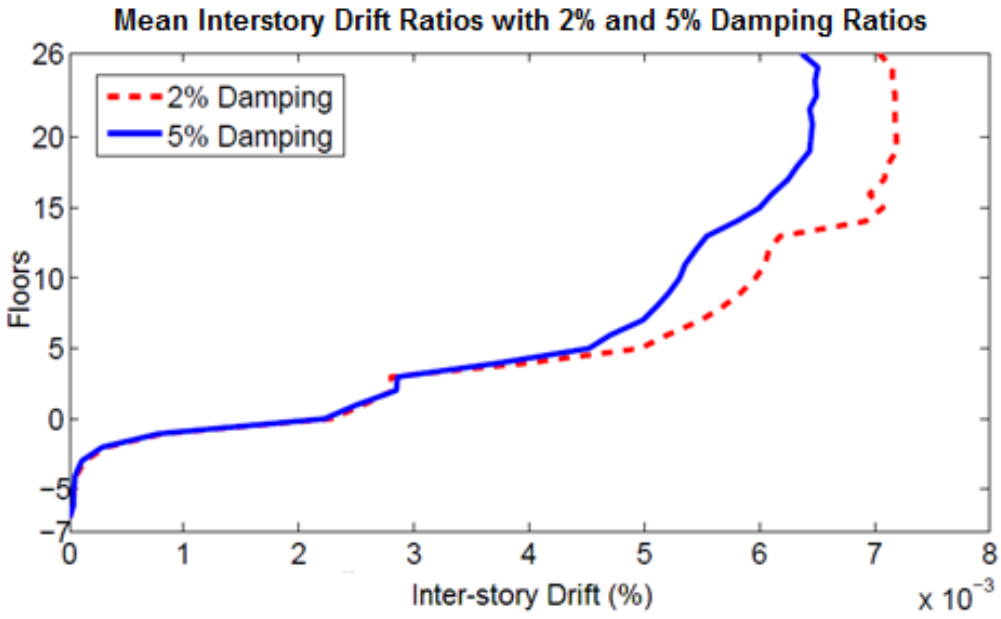

Figure 7.25. Mean Interstory drift ratios of the updated FEM's with 2% and 5% viscous damping ratios.

In order to quantify the probability of failure under the selected input motions, probability density functions in terms of interstory drift ratios were established in Figure 7.2.6. To compare the failure probabilities based on the probability density function in the Figure 7.26, 1% and 0.5% threshold values can be chosen again. The probability of exceeding 1% threshold is 12% for the updated FEM with the identified viscous damping ratio while it is 10% for the updated FEM with the code based viscous damping ratio. For 0.5% threshold value, the probability of exceedance is 52% for the updated FEM with 2% viscous damping ratio while it is 44% for the updated FEM with viscous 5% damping ratio.

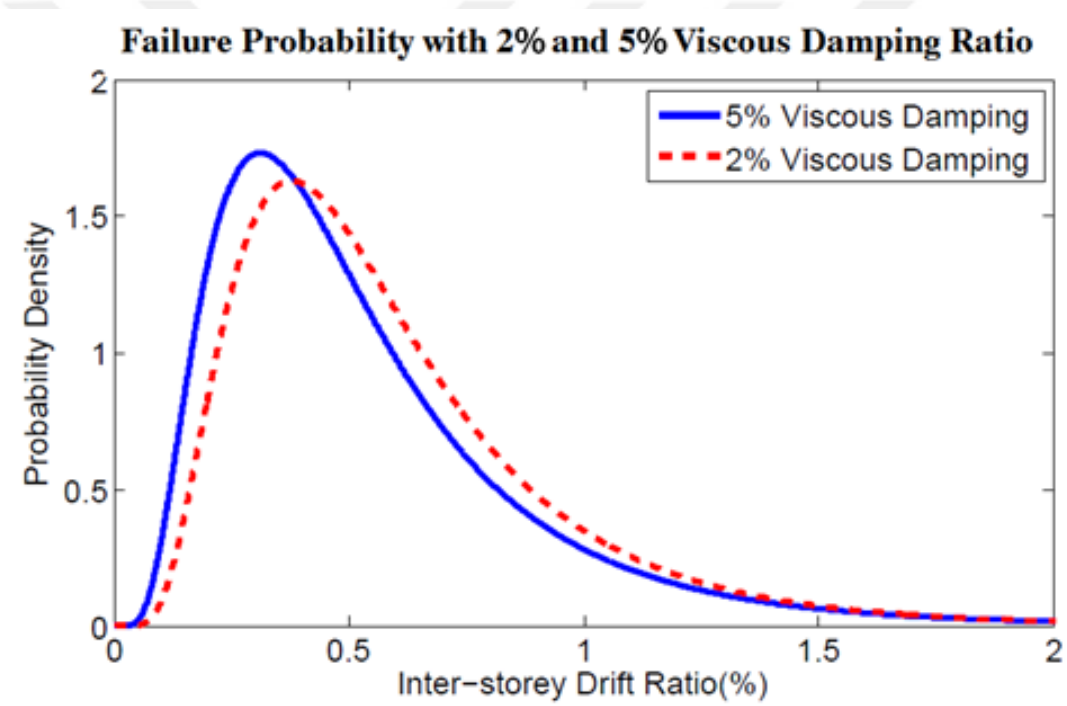

Figure 7.26. Probability density functions of the updated FEM's with 2% and 5% viscous damping ratios.

8. CONCLUSIONS AND FUTURE WORK

8.1. Conclusions

In this study, in order to investigate the effect of identified modal shapes, frequencies and viscous damping on seismic performance assessment of tall buildings, the system identification of a twenty six storey tall building is performed with the vibration measurements. The FEM of the building is generated and updated based on the identified modal values in order to represent the real dynamic characteristics. In the first place, NLTH analyses are performed with the updated and the non-updated FEM in order to observe the influence of utilizing the identified modal frequencies and shapes. 5% viscous damping ratio is used in both FEM's. Secondly, NLTH analyses are carried out with updated FEM considering the identified (2%) and 5% viscous damping ratios in order to observe the influence of using the identified viscous damping. The 5% viscous damping ratio is chosen due to the fact that it is the highest damping ratio suggested in seismic codes, including Turkish Seismic Code. The main findings are as following.

(i) At design practice, the modelling of seismic gaps which provides friction is usually omitted. However, it is observed that their contribution to the stiffness, consequently, to the dynamic characteristics of the structures is very crucial.

(ii) Mode shapes of higher modes may be susceptible to stiffness variations along building more than the fundamental mode, resulting in higher static forces imposed by these modes. The excitation of higher modes may be also much more than the ones of the fundamental mode, depending on the frequency content of the input motions. Consequently, large seismic demands in tall buildings may arise from the combination of these high static and dynamic forces of higher modes. Therefore, it is important to represent the actual static forces of higher modes by the virtue of FEM Updating Procedures. Table 8.1 displays the probabilities of exceeding 1% and 0.5% interstory drift ratios for the non-updated and the updated FEM's and their differences.

Table 8.1. Probabilities of exceeding the treshold interstory drift ratios for the updated and the non-updated FEM's

Treshold Interstory Drift	**Non-updated FEM**	**Updated FEM**	**Difference**
1	16%	10%	-60
0.5%	55%	44%	-25

(iii) The response of the tall building to the four small magnitude earthquake verify that the tall building is sensitive to the excitation of higher modes during the expected seismic events.

(iv) The damping ratio offered by Turkish Design Code is much more than the identified one. In addition, it is difficult to select a viscous damping ratio for a particular structure based on the researches and guidelines. Table 8.2 displays the probabilities of exceeding 1% and 0.5%drift ratios for the updated FEM's with the identified viscous damping ratio (2%) and the code based viscous damping ratio (5%) and their differences.

Table 8.2. Probabilities of exceeding the treshold interstory drift ratios for the updated FEM's with the identified and code based viscous damping ratios.

Treshold Interstory Drift	**Updated FEM (5% Damping Ratio)**	**Updated FEM (2% Damping Ratio)**	**Difference**
1	10%	12%	17%
0.5%	44%	52%	16%

The outcomes indicate that the accurate representation of modal frequencies, shapes and viscous damping ratios in FEM's is very crucial in seismic performance assessment of tall buildings. The use of unrealistic modal values may lead to unsafe or conservative designs. Therefore, system identification studies are recommended to verify the result of nonlinear simulations of tall buildings in order to improve the current seismic design practice.

8.2. Future Work

(i) The nonlinear FEM of the structure may be developed in a software which has many features to conduct advanced nonlinear analysis of structures. So, the shear walls can be modelled with fiber-hinge models and different cyclic material behaviors can be incorporated.

(ii) If any strong earthquake occurs in Istanbul and the response of the structure to this earthquake is recorded during this seismic event, the acceleration responses obtained from the records and the FEM can be compared. The effect of cyclic material behaviors and hinge models on the reliable generation of FEM of the structure can be discussed.

(iii) Other identification methods such as Stochastic Subspace Identification (SSI) and ERA (Eigensystem Realization Algorithm) can be adopted so that the effect of system identification methods can be discussed.

(iv) Probabilistic FEM updating methods such as Error-Domain Falsification (Goulet *et al.*, 2013) may be utilized.

(v) The Matlab code which performs the Automatic analysis of the recorded data three times in a day can be developed by creating a user interface. This code may be also enhanced to produce a real-time monitoring software so that the modal parameters of the structure can immediately obtained right after any seismic events occur.

REFERENCES

American Concrete Institute, *ACI318-08: Building code requirements for structural concrete and commentary*, 2008.

Bernal, D., "Viscous damping in inelastic structural response", *Journal of structural engineering*, Vol. 120, No. 4, pp. 1240–1254, 1994.

Blakeley, R., R. Cooney and L. Megget, "Seismic shear loading at flexural capacity in cantilever wall structures", *Bulletin of the New Zealand National Society for Earthquake Engineering*, Vol. 8, No. 4, pp. 278–290, 1975.

Borochek, R. L. and F. V. Yanez, "Experimental verification of basic analytical assumptions used in the analysis of structural wall buildings", *Engineering Structures*, Vol. 22, No. 6, pp. 657–669, 2000.

Boutin, C., S. Hans, E. Ibraim and P. Roussillon, "In situ experiments and seismic analysis of existing buildings. Part II: Seismic integrity threshold", *Earthquake engineering & structural dynamics*, Vol. 34, No. 12, pp. 1531–1546, 2005.

Brincker, R., L. Zhang and P. Andersen, "Modal identification from ambient responses using frequency domain decomposition", *Proc. of the 18*'International Modal Analysis Conference (IMAC), San Antonio, Texas*, 2000.

British Standard, *Eurocode 8: Design of structures for earthquake resistance*, 2005.

Brownjohn, J. M. and C.-K. Ang, "Full-scale dynamic response of high-rise building to lateral loading", *Journal of performance of constructed facilities*, Vol. 12, No. 1, pp. 33–40, 1998.

Brownjohn, J., T. Pan and X. Deng, "Correlating dynamic characteristics from field measurements and numerical analysis of a high-rise building", *Earthquake*

engineering & structural dynamics, Vol. 29, No. 4, pp. 523–543, 2000.

Brownjohn, J. M. W. and T. C. Pan, "Response of tall buildings to weak long distance earthquakes", *Earthquake engineering & structural dynamics*, Vol. 30, No. 5, pp. 709–729, 2001.

Catbas, F. N., M. Susoy and D. M. Frangopol, "Structural health monitoring and reliability estimation: Long span truss bridge application with environmental monitoring data", *Engineering Structures*, Vol. 30, No. 9, pp. 2347–2359, 2008.

Catbas, F. N., F. Moon and A. E. Aktan, "An Integrated View for Structural Identification of Civil Infrastructure Systems: An Overview of a Collaborative ASCE Committee Effort", *Structures Congress 2010*, pp. 440–446, ASCE, 2010.

Catbas, F. N., H. B. Gokce and M. Gul, "Nonparametric analysis of structural health monitoring data for identification and localization of changes: Concept, lab, and real-life studies", *Structural Health Monitoring*, pp. 613–626, 2012.

Celebi, M., "Recorded earthquake responses from the integrated seismic monitoring network of the Atwood building, Anchorage, Alaska", *Earthquake Spectra*, Vol. 22, No. 4, pp. 847–864, 2006.

Celebi, M., L. Phan and R. Marshall, "Dynamic characteristics of five tall buildings during strong and low-amplitude motions", *The structural design of tall buildings*, Vol. 2, No. 1, pp. 1–15, 1993.

Celebi, M., A. Sanli, M. Sinclair, S. Gallant and D. Radulescu, "Real-time seismic monitoring needs of a building owner-and the solution: a cooperative effort", *Earthquake Spectra*, Vol. 20, No. 2, pp. 333–346, 2004.

Charney, F. A., "Unintended consequences of modeling damping in structures", *Journal of structural engineering*, Vol. 134, No. 4, pp. 581–592, 2008.

Chopra, A. K., *Dynamics of structures*, Vol. 3, Prentice Hall New Jersey, 1995.

Chopra, A. K. and R. K. Goel, "A modal pushover analysis procedure for estimating seismic demands for buildings", *Earthquake Engineering & Structural Dynamics*, Vol. 31, No. 3, pp. 561–582, 2002.

Chopra, A. K., R. K. Goel and C. Chintanapakdee, "Evaluation of a modified MPA procedure assuming higher modes as elastic to estimate seismic demands", *Earthquake Spectra*, Vol. 20, No. 3, pp. 757–778, 2004.

Computers and Structures INC, *SAP2000 - integrated finite element analysis and desing of structures. Analysis reference*, 1997.

Dynamic Design Solutions NV (DDS), Leuven, Belgium, *FEMtools Theoretical Manual, Version 2.1.0*, 2001.

Erdik, M., M. Demircioglu, K. Sesetyan, E. Durukal and B. Siyahi, "Earthquake hazard in Marmara region", *EGS-AGU-EUG Joint Assembly*, Vol. 1, p. 259, 2003.

Erduran, E., "Evaluation of Rayleigh damping and its influence on engineering demand parameter estimates", *Earthquake Engineering & Structural Dynamics*, Vol. 41, No. 14, pp. 1905–1919, 2012.

Fajfar, P. and M. Fischinger, "N2-A method for non-linear seismic analysis of regular buildings", *Proceedings of the Ninth World Conference in Earthquake Engineering*, Vol. 5, pp. 111–116, 1988.

Federal Emergency Management Agency, Building Seismic Safety Council, Washington DC, USA, *FEMA-356: Prestandard and commentary for the seismic rehabilitation of buildings*, 2000.

Goel, R. K. and A. K. Chopra, *Vibration properties of buildings determined from recorded earthquake motions*, Earthquake Engineering Research Center, University

of California, 1997.

Goulet, J.-A., C. Michel and I. F. Smith, "Hybrid probabilities and error-domain structural identification using ambient vibration monitoring", *Mechanical Systems and Signal Processing*, Vol. 37, No. 1, pp. 199–212, 2013.

Hall, J. F., "Problems encountered from the use (or misuse) of Rayleigh damping", *Earthquake engineering & structural dynamics*, Vol. 35, No. 5, pp. 525–545, 2006.

Huang, Y.-N., A. S. Whittaker and N. Luco, "Orientation of maximum spectral demand in the near-fault region", *Earthquake Spectra*, Vol. 25, No. 3, pp. 707–717, 2009.

Imbsen Sofrware Systems, *XTRACT - Cross Section Analysis Program for Structural Engineers*, 2004.

International Conference of Building Officials, California,USA, *UBC: Uniform building code*, 1997.

Istanbul Metropolitan Municipality, Istanbul, Turkey, *Istanbul Seismic Hazard Maps*, `http://www.Ibb.gov.tr/tr/Subsites/Depremsite/Pages/Avrupayakasıguneyimikrobolgelemeprojesi.aspx`.

International Conference of Building Officials, California, USA, *ATC: Uniform building code*, 1997.

Iqbal, M. and A. Derecho, "Inertia forces over height of reinforced concrete structural walls during earthquakes", *ACI Special Publication-Reinforced Concrete Structures Subjected to Wind and Earthquake Forces, SP-63*, pp. 173–196, 1980.

Jeary, A., "Damping in structures", *Journal of wind engineering and industrial aerodynamics*, Vol. 72, pp. 345–355, 1997.

Jeary, A., "Damping in tall buildings—a mechanism and a predictor", *Earthquake*

Engineering & structural dynamics, Vol. 14, No. 5, pp. 733–750, 1986.

Jehel, P., P. Léger and A. Ibrahimbegovic, "Initial versus tangent stiffness-based Rayleigh damping in inelastic time history seismic analyses", *Earthquake Engineering & Structural Dynamics*, Vol. 43, No. 3, pp. 467–484, 2014.

Kasai, K., W. Pu and A. Wada, "Response of Passively-Controlled Tall Buildings in Tokyo during 2011 Great East Japan Earthquake", *Proceedings of the 15th World Conference on Earthquake Engineering*, 2012.

Keintzel, E., "Seismic design shear forces in RC cantilever shear wall structures", *European earthquake engineering*, Vol. 3, pp. 7–16, 1990.

Klemencic, R., J. A. Fry, J. D. Hooper and B. G. Morgen, "Performance-based design of ductile concrete core wall buildings-issues to consider before detailed analysis", *The Structural Design of Tall and Special Buildings*, Vol. 16, No. 5, pp. 599–614, 2007.

Kreslin, M. and P. Fajfar, "The extended N2 method considering higher mode effects in both plan and elevation", *Bulletin of Earthquake Engineering*, Vol. 10, No. 2, pp. 695–715, 2012.

Koh, B. and S. Dyke, "Structural health monitoring for flexible bridge structures using correlation and sensitivity of modal data", *Computers & structures*, Vol. 85, No. 3, pp. 117–130, 2007.

Kohler, M. D., P. M. Davis and E. Safak, "Earthquake and ambient vibration monitoring of the steel-frame UCLA Factor building", *Earthquake Spectra*, Vol. 21, No. 3, pp. 715–736, 2005.

Lemnitzer, A., L. M. Massone, D. A. Skolnik, C. Juan and J. W. Wallace, "Aftershock response of RC buildings in Santiago, Chile, succeeding the magnitude 8.8 Maule earthquake", *Engineering Structures*, Vol. 76, pp. 324–338, 2014.

Léger, P. and S. Dussault, "Seismic-energy dissipation in MDOF structures", *Journal of Structural Engineering*, Vol. 118, No. 5, pp. 1251–1269, 1992.

Li, Q., J. Fu, Y. Xiao, Z. Li, Z. Ni, Z. Xie and M. Gu, "Wind tunnel and full-scale study of wind effects on China's tallest building", *Engineering structures*, Vol. 28, No. 12, pp. 1745–1758, 2006.

Li, Q., J. Fang, A. Jeary, C. Wong and D. Liu, "Evaluation of wind effects on a supertall building based on full-scale measurements", *Earthquake engineering & structural dynamics*, Vol. 29, No. 12, pp. 1845–1862, 2000.

Li, Q., Y. Xiao, C. Wong and A. Jeary, "Field measurements of wind effects on the tallest building in Hong Kong", *The Structural Design of Tall and Special Buildings*, Vol. 12, No. 1, pp. 67–82, 2003.

Liel, A. B., C. B. Haselton, G. G. Deierlein and J. W. Baker, "Incorporating modeling uncertainties in the assessment of seismic collapse risk of buildings", *Structural Safety*, Vol. 31, No. 2, pp. 197–211, 2009.

Lord, J.-F., C. E. Ventura, E. Dascotte, R. Brincker and P. Andersen, "FEM Updating Using Ambient Vibration Data from a 48-Storey Building in Vancouver, British Columbia, Canada", pp. 2142–2149, 2003.

Maniatakis, C. A., I. N. Psycharis and C. C. Spyrakos, "Effect of higher modes on the seismic response and design of moment-resisting RC frame structures", *Engineering Structures*, Vol. 56, pp. 417–430, 2013.

Maniatakis, C. A., I. N. Psycharis and C. C. Spyrakos, "Effect of higher modes on the seismic response and design of moment-resisting RC frame structures", *Engineering Structures*, Vol. 56, pp. 417–430, 2013.

Ministry of Public Works and Settlement, Ankara, Turkey, *Specifications for buildings to be built in seismic areas*, 2007.

Moaveni, B., A. R. Barbosa, J. P. Conte and F. M. Hemez, "Uncertainty analysis of system identification results obtained for a seven-story building slice tested on the UCSD-NEES shake table", *Structural Control and Health Monitoring*, Vol. 21, No. 4, pp. 466–483, 2014.

Moaveni, B., X. He, J. P. Conte, J. I. Restrepo and M. Panagiotou, "System identification study of a 7-story full-scale building slice tested on the UCSD-NEES shake table", *Journal of Structural Engineering*, 2011.

Moaveni, B., A. Stavridis, G. Lombaert, J. P. Conte and P. B. Shing, "Finite-element model updating for assessment of progressive damage in a 3-story infilled RC frame", *Journal of Structural Engineering*, Vol. 139, No. 10, pp. 1665–1674, 2012.

Moaveni, B., J. P. Conte and F. M. Hemez, "Uncertainty and sensitivity analysis of damage identification results obtained using finite element model updating", *Computer-Aided Civil and Infrastructure Engineering*, Vol. 24, No. 5, pp. 320–334, 2009.

Moehle, J. P., "The tall buildings initiative for alternative seismic design", *The Structural Design of Tall and Special Buildings*, Vol. 16, No. 5, pp. 559–567, 2007.

Naeim, F., "Performance of 20 extensively-instrumented buildings during the 1994 Northridge earthquake", *The Structural Design of Tall Buildings*, Vol. 7, No. 3, pp. 179–194, 1998.

Panagiotou, M. and J. I. Restrepo, "Dual-plastic hinge design concept for reducing higher-mode effects on high-rise cantilever wall buildings", *Earthquake Engineering & Structural Dynamics*, Vol. 38, No. 12, pp. 1359–1380, 2009.

Panagiotou, M., J. I. Restrepo and J. P. Conte, "Shake-table test of a full-scale 7-story building slice. Phase I: Rectangular wall", *Journal of Structural Engineering*, 2010.

Pasific Earthquake Engineering Research (PEER), University of California, Berkeley, California, USA, *PEER NGA West2 Data Base*.

Pekelnicky, R. and C. Poland, "ASCE 41-13: Seismic evaluation and retrofit of existing buildings", *SESOC 2012 Convention*, 2012.

Petrini, L., C. Maggi, M. N. Priestley and G. M. Calvi, "Experimental verification of viscous damping modeling for inelastic time history analyzes", *Journal of Earthquake Engineering*, Vol. 12, No. S1, pp. 125–145, 2008.

Priestley, M. and D. Grant, "Viscous damping in seismic design and analysis", *Journal of Earthquake Engineering*, Vol. 9, No. spec02, pp. 229–255, 2005.

Pu WC, K. T., Kasai K, "Response of conventional seismic-resistant tall buildings in Tokyo during 2011 great east Japan earthquake", *Proceedings of the 15th World Conference on Earthquake Engineering*, 2012.

Safak, E. and M. Celebi, "Seismic response of Transamerica building. II: system identification", *Journal of Structural Engineering*, Vol. 117, No. 8, pp. 2405–2425, 1991.

Safak, E. and M. Çelebi, "Recorded seismic response of Pacific Park Plaza. II: System identification", *Journal of Structural Engineering*, Vol. 118, No. 6, pp. 1566–1589, 1992.

Sangarayakul, C. and P. Warnitchai, "Approximate modal decomposition of inelastic dynamic responses of wall buildings", *Earthquake Engineering & Structural dynamics*, Vol. 33, No. 9, pp. 999–1022, 2004.

Satake, N., K.-i Suda, T. Arakawa, A. Sasaki and Y. Tamura, "Damping evaluation using full-scale data of buildings in Japan", *Journal of Structural Engineering*, Vol. 129, No. 4, pp. 470–477, 2003.

Skolnik, D., Y. Lei, E. Yu and J. W. Wallace, "Identification, model updating, and response prediction of an instrumented 15-story steel-frame building", *Earthquake Spectra*, Vol. 22, No. 3, pp. 781–802, 2006.

Skolnik, D., E. Yu, J. Wallace and E. Taciroglu, "Modal System Identification & Finite Element Model Updating of a 15-story Building using Earthquake & Ambient Vibration Data", *Structural Engineering Research Frontiers*, pp. 1–14, ASCE, 2007.

Smith, R. J. and M. R. Willford, "The damped outrigger concept for tall buildings", *The Structural Design of Tall and Special Buildings*, Vol. 16, No. 4, pp. 501–517, 2007.

Smith, R., R. Merello and M. Willford, "Intrinsic and supplementary damping in tall buildings", *Proceedings of the ICE-Structures and Buildings*, Vol. 163, No. 2, pp. 111–118, 2010.

Soyoz, S., M. Q. Feng and M. Shinozuka, "Structural reliability estimation with vibration-based identified parameters", *Journal of engineering mechanics*, Vol. 136, No. 1, pp. 100–106, 2010.

Structural Vibration Solutions, Denmark, *ARTeMIS Extractor: Ambient Response Testing and Modal Identification Software, User's Manual*, 2001.

Tall Building Initiative-PEER, California, USA, *PEER/ATC-72-1: Modeling and acceptance criteria for seismic design and analysis of tall buildings*, 2010.

Teughels, A. and G. De Roeck, "Structural damage identification of the highway bridge Z24 by FE model updating", *Journal of Sound and Vibration*, Vol. 278 ,No. 3, pp. 589-610, 2004.

The mathworks INC, *MATLAB User's Guide*, 2015.

Turkish Standards Institute, Ankara, Turkey, *TS500: Requirements for design and construction of reinforced concrete structures*, 2000.

Van Overschee, P. and B. De Moor, "N4SID: Subspace algorithms for the identification of combined deterministic-stochastic systems", *Automatica*, Vol. 30, No. 1, pp. 75–93, 1994.

Ventura, C., J. Lord, M. Turek, R. Brincker, P. Andersen and E. Dascotte, "FEM updating of tall buildings using ambient vibration data", *Proceedings of the Sixth European Conference on Structural Dynamics (EURODYN)*, pp. 4–7, 2005.

Venture, N. C. J., "Selecting and scaling earthquake ground motions for performing response-history analyses", *NIST GCR*, pp. 11–917, 2011.